Ana Rita Alves Pereira de Ferreira Monteiro

Investigating the expression of genes and proteins in Glioblastoma during hypoxia

UAlg
UNIVERSIDADE DO ALGARVE
Biomedical Sciences and Medicine Department

Year 2017/2018

Ana Rita Alves Pereira de Ferreira Monteiro

Investigating the expression of genes and proteins in Glioblastoma during hypoxia

Master in Oncobiology –
Molecular Mechanisms of Cancer

Work Supervised by:

Dr. Patrícia Madureira, Cancer Biology and Progression Laboratory, Centre for Biomedical Research (University of Algarve) and Brain Tumour Research Centre of Excellence (University of Portsmouth);

Dr. Ana Teresa Maia, Centre for Biomedical Research and Department of Biomedical Sciences and Medicine (University of Algarve).

UAlg
UNIVERSIDADE DO ALGARVE
Biomedical Sciences and Medicine Department

Year 2017/2018

Investigating the expression of genes and proteins in Glioblastoma during hypoxia

Statement of authorship

I hereby declare that I am the author of this work, which is, to the best of my knowledge and belief, original, except as acknowledged in the text. Authors and work consulted are properly cited in the text and listed in the references in the required format. The material has not been previously submitted, in whole or in part, for a degree at this or any other university.

_____

Signature

Acknowledgements

I am enormously grateful to my supervisor, Dr. Patrícia Madureira for giving me the wonderful opportunity to work in a such amazing lab as the one from the Brain Tumour Research Excellence center at University of Portsmouth. I am immensely thankful for all the shared knowledge, encouragement and patience, as well the friendship, support and warm welcome in Portsmouth. My wish is that future will bring us to work together again.

A big thank you to Dr. Richard Hill who also supervised, helped and taught me during the 10 months I spend in the laboratory.

I would also like to express my profound gratitude to my co-supervisor Dr. Ana Teresa Maia, who took time from an incredibly busy schedule to assist me with my dissertation. I am truly thankful for the help and attentiveness.

I am extremely grateful to Professor Geoffrey J. Pilkington and everyone in the Brain Tumour Research Excellence center laboratory from University of Portsmouth, for accepting me and giving me the chance to learn and grow as a person and a scientist in a challenging environment.

A big thanks to all my friends in Portsmouth, particularly Mohsen Seifi, Noor Alabdullah and Tarek Zaidieh who gave support and motivation in harder days and who made me feel like at home. I am also enormously grateful to my dear friend Diana Leite for all the help in the laboratory, as well the friendship, companionship, shared laughs and for making my days happier.

I am also immensely grateful to my friends and dear colleagues Juliana Machado and Catarina Martins. Thank you for accommodating me in your office, homes and hearts.

A heartfelt gratitude goes to everyone from “Grupeta dos 10 magníficos”, who are indeed the best friends in the world. Thank you for these 8 years of friendship and for all the encouragement words.

For all the love and caring, I am infinitely grateful to Daniel Duarte who despite being miles away from me, kept close at all times. You proved there is no distance for love.

Most importantly, I am eternally grateful to my parents Elisabete Pereira and Samuel Monteiro who supported me financially through this opportunity, for being by me side at all times and for loving me unconditionally and for making of me what I am today. I owe you all my triumphs. Also, a tremendously heartfelt gratitude to by brother Miguel Monteiro and sister Joana Monteiro.

“Nature is the source of all true knowledge. She has her own logic, her own laws, she has no effect without cause nor invention without necessity.”

Leonardo da Vinci

Abstract

Glioblastoma multiforme (GBM), grade IV Astrocytoma, is the most common and deadly form of brain cancer. Despite the low incidence rate (3.2 per 100.000 people), patient's median survival is only 14 months. Notwithstanding all new diagnostic tools, GBM remains a therapeutic challenge, being extremely difficult to prevent recurrence. Therefore, it is essential to conduct research in order to understand the molecular pathways in the core of GBM aggressiveness and swift evolution.

GBM is often characterized by hypoxic regions where oxygen levels are extremely low. As a natural consequence of tumour growth and expansion, some areas of the tumour become distanced from the blood vessels and consequently, from the oxygen supply. In such a critical environment, cells activate pro-survival and malignancy mechanisms such as the metabolic switch, invasion and angiogenesis. Hence we investigated the expression of genes featuring these survival mechanisms and identified a panel of hypoxia-driven-malignancy markers.

To conduct this study, two GBM patient´s biopsy-derived cell lines (UP-029 and SEBTA-023) were used and cultured under hypoxic conditions for a selected set of time-points (time-course). To characterize the hypoxic response of these cells, hypoxia profiler microarrays were ran for normoxia, 6 and 48 hours of hypoxia (1% O_2). Once identified the induced and repressed genes, these were analyzed and validated through qRT-PCR assays. Finally, western-blot analysis was performed to detect target proteins and correlate with the previously obtained gene expression data. Our study validated *ANGPTL4*, *PIGF, VEGFA*, *GLUT1*, *PFKB4*, *PFKB3*, *BNIP3*, *DDIT4*, *NDRG1* and *CAIX* genes as relevant in GBM's hypoxia-mediated response. We also pointed out *MXI1*, *HNF4A* genes as likely significant factors in GBM hypoxia. Furthermore, we hypothesize *PFKB3* as an adaptive resistance marker in GBM and the repression of *TFRC* as required mechanism for GBM progression.

Keywords: Glioblastoma (GBM); Hypoxia; Angiogenesis; Glycolysis; Invasion

Resumo

O Glioblastoma multiforme (GBM) é a forma mais comum e letal de cancro no sistema nervoso central. Devido às suas caraterísticas altamente invasivas e malignas, o Glioblastoma foi considerado pela *World Health Organization* (WHO) como um Astrocitoma grau IV. Contrariamente a outros tipos de cancro de igual grau, a capacidade de invasão do GBM é limitada ao tecido cerebral.

Apesar dos avanços nas tecnologias de diagnóstico e dos constantes progressos na investigação do cancro, o tratamento do GBM é meramente paliativo. A seletividade farmacológica da barreira hemato-encefálica, a elevada heterogeneidade tumoral e influência destrutiva do tumor no tecido nervoso, refletem-se na ineficiência das terapias aplicadas.

Clinicamente, o GBM manifesta-se através de pressão intracranial, cefaleias e/ou défices neurológicos tais como, alterações visuais, alterações da fala, dificuldades cognitivas e até modificações na personalidade. Embora, menos frequentes, convulsões também se encontram descritas como um dos sintomas.

A taxa de incidência deste tipo de carcinoma é de facto baixa, sendo que em 100000 apenas 3.2 pessoas são afetadas. Não obstante, a média de sobrevida destes pacientes é somente 14 meses. Conduzir investigações no sentido de entender os mecanismos moleculares que se encontrar subjacentes à expansão e agressividade do GBM torna-se, portanto, essencial.

Uma das características mais proeminentes do GBM são as regiões hipóxicas, onde os níveis de oxigénio são extremamente baixos. Esta é uma consequência natural, derivada da expansão tumoral e do incremento da distância de difusão de oxigénio. Estabelecido um microambiente como este, crítico para a sobrevivência celular, as células tumorais ativam mecanismos de malignidade tais como "*switch*" metabólico, angiogénese e invasão. Desta forma as células adquirem vantagem clonal e capacidade migratória para invadirem zonas de tecido cerebral saudável. Para além do incremento da malignidade, a elevada capacidade invasiva destas

células constitui um risco em termos de recorrência. De um modo geral, a hipóxia integra-se como um marcador de mau prognostico.

Para este estudo, duas linhas celulares obtidas através de biópsias de pacientes com GBM (UP-029 e SEBTA-023), foram incubadas a diferentes tempos de hipóxia. Após extração de ácido ribonucleico (ARN), realizou-se um *microarray* de perfil de hipóxia a três amostras em diferentes condições: normóxia (controlo), 6 e 48 horas. O método do *microarray* baseia-se na tecnologia de reações de polimerase em cadeia e em tempo real (*RT-PCR*). Este, por sua vez, é um método de quantificação de expressão génica através da geração de cópias (por ciclo de PCR) a partir de um ADN molde. Isto origina uma correlação entre a quantidade inicial de cópias e a quantidade acumulada a cada ciclo. Desta maneira, foi possível quantificar a expressão génica de 84 genes previamente descritos na literatura como relacionados na resposta hipóxica em diversos tipos de cancro. Este ensaio permitiu-nos identificar em larga escala diversos marcadores de hipóxia que foram diferencialmente expressos com significância. Do painel analisado, destacaram-se os genes *ANGPTL4, NDRG1, CAIX, PFKB4* e *VEGFA* como relevantemente induzidos tanto nas UP-029 como nas SEBTA-023. Para além destes, os genes *MXI1, HNF4A* e *TFRC* foram estabelecidos como significativamente sub-expressos durante a hipóxia nas duas linhas celulares de GBM.

Continuando com a análise, estudámos através de ensaios de *RT-PCR* quantitativo os vários genes distinguidos acima, tal como outros apenas diferencialmente expressos numa das linhas celulares durante a hipóxia. Cada gene foi analisado em quatro condições diferentes: normóxia, 6, 24 e 48 horas de hipóxia, em pelo menos três corridas diferentes. O método de $2^{-\Delta\Delta CT}$ foi usado para calcular o *fold-change* de cada gene, que nos transmite a magnitude biológica da expressão de um gene relativamente a um controlo. De modo a estudar a significância estatística dos resultados, usámos *Students T-test* (tipo 2, cauda 2) para calcular os *P-values* de cada amostra. Considerámos três níveis de significância para *P-values* inferiores que 0.05 (*), 0.01 (**) e 0.001 (***).

Desta análise de RT-PCR quantitativo, para além dos genes previamente distinguidos, também os genes *PIGF*, *PDK1*, *PFKB3*, *BNIP3*, *DDIT4* e *SLC16A3*

foram detetados como significativamente induzidos nas linhas celulares UP-029 e SEBTA-023. Validámos, também, o gene *TFRC* como significativamente sub-expresso durante a hipóxia.

De modo a analisar a expressão de proteínas de alguns deste fatores, realizaram-se ensaios de *Western-blot*. Esta é uma técnica vastamente usada em laboratório que permite a identificação de proteínas específicas de uma amostra de proteína total. Este método consiste na separação de proteínas por pesos moleculares através da aplicação de voltagem. Para tal, a amostra proteica é desnaturada através de calor e posteriormente pipetada num gel de eletroforese. As proteínas (carga negativa) migram através do gel na direção do polo positivo, assim que aplicada voltagem. Desta forma, as moléculas menores migram mais rapidamente e facilmente para a base do gel que as de maior peso molecular, que ficam mais próximas do topo. Após separação e transferência para uma membrana de nitrocelulose, é possível sinalizar estas proteínas através de complexos de anticorpos e fluoróforos. Assim, pudemos detetar a expressão proteica de alguns genes de interesse em diferentes condições: normóxia, 1, 2, 3, 6, 24 e 48 horas de hipóxia.

Realizou-se uma análise de expressão proteica de HIF1α para confirmar a indução da resposta hipóxica. Uma vez que é regulado a nível da proteína, foram detetadas, de facto, bandas de HIF1α durante a hipóxia , apesar de não se observarem induções significantes da expressão génica. Como *CAIX*, foi significativamente expresso a nível do gene, foram também realizados *blots* para a proteína correspondente. A proteína CAIX foi detetável nas amostras de 6, 24 e 48 horas de hipóxia, especialmente nas células SEBTA-023.

A proteína EGFR, vastamente descrita em GBM, foi também analisada. Curiosamente não foi detetável nas células UP-029, mas sim nas SEBTA-023, em todas as amostras. À semelhança de EGFR, os *blots* das proteínas UpaR, VEGFC e S100A10 foram também analisados. As proteínas UpaR e S100A10 foram detetadas em ambas as linhas celulares, com distinção nas amostras SEBTA-023. Nas células UP-029 a baixa deteção de proteína pode-se justificar por uma activação mais tardia

da expressão de factores de invasão. Curiosamente a expressão de VEGFC, detetável em ambas as linhas, diminuí em simultaneidade com o aumento de horas de hipóxia.

Em suma, o nosso estudo identificou *ANGPTL4, NDRG1, CAIX, PFKB4*, *VEGFA*, *PIGF*, *PDK1*, *PFKB3*, *PFKB4*, *BNIP3*, *CAIX*, *DDIT4*, *NDRG1* e *SLC16A3* como genes significativamente induzidos e *HNF4A* e *TFRC* como genes significativamente sub-expressos em GBM. Extrapolámos, que por vezes a indução das expressões de genes e proteínas de invasão é uma resposta tardia após um período considerado crónico de hipóxia. De futuro, deveriam ser estudados tempos de hipóxia mais prolongados, como 72 e 96 horas. Sugerimos, também, *PFKB3* como um provável marcador de resistência à terapia, uma vez que já se encontra descrito noutros tumores, e neste estudo foi significativamente induzido. Conjuntamente, propõe-se o *TFRC* como um possível fator importante no impedimento da progressão do GBM, uma vez que foi sub-expresso nas diferentes análises. Estudos relativos a estes dois genes deverão ser conduzidos no futuro, para confirmar as hipóteses acima. Seria também relevante repetir este estudo aumentando o número de linhas celulares de modo a elevar a sensibilidade da seleção de possíveis novos marcadores de invasão em hipóxia.

Palavras-chave: Glioblastoma (GBM); Hipóxia; Angiogénese; Glicólise; Invasão

List of Contents

List of Figures

Chapter I

Chapter II

Chapter III

List of Tables

Chapter I

Chapter II

Glossary

A

ADM: Adrenomedullin
AIIt: AnnexinA2-S100A10 heterotetramer
ANGPTL4: Angiopoietin like 4
Apaf-1: Apoptotic protease activating factor 1
APS: Ammonium persulfate
ATP: Adenosine triphosphate
ATRX: Alpha-thalassemia/mental retardation X-linked syndrome protein

B

BCA: Bicinchoninic acid
Bcl-2: B-cell lymphoma 2
BNIP3: BCL2 Interacting protein 3
BTR: Brain tumour research centre

C

CAIX: Carbonic anhydrase IX
cAMP: Cyclic adenosine monophosphate
cDNA: Complementary DNA
CDKN: Cyclin-dependent kinase inhibitor
CDK4: Cyclin-dependent kinase
CD133: Prominin-1
CNS: Central nervous system
CT: Cycle threshold
CTCF: CCCTC-binding factor
CTV: Clinical target volume

D

DDIT4: DNA-damage-inducible transcript four
DMEM: Dulbecco's modified eagle's medium
DNA: Acid deoxyribonucleic

E

ECM: Extracellular matrix
EGFR: Epithelial growth factor receptor
EGLN2: *Egl* nine homolog 2
EGR1: Early growth response 1
EMT: Epithelial-to-mesenchymal transition
EPO: Erythropoietin
ERK: Extracellular signal-regulated kinase
E2F: E2 factor

F

FBS: Fetal bovine serum
FDA: Food and drug administration
F3: Coagulation factor III

G

GABRA1: Gamma-aminobutyric acid receptor
GADP: Glyceraldehyde-three-phosphate
GBM: Glioblastoma
G-CIMP: Glioma CpG island methylator phenotype
GDC: Genomic DNA contamination
gDNA: Genomic DNA
GLUT: Glucose transporter
GSC: Glioblastoma stem cell
GTV: Gross tumour volume

H

HBSS: Hank's balanced salted solution
HDAC1: Histone deacetylase
HIF: Hypoxia inducible factor
HKG: Housekeeping genes
HK2: Hexokinase 2
HMOX1: Heme-oxygenase one
HNF4A: Hepatocyte nuclear factor 4 alpha
HPRT*:* Hypoxanthine phosphoribosyltransferase 1

I

IDH1: Isocitrate dehydrogenase 1
IER2: Immediate early response 2

K

KDM: Lysine histone demethylases
Klf4: Kruppel-like factor 4
KPS: Karnofsky performance scale

L

LDHA: Lactate dehydrogenase A
LOH: Loss of heterozygosity
LOX: Lysil oxidase

M

MAPK: Mitogen-activated protein kinase
MDM2: Mouse double minute 2 homolog
MET: Hepatocyte growth factor receptor
MEK: Methyl ethyl ketone
MGMT: O^6 –methylgunine-DNA methyltransferace
MMP: Matrix metalloproteinase
mRNA: Message acid ribonucleic
MTIC: *5-(3-methyltriazen-1-yl)imidazole-4-carboxamide*
mTOR: Mammalian target of rapamycin
MXI1: Max interactor 1

N

NADPH: Nicotinamide adenine dinucleotide phosphate dehydrogenase
NDRG1: N-myc downstream regulator 1
NEFL: Negative elongation factor
Neurod1: Neurogenic differentiation 1
NF-Kb: Nuclear factor kappa B
NF1: Neurofibromatosis 1
Ngn: Neurogenin
NRES: National research ethics service
NRP: Neuropilin

O

O^2: Oxygen
Oct4: Octamer-binding transcription factor four
ORs: Organs at risk

P

PBS: Phosphate Buffered Saline
PCNA: Proliferating cell nuclear antigen
PDGFR: Platelet-derived growth factor receptors
PDK1: Pyruvate Dehydrogenase Kinase 1
PFKB: *6-phosphofructo-2kinase/fructose-2,six-biphosphate*
PI3K: Phosphatidylinositol-4,5-bisphosphate 3-kinase
PLAU: Plasminogen Activator Urokinase
PLGF: Placenta growth factor
PPC: PCR positive controls
pRB: Phosphorylated retinoblastoma
PTEN: Phosphatase and Tensin Homolog
PTV: Planning target volume
PHD1-3: Prolyl hydroxylases 1-3
P21: Protein 21

R

RIN: RNA Integrity Number
RISC: Recurrence-initiating stem-like cancer
ROS: Reactive Oxygen Species
RNA: Acid Ribonucleic
RTC: Reverse transcription control
RT-PCR: Real-time Reverse-Transcription Polymerase Chain Reaction

S

SDS: Sodium dodecyl sulphate
SDS-PAGE: Sodium dodecyl sulphate poly-acrylamide gel
SERPINE1: Serpin Peptidase Inhibitor Clade E
SOX2: Sex determining region Y-box 2
SYT1: Synaptotagmin-1

T

TBS-T: Tris-buffered saline-tween20
TEMED: N, N', N'-Tetramethylethylenediamine
TET: Ten-Eleven translocation
TFRC: Transferrin receptor
TNFRSF1A: Tumour necrosis factor receptor 1A
tPA: Tissue type-plasmin activator
TP53: Tumour protein 53
TRADD: Tumor necrosis factor receptor type 1-associated death domain

U

uPA: Urokinase type-plasmin activator
uPAR: Urokinase type-plasmin activator receptor
USF2: Upstream transcription factor 2

V

VEGF: Vascular endothelial growth factor
VEGFR: Vascular endothelial growth factor receptor
VHL: Von Hippel-Lindau

W

WHO: World Health Organization
WT: Wild-type

Others:

α-KG: α-Ketoglutarate
2-HG: 2-hydroxyglutarate
1,3BPG: D-1,2-bisphosphoglycerate
ΔΔCT: delta-delta cycle threshold

CHAPTER I

INTRODUCTION

1. Introduction

Glioblastoma (GBM) is the most common form of brain cancer, with its origin in glial cells or neural stem cells from the central nervous system (CNS) (Lombardi & Assem, 2017). Due to its highly invasive and aggressive nature, GBM is classified by the WHO (World Health Organization) as a grade IV Astrocytoma (Gupta & Dwivedi, 2017). Unlike other grade IV malignancies, GBM invasiveness seems to be exclusive to the brain microenvironment. Nevertheless, the destructive influence on brain tissue, and the heterogeneity of the tumour and its associated microenvironment, constitute great obstacles for the efficacy of current therapies (Lombardi M, Assem M, 2017). In fact, within all human tumours, GBM is considered one of the most lethal and difficult to treat (Paolillo, Boselli, & Schinelli, 2018).

The clinical presentation of GBM may vary depending on the location of the tumour. The most common symptoms include increased intracranial pressure, headache and focal or progressive neurologic deficits. Nearly 25% of the patients have seizures as an early event, while at a later stage close to 50% suffer from this symptom (Davis, 2016).

The known risk factors for GBM are ionizing radiation and genetic diseases. Patients that undergo therapeutic radiation for another tumour or condition may be affected in the future by a radiation-induced GBM. Also, there is an increased risk of GBM in patients suffering from genetic diseases such as neurofibromatosis 1 and 2, tuberous sclerosis, Li-Fraumeni syndrome, retinoblastoma and Turcot Syndrome. Approximately 1% of GBM patients are known to have a hereditary disease. Environmental exposures to chemicals such as smoking, pesticides, petroleum refining, etc. may also be correlated to GBM (Davis M, 2016). Electromagnetic fields and nonionizing radiation from cell phones were not proved to lead to GBM development (Davis M, 2016).

GBM incidence is slightly higher in men than women, as well as in Caucasians as compared to other ethnicities. The average incidence rate is 3.2 per 100.000 people. The median survival after surgery and chemotherapy acknowledged by population-based studies is only 14 months (Delgado-López & Corrales-García, 2016;

Davis M, 2016). Even though more common in advanced ages (median 64 years old), GBM may occur at any age. In fact, GBM is the most common pediatric solid tumour. The prognosis in children is slightly better than in adults, due to biological dissimilarities, however it still remains poor (Das K & Kumar R, 2017; Davis M, 2016). Despite all treatment efforts, about 70% of GBM patients experience disease progression within one year of diagnosis and less than 5% (adulthood GBM) and 20% (pediatric GBM) survive five years after the diagnosis. Indeed, second line treatments are basically palliative care in order to optimize life quality (Das & Kumar, 2017; Davis, 2016).

Despite all new diagnostic tools, GBM remains the most deadly type of malignant brain tumour with a very low median survival rate (Monteiro, Hill, Pilkington, & Madureira, 2017). Nowadays, the inability to predict sensitivity or resistance to therapies as well the challenge of achieving an optimal CNS bioavailability lead to an unfortunate scenario for GBM patients (Lombardi M, Assem M, 2017). Studies regarding this disease are imperative in order to improve prophylaxis, early diagnosis, prognosis and treatment prediction to lead to a better outcome. Moreover, understanding the molecular pathways in the core of GBM aggressiveness and swift evolution may be half way towards a paradigm change (Lombardi M, Assem M, 2017).

1.1 Glioblastoma classification

GBM can be assembled into two distinct groups: primary and secondary. Primary GBM, most common (approximately 90% of all cases), develop from a glioma precursor cell without evidences of precursor lesions. On the other hand, secondary GBM is the consequence of a lower-grade glioma (e.g. Grade II astrocytoma) progression. While primary GBM is more common in elderly, secondary GBM manifests preferentially in younger patients. Although histologically similar, primary and secondary GBMs are differentiated by distinct genetic and epigenetic landscapes (Ohgaki & Kleihues, 2013).

1.1.1 Primary Glioblastoma

Primary GBMs are typically characterized by *PTEN* mutations, loss of chromosome 10 and overexpression of the Epithelial Growth Factor receptor (EGFR) (Ohgaki & Kleihues, 2013). Although the loss of heterozygosity (LOH) of chromosome 10q may

be found on both GBM types and linked to loss of PTEN in the secondary tumours, spontaneous mutations of *PTEN* are exclusive of primary GBM (Mansouri, Karamchandani, & Das, 2017). The LOH of chromosome 10 represents by itself a poor molecular prognosis marker. Indeed, this loss can, in some cases, be linked with the *PTEN* inactivation, since this tumour suppressor gene cytogenetic location is 10q23.3, as illustrated on Figure 1.1 (Balesaria et al., 1999).

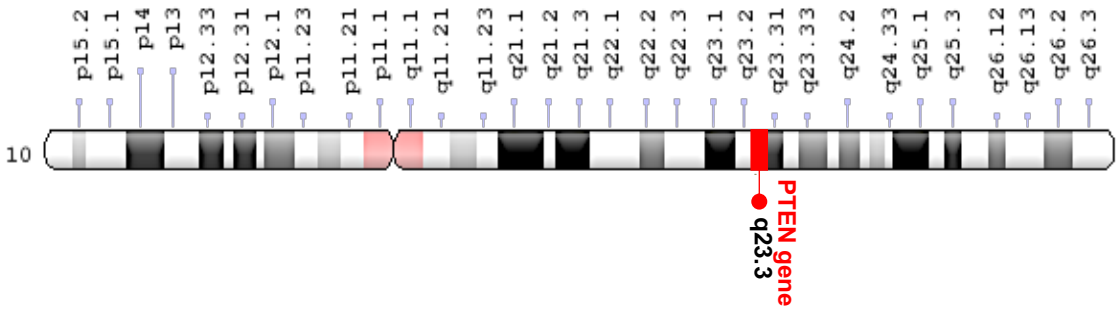

Figure 1.1. PTEN gene cytogenetic location on Chromosome 10. Schematic representation of chromosome 10, highlighting the location of the *PTEN* gene in red. Adapted from https://ghr.nlm.nih.gov/gene/PTEN/location.png

PTEN (Phosphatase and tensin homolog) mutation is believed to be an early event of glioma carcinogenesis (Feng et al., 2016). When lacking this protein, PI3K/AKT/mTOR pathway becomes constitutively activated, leading to an immortal path of uncontrolled growth and survival. PTEN, as the major regulator of this pathway (shown in Figure 1.2), is a key tumour suppressor and as such its inhibition fuels the carcinogenesis process (Chalhoub & Baker, 2009).

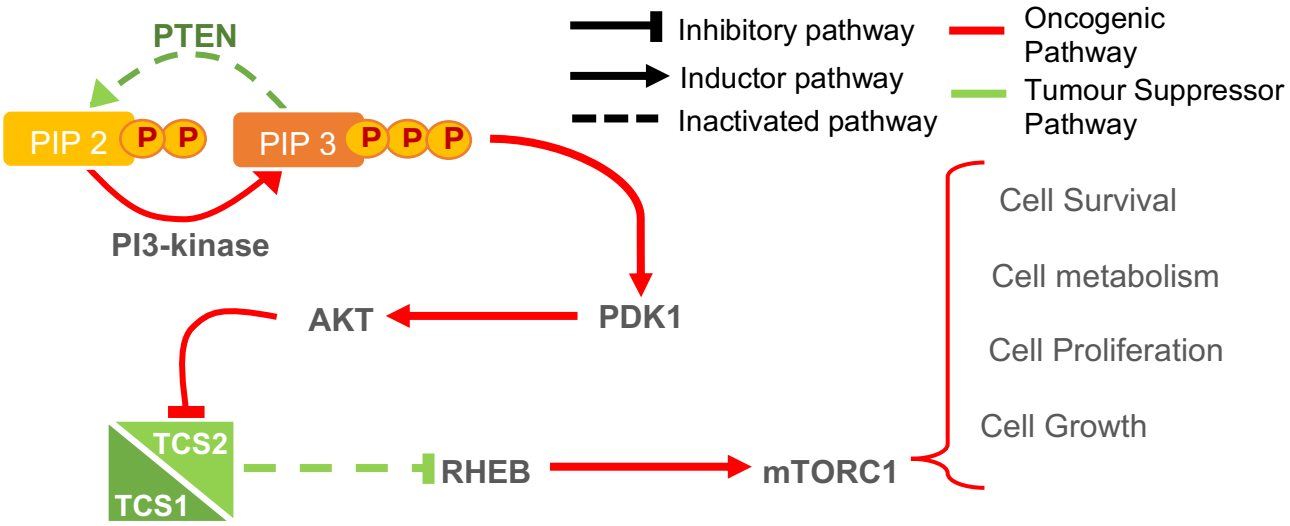

Figure 1.2. PI3K oncogenic pathway, when PTEN is inactivated. When PTEN protein is inactivated PIP3 remains active. This will lead to and over-activation of the mTOR that signals for cell survival, metabolism, proliferation and growth.

Along with *PTEN* loss, the EGFR over-activation is intimately related with cell survival, proliferation and invasion pathways, which constitute imperative hallmarks for cancer progression. Indeed, this protein is overexpressed in ~60% of primary GBMs, featuring a more aggressive phenotype (HONGSHENG et al., 2017). This membrane receptor signals to some of the most important oncogenic pathways, the MAPK/ERK and the PI3K/AKT/mTOR pathways, both illustrated on Figure 1.3.

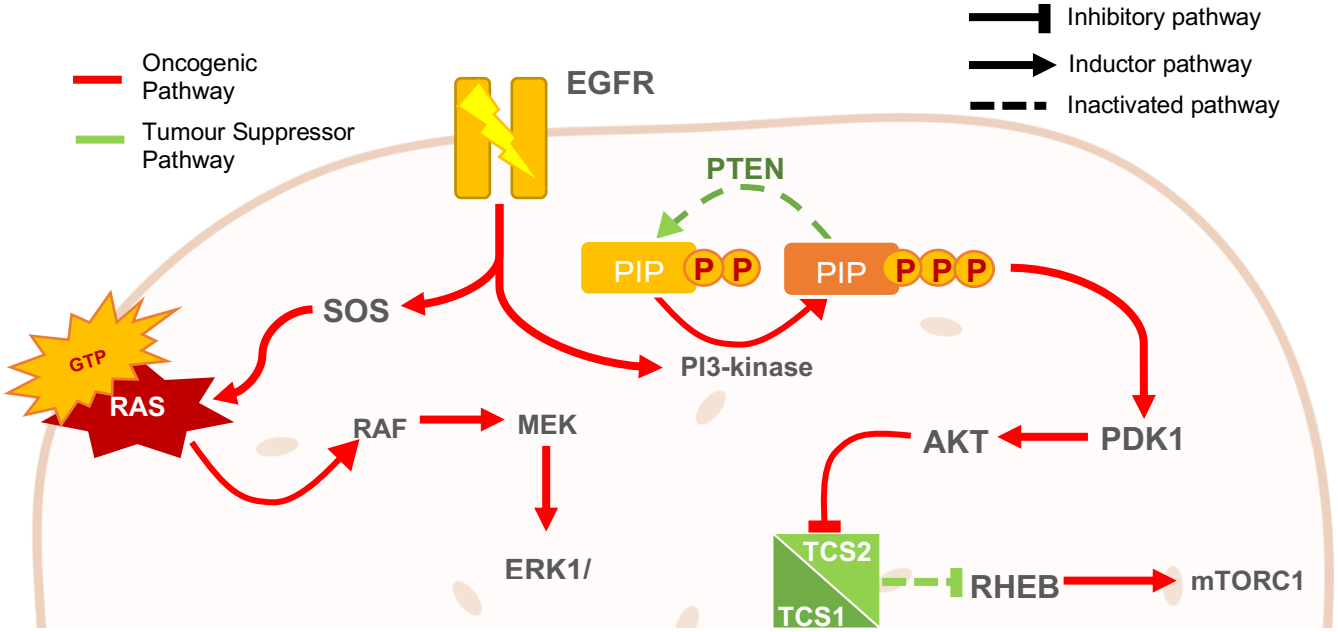

Figure 1.3. EGFR induced signaling pathways. EGFR induces two oncogenic pathways, when mutated, which leads to overactivation of the RAS-RAF-MEK-ERK and AKT-mTOR signaling chains.

Nearly 88% of gliomas develop alterations in the MAPK/ERK pathway, which is translated in a poor survival prognosis. Moreover, this signaling pathway is also known to lead to increased therapy resistance (Pandey, Bhaskara, & Babu, 2016). Additionally, the over-activation of the PI3K/AKT/mTOR pathway is also a poor prognostic marker (X. Li et al., 2016). Not only the lack of *PTEN* contributes for the abnormal PI3K activity, constitutively active EGFR also induces this pathway. In fact, both *EGFR* and *PTEN* mutational events seem to be harbored in a significant number of GBMs as mutually inclusive genetic events (Arif et al., 2015).

1.1.2 Secondary Glioblastoma

Secondary GBM mutational landscapes frequently show *TP53* and *ATRX* loss, chromosomes 1p and 19q co-deletion and Isocitrate dehydrogenase 1 (*IDH1)* mutations. Indeed, *IDH1* mutation is a well-established molecular marker of all secondary GBMs, while *TP53*, *ATRX* mutations and co-deletion of both chromosomes

1p and 19q depend on the type of precursor tumour. *TP53* and *ATRX* loss are mutational marks of an astrocytoma precursor. On the other hand, loss of chromosomes 1p and 19q are typical of oligodendrogliomas (Mansouri, Karamchandani, & Das, 2017). More than a molecular marker, *IDH1* mutations are of great clinical significance since they represent a better prognosis (Cohen A, Holmen S & Colman H, 2013).

Mutations targeting *IDH1* result in the loss of this enzyme normal activity. While in the healthy system, this protein has the catalytic function of producing α-Ketoglutarate (α-KG) and NADPH, in a tumour environment, mutated *IDH1* produces 2-hydroxyglutarate (2-HG) and NADP+, as exhibited in figure 1.4.

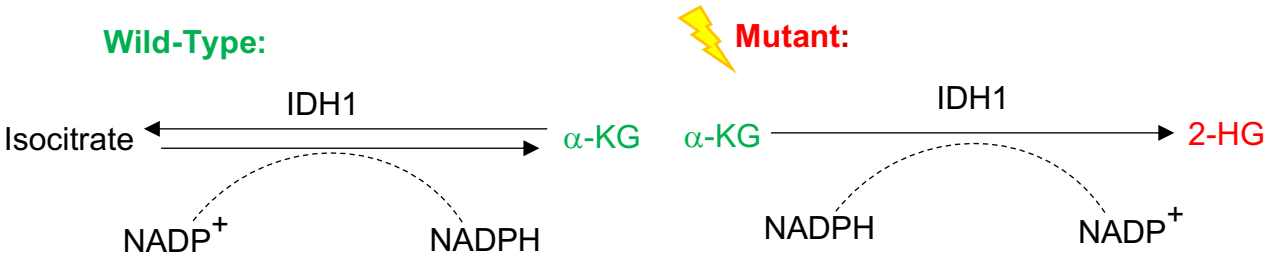

Figure 1.4. Comparison of IDH1 Wild-type (wt) with IDH1 Mutant. The catalytic reaction lead by wt IDH1 has as products NADPH and α-KG. When mutated, $NADP^+$ and 2-HG are the catalytic products.

NADPH is a very important metabolite for proliferation, since it is involved in cellular processes such as defense against oxidative stress, glycolysis and synthesis of fatty acids. However, *IDH1* mutations result in a decrease of NADPH cellular levels as this molecule acts as an electron donor to produce 2-HG. It is not yet clear if the reduced levels of this metabolite is the reason why secondary GBMs have a slower tumour growth rate (Yang, Ye, Guan, & Xiong, 2012). Since NADPH is a critical metabolite for the cellular detoxifying process against Reactive Oxygen Species (ROS), this could also be a possible cause for mutated *IDH1* better prognosis (van Lith et al., 2014).

Similarly, α-KG plays an important role in GBM tumour cell metabolism. As the only structural difference between α-KG and 2-HG molecules is the replacement of the 2-ketone group for a hydroxyl group. This leads to 2-HG acting as a competitive antagonist. This results in the inhibition of many α-KG-dependent dioxygenases, such as lysine histone demethylases (KDMs) and Ten-Eleven Translocation (TET) family of

DNA hydroxylases. In this way high 2-HG concentrations in GBM cells lead to a global DNA hypermethylation phenotype, illustrated in Figure 1.5, altering gene expression and inhibiting differentiation (Maus & Godefridus, 2017).

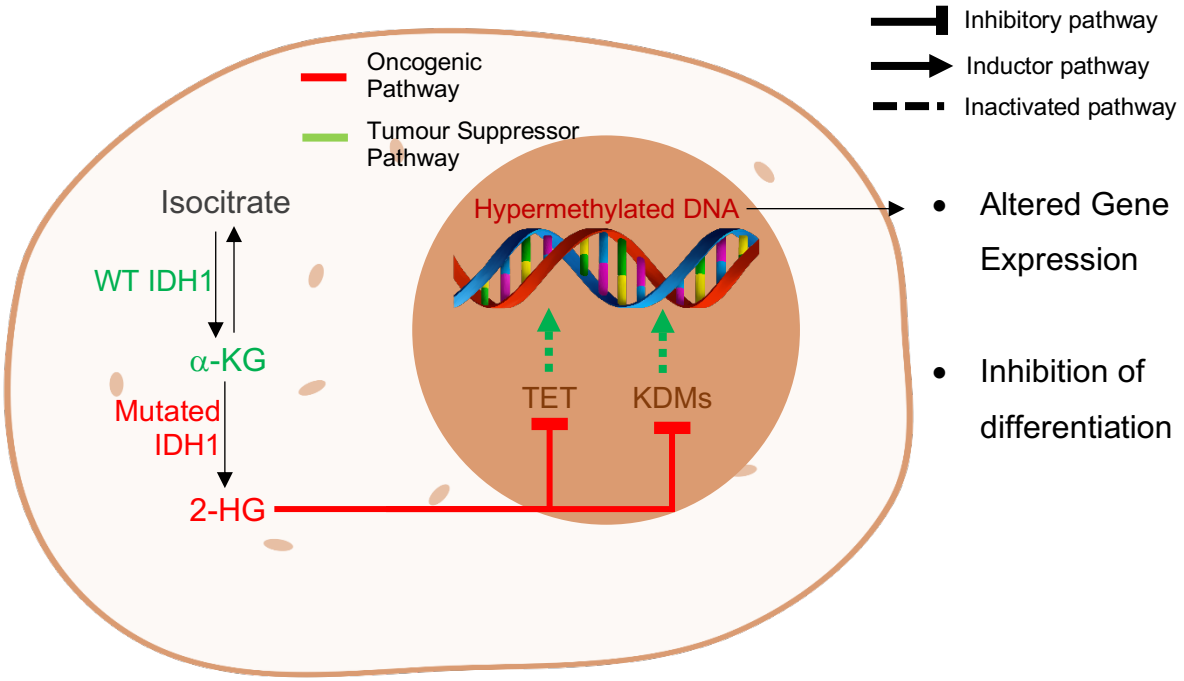

Figure 1.5. Mutated *IDH1* generates 2-HG which by inhibiting TET and KDMs leads to genome hypermethylation. This will result in altered gene expression and inhibition of differentiation.

Although not yet clear how *IDH1* mutations are translated into better outcomes, the hypermethylated phenotype resultant from *IDH1* mutations may be a main reason by affecting the expression of DNA repair proteins (such as MGMTs), leaving cells vulnerable to DNA alkylating therapeutics. Additionally, the fact that mutated *IDH1* lacks the ability to reverse 2-HG or α-KG into Isocitrate, as illustrated in Figure 1.4, may also be related with a better outcome. Isocitrate is a substrate to generate citrate for lipid synthesis, central in cell proliferation and maintenance. Therefore, low levels of citrate may have a great impact on cell survival (van Lith et al., 2014).

Even though IDH1 is a central molecular marker for the identification of secondary GBMs, there are more mutational hints in these tumour landscapes. Not only these hints may characterize a tumour as a secondary GBM, it might even represent evidences of a specific precursor tumour.

Astrocytomas are brain tumours with origin in the star-shaped brain glial cells called astrocytes (Killela et al., 2013). As mentioned before, *TP53* and *ATRX* losses

are both common in astrocytomas. Indeed, the loss of *TP53* is one of the most frequent and earliest mutations in the developing astrocytoma. This early event results of a mutation G:C→A:T on the CpG sites that mostly occur in the hotspot codons 248 and 273 (Ohgaki & Kleihues, 2007). In its wild-type form, TP53 is a transcription factor activated when DNA damage is detected in the cell cycle. Subsequently, this protein is involved in processes such as the regulation of cell cycle arrest and apoptosis, illustrated in Figures 1.6a and 1.6b (Sionov & Haupt, 1999).

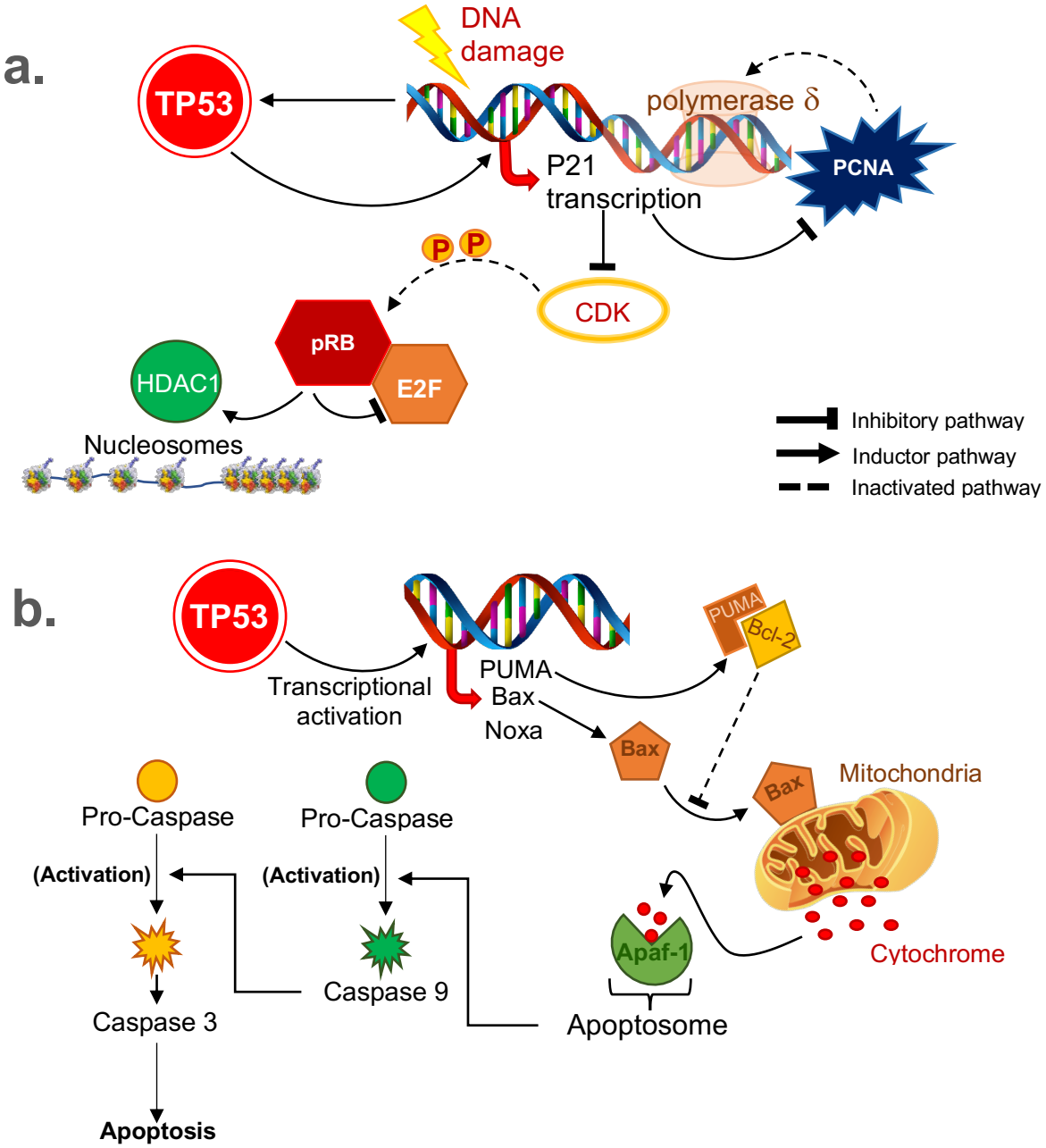

Figure 1.6. TP53 Wild-Type tumour suppressor pathway for: **a. cell cycle arrest** TP53 arrests the cell cycle in the G1 phase by inducing the expression of P21. When inhibiting CDKs via P21, pRB maintains itself in a hypophosphorylated state, sequestering E2F transcription factor. E2F is repressed, as well the transcription of its target genes required for the transition to S phase. Additionally, pRB recruits HDAC1 which promotes the compaction of the nucleosomes to prevent transcription. P21 is

also able to halt cellular growth by preventing PCNA (Proliferating Cell Nuclear Antigen) from activating DNA polymerase δ, central in DNA replication (Sionov & Haupt, 1999); **b. cell apoptosis** TP53 also induce apoptosis if the DNA damage is too extensive or irreversible. Bax releases cytochrome c from the mitochondria, subsequently activating caspase-9 (Haupt S., Berger M., Goldberg Z., & Haupt Y., 2003). PUMA encodes for two proteins: PUMA-α and PUMA-β that bind to Bcl-2 to release cytochrome c and induce cell death in a c/Apaf-1-dependent way (Nakano & Vousden, 2001). When released by Bax and PUMA proteins, cytochrome c binds to the Apoptotic Protease Activating Factor 1 (Apaf-1) forming the Apoptosome. This complex triggers Pro-Caspase 9, turning it into Caspase 9 (activated form), which will in its turn trigger Pro-Caspase 3 (into Caspase 3), finally leading to apoptosis (Ooi & Ma, 2013). Lastly, Noxa has been indicated as functioning through an analogous pathway to Bax (Shibue et al., 2003).

ATRX (alpha-thalassemia/mental retardation X-linked syndrome protein), member of the SN2 family of chromatin-remodeling proteins, has a key role in gene expression regulation. This protein exists in two isoforms which take part in the maintenance of the stability of the genome and chromatin structure at telomeres (Hoelper, Huang, Jain, Patel, & Lewis, 2017; Jones et al., 2017). Although ATRX role in gliomas is not yet fully understood, low expression levels of this protein have been linked with tumours which overexpress genes involved in signal transduction (GTP-related) as well as in transport, modification, and ubiquitination of proteins (Jones et al., 2017). Moreover, tumours with this mutation exhibit lengthening of the telomeres (Hoelper et al., 2017).

It has been shown that *ATRX* and *TP53* loss, alongside with *IDH1* mutations are the 3 oncogenic hits required to arrest astrocytoma stem cells differentiation. This event promotes gliomaneogenesis by maintaining these cells in a perpetual self-renewing and invasive state. *SOX2* was identified as downregulated in tumours harboring these 3-hits. *SOX2* expression depends on the CTCF-dependent chromatin loop to be able to reach its enhancer 700 kb downstream. However, the 3 P53-ATRX-IDH1 hits induce the hypermethylation of the CTCF motifs which flank the *SOX2* locus, meaning that the loop is disrupted, clarified in Figure 1.7 (Modrek et al., 2017).

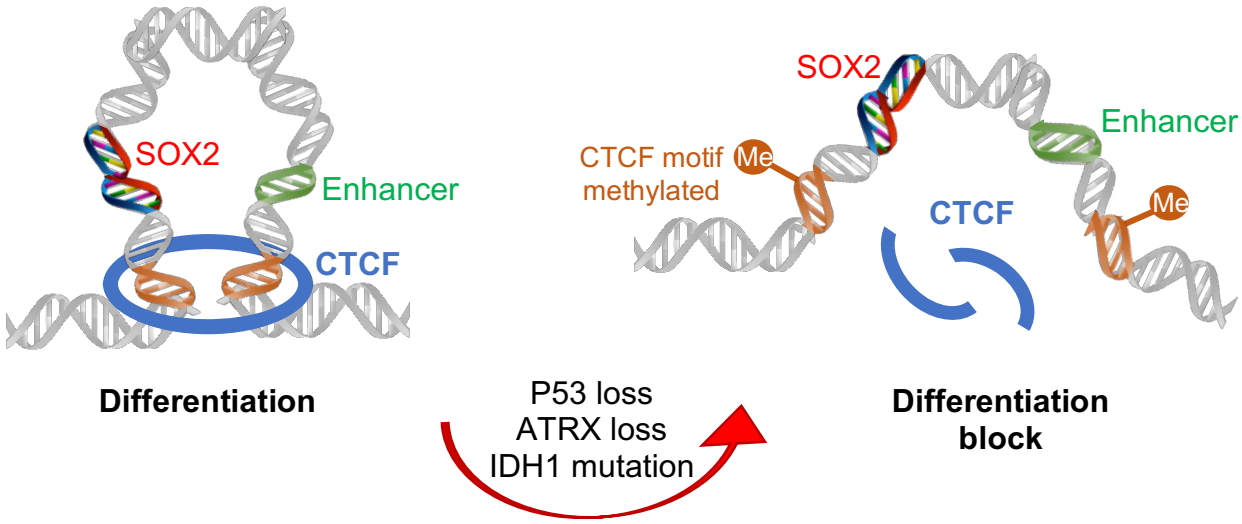

Figure 1.7. The role of the 3-hits theory, which will lead to the maintenance of the pluripotency phenotype by inactivation of CTCF induced chromatin loop and SOX2 enhancer.

Although SOX2 is mainly known for its role in promoting pluripotency, in the brain it may promote the transcription of pro-neurogenic factors such as Neurod1, Ngn1 and Ngn2 (Amador-Arjona et al., 2015). Downregulation of *SOX2* was shown to be concurrent with downregulation of these pro-neurogenic genes, which may explain the differentiation blockage (Modrek et al., 2017).

Secondary GBMs may also evolve from an oligodendrioma precursor. This rare type of glioma (<4%) has origin in the oligodendrocyte cells which give support and insulation to the axons in the CNS. Classically, oligodendrogliomas feature loss of heterozygosity for chromosome arms 1p and 19q as a result from an aberrant translocation *t* (1:19) (q10:p10). This molecular marker, besides its origin identification purpose, is of a high clinical significance since it seems to be associated with sensitivity to chemotherapy and improved outcome (Wesseling, Van Den Bent, & Perry, 2015). Simultaneous loss of 1p and 19q alleles is indeed one of the earliest events in the majority of oligodendrogliomas. Such fact suggests that this genetic modification confers a selective growth advantage to oligodendroglioma cells. However, it is yet unknown which underlying molecular mechanisms are implicated in tumour progression (Reifenberger & Louis, 2003).

1.1.3 Molecular Classification of Glioblastoma Subtypes

Regardless of their primary or secondary origin, GBMs can be categorized into 4 molecular subtypes: classical, mesenchymal, proneural and neural. This molecular classification of GBMs is based in mutational patterns that bear a resemblance with

the expression profiles of their putative cells of origin (Verhaak et al., 2010). Mesenchymal tumours are enriched with both mesenchymal and astroglial signatures. While, proneural tumours have a clear sign of an oligodendrocyte development (Alcantara Llaguno & Parada, 2016). The neural subtype has an alignment of genes which functions are related with the nervous system function and development. On the other hand, similarly to the mesenchymal subtype, classical tumours have stem cell markers (Lombardi & Assem, 2017). Each subtype is associated to a singular molecular signature, indicative of the cell of origin. Yet, the clinical and scientific significance of this categorization relies not in the cell of origin but in the mutational markers of each tumour type that may or not confer a better prognosis and an enhanced therapeutic response. Distinctive mutated molecular pathways may establish advantages or disadvantages in terms of therapy response (Verhaak et al., 2010).

1.1.3.1 Classical

The classical subtype commonly characterized by the amplification of chromosome 7 paired with loss of chromosome 10, features the amplification of *EGFR* and loss of *PTEN* and *CDKN2A* (Lombardi & Assem, 2017; Verhaak et al., 2010).

1.1.3.2 Mesenchymal

Mesenchymal tumours similarly to the classical subtype, harbor the amplification of chromosome 7 and loss of chromosome 10, amplification of *EGFR* and loss of *PTEN*. However, this subtype has the particularity of *NF1* mutations and overexpression of the tumour necrosis factor pathway genes *TRADD*, *RELB* and *TNFRSF1A* (a potential consequence of the high overall necrosis associated with this class) (Lombardi & Assem, 2017; Verhaak et al., 2010).

1.1.3.3. Proneural

In the proneural subtype, both *PDGFRA* and *IDH1* mutations are major features. Although amplification of *PDGFRA* is frequently seen in all GBM classes, the rates of amplification are much higher in proneural tumours. Curiously, in these tumours it seems that *IDH1* and *PDGFRA* mutations are mutually exclusive events, rarely occurring at the same time. Besides these, *TP53* mutations are also common in this GBM sub-type (Verhaak et al., 2010).

1.1.3.4 Neural

In neural tumours, the expression of neuronal markers such as *NEFL*, *GABRA1*, *SYT1* and *SLC12A5* is extremely common (Dunn et al., 2012; Verhaak et al., 2010).

Table 1.1. The 4 molecular classifications of Glioblastomas and their respective prognosis, cell of origin, chromosomal aberration and altered pathways (Verhaak et al., 2010; Lombardi & Assem, 2017). ↑ = amplification; ↓ = Downregulation

	CLASSICAL	MESENCHYMAL	PRONEURAL	NEURAL
Prognosis	Poor	Poor	Good	Good
Cell Origin	Stem cells	Stem cells/Astroglial	Oligodendroglial	Neural
Chromosomal Aberration	↑Chromosome 7 ↓Chromosome 10	↑ Chromosome 7 ↓ Chromosome 10	No chromosomal aberrations	No chromosomal aberrations
Altered pathways	↑EGFR Loss of PTEN and CDKN2	↑EGFR NF-Kb pathway proteins Loss of PTEN ↓NF1	↑ PDGFA or mutation of IDH1 Loss of PT53	↑ NEFL, GABRA1, SYT1 and SLC12A5

This molecular categorization of GBMs fits into the generic primary and secondary classes with different incidence rates, as shown in Figure 1.8. Indeed, primary GBMs may be associated with any of the four subtypes. However, secondary GBMs are exclusively proneural tumours, being this the only class comprehending *IDH1* mutations (Morokoff, Ng, Gogos, & Kaye, 2015).

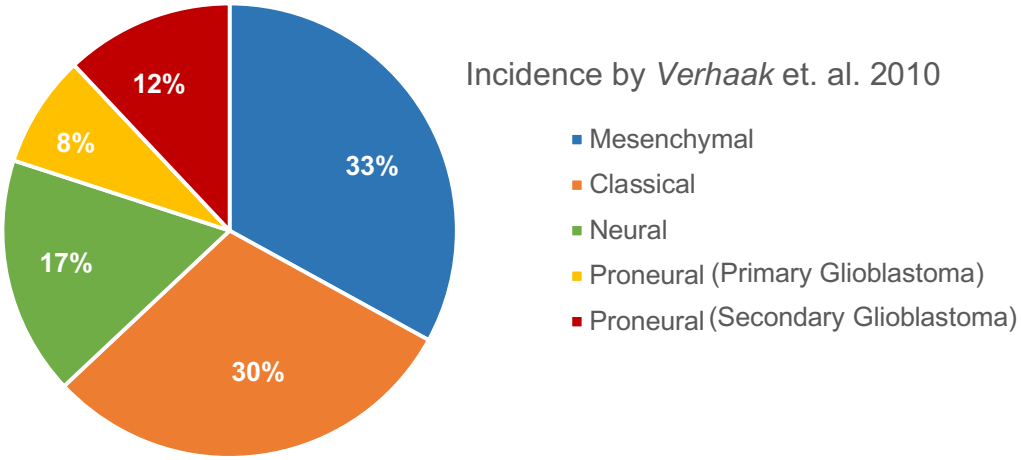

Figure 1.8. The 4 molecular classifications of GBMs, sorted into the primary and secondary categories and their respective incidence by *Verhaak et al.* (adapted from Morokoff, Ng, Gogos, & Kaye, 2015).

Recently, a new cluster of tumours has been documented: G-CIMP+. This molecular subgroup identification is based on the CpG island methylator phenotype existent in several GBMs within the four categories previously mentioned, yet predominant in tumours which harbor *IDH1* mutations (proneural secondary GBMs) (Malta et al., 2017; Mansouri et al., 2017).

Generally, these tumours tend to relate with a better outcome and improved overall survival translated from the effectiveness of chemotherapy. In G-CIMP+ tumours, the MGMT promoter methylation has been established as a favorable prognostic molecular biomarker. Moreover, patients with triple combined G-CIMP+ tumours, which harbor the co-deletion of 1p/19q chromosomes, *IDH* mutations and *MGMT* methylation, have a significantly improved overall survival than those who only carry the *MGMT* methylation biomarker (Malta et al., 2017).

1.2 Therapeutic strategies

Despite all progresses in broad-spectrum cancer therapies development and diagnostic technologies, GBM shows one of the worst prognosis, with a high mortality rate. Currently, maximal surgical resection followed by concomitant radiotherapy and temozolomide chemotherapy is the standard treatment for newly diagnosed tumours. Still, there is no standard of care for recurrent or progressive GBM, despite the numerous clinical trials. Due to the disease heterogeneity (multiple molecular and histological subtypes) and small control groups (low incidence), it is difficult to identify the effectiveness of therapies in trials. Alternative therapies, in these cases, vary within reoperation, re-irradiation, systemic therapies (new chemotherapies, i.e. Bevacizumab) or combined modality therapies (surgery/radiotherapy/chemotherapy) (Fernandes et al., 2017).

1.2.1 Surgery

Surgery is the first therapeutic approach for GBM treatment, aiming to resect maximal tumour mass as possible within safety parameters in order to extract tissue for pathological diagnosis and delay tumour progression. The more extensive the resection is, the longer is the life expectancy. However, the main barrier this method faces is the fine balance between the tumour tissue removal and the preservation of brain functions and healthy tissue. As a matter of fact, surgeries to tumours located

within the eloquent cortex have high risk of postoperative neurological deficits (Fernandes et al., 2017).

Prior to surgery, the candidates are determined as good surgical candidates through the Karnofsky Performance Scale (KPS), shown in table 1.2. Normally, only patients with a KPS index equal or greater to 70 are considered for a surgical intervention. Nonetheless, selected patients with lower indexes may sometimes benefit from surgery, exhibiting improved survival and quality of life after tumour reduction (Young, Jamshidi, Davis, & Sherman, 2015). *Marina et al.* revealed that patients with preoperative KPS lower than 50, indeed improved their KPS status after surgery increasing their survival time and functional grade (Marina et al., 2011; Young et al., 2015). It is essential to understand that the surgical approach may differ between individuals, taking in consideration the localization of the tumour, pre- and postoperative KPS, survival extension and life quality (Young et al., 2015).

Table 1.2. Karnofsky performance status adapted from *Young et al., 2015*

GENERAL RANKING	FUNCTIONAL CRITERIA (%)
Able to carry on normal activity and to work; no special care needed	100%: No Complains; No evidence of disease;
	90%: Able to carry on normal activities; minor signs or symptoms of disease;
	80%: Normal activity with effort; Some signs or symptoms of disease;
Unable to work; able to live at home and care for most personal needs; varying amount of assistance needed	70%: Cares for self; Unable to carry on normal activity or to do active work;
	60%: Requires occasional assistance but is able to care for most personal needs;
	50%: Requires considerable assistance and frequent medical care;
Unable to care for self; requires equivalent of institutional or hospital care; disease may be progressing rapidly	40%: Disabled; Requires special care and assistance;
	30%: Severely disable; hospital admission is indicated although death not imminent;

	20%: Very Sick; Hospital admission necessary; Active supportive treatment necessary;
	10%: Moribund; Fatal processes progressing rapidly;
	0%: Dead.

1.2.2 Radiotherapy

After surgery and previously to radiotherapy, patients are administered with dexamethasone, a corticosteroid, in order to prevent brain swelling. This is particularly important in patients whose tumour exerts were significant. Also, it may prevent radiotherapy associated brain swelling that can worsen the patient's symptoms (Kostaras, Cusano, Kline, Roa, & Easaw, 2014).

Currently, the standard radiotherapy is given in concomitance with chemotherapy and may vary between 5.000-6.000 cGy doses fractionated over 30 days, in order to allow healthy cells of the irradiated zone to recover. Postoperative radiotherapy in these doses has been validated as beneficial in terms of survival advantage. However, dose-escalation beyond these values resulted in increased toxicity without being beneficial in terms of survival (Barani & Larson, 2015).

Notwithstanding the standards and what is considered the ideal dose, how radiotherapy is applied may depend on the age of the patient, tumour size and location. Normally, patients up to 70 years old, with a reasonable KPS status receive standard treatment of 6.000 cGy in fractions of 2 Gy. Whereas 70 years old patients should receive a less aggressive treatment of 4.000 cGy in fractions of 2,66 Gy (Cabrera et al., 2016). As a localized treatment, it is crucial to perform imaging diagnostics of the tumour prior to therapy. This helps define the target volume and localization. There are four important notions that help with the radiotherapy planning concerning the volume and localization, as well as the effectiveness and safety: Gross Tumour Volume (GTV); Clinical Target Volume (CTV); Planning Target Volume (PTV) and Organs at Risk (ORs). The first, GTV refers to the volume to be irradiated which can be seen and imaged (primary tumour). Secondly, the CTV means to target the spreading cells surrounding the primary tumour, which cannot be fully imaged.

Following, the PTV contains the CTV irradiated volume with slightly wider margins to account for possible variations in the beam alignment, patient position, organ motion and deformation. Finally, it is important to consider the volumes to be irradiated, in order to protect the ORs from being targeted with a higher-than-safe dose (Burnet, Thomas, Burton, & Jefferies, 2004).

The side effects of radiotherapy usually start in the first week after initiating treatment and include hair loss, nausea and fatigue ("Side effects of radiotherapy | Brain tumour (primary)," 2015). Although rare, patients may also experience side effects that start months or years after treatment, once the brain tissue damage can reduce the blood supply to certain areas of the brain. This effects may vary between impaired memory, confusion and personality changes ("Long term side effects of radiotherapy | Brain tumour (primary)," 2015).

1.2.3 Chemotherapy

Following surgery adjuvant chemotherapy is given in concomitance with radiotherapy. Despite all lines of treatments GBM prognosis remains one of the poorest within all cancer types. Dysregulation of signaling pathways is widely studied nowadays and therapeutic approaches have been made to target proteins within these pathways. Several oncogenic pathways inhibitors have been tested in pre-clinical and clinical trials for this type of cancer. It is assumed that in the future, combinations of these drugs with cytotoxic chemotherapeutic (p.e. Temozolomide) and radiation could improve the prospective survival of GBM patients. However, cytotoxic chemotherapy remains for the moment the standard treatment as the most advantageous in terms of survival, within all approved drugs (Minniti, Muni, Lanzetta, & Enrici, 2009).

1.2.3.1 Temozolomide

Temozolomide is a cytotoxic alkylating agent reportedly discovered by a mix of "intelligence, guesswork, dogged persistence and luck" in 1970 (Newlands, Stevenst, Wedge, Wheelhouse, & Brock, 1997). This orally administrated drug is non-enzymatically hydrolyzed into *5-(3-methyltriazen-1-yl)imidazole-4-carboxamide* (MTIC) at physiological pH, its active form. MTIC, once activated, alkylates DNA at N^7 position of guanine (most common), O^3 position of adenosine and O^6 position of guanosine (most critical). The methylation of these residues leads to DNA strand

breaks and subsequent cell apoptosis (Temozolomide, DrugBank Database, 2005). The cytotoxic effect of this drug is correlated with the intracellular levels of MGMT. As a critical DNA repair protein, MGMT has the ability to reverse temozolomide's strand-breaking action. High levels of MGMT are associated with temozolomide resistance. On the other hand, MGMT epigenetic silencing (methylation) is correlated with enhanced temozolomide sensitivity, which predicts a good outcome as benefit from this therapy. It has been reported that the 2-year survival rates for patients treated with radiotherapy and temozolomide with no MGMT methylation was 14%, whereas in patients with MGMT silencing, it was 46%. Nevertheless, it has been demonstrated through clinical trials that temozolomide increases significantly survival rates with minimal additional toxicity, when added to radiotherapy. Indeed, the reported 2-year survival rate for radiotherapy and temozolomide in concomitance was 27%, while radiotherapy by itself was only 10% (Minniti et al., 2009).

1.2.3.2 Carmustine

Carmustine is an alkylating agent which cross-links in the DNA and RNA to inhibit its synthesis and translation, respectively (Carmustine, DrugBank Database, 2005). In addition, Carmustine causes oxidative stress by inhibiting glutathione reductase, leading to activation of caspase-3 and apoptosis (Castaldo, Freitas, Conchinha, & Madureira, 2016). Systemic administration of this drug has demonstrated low efficacy in GBM treatment. However, a different method was developed: Carmustine wafers (Gliadel® wafers). This new method consists in a controlled release of carmustine from biodegradable polymer wafers that are placed in the cavity left by the surgical removal of the brain tumour. This approach not only reduced systemic toxicity, but it also increased the effectiveness of the therapy (Lin & Kleinberg, 2008). Carmustine wafers are approved to treat newly-diagnosed and recurrent GBM as an adjuvant treatment, alone or in combination with temozolomide, when surgical removal of the tumour is possible. Trials have not yet been conducted in order to compare carmustine wafers treatment to temozolomide, as single therapies. Despite the therapeutic benefits of this approach, risks associated with this treatment should not be disregarded. Cerebral edema, healing abnormalities, intracranial infections, seizures, intracranial hypertension and cerebrospinal fluid leaks are among the side effects that may be experienced by the patients who undergo this treatment and should be taken into consideration when prescribing it (Chowdhary,

Ryken, & Newton, 2015). Plus, combination of carmustine wafers with the standard treatment may carry the risk of increased secondary events and might not significantly improve the outcome (De Bonis et al., 2012).

1.2.3.3 Targeted therapies

As mentioned above, GBM is characterized by aberrant activation of signaling pathways that lead to tumour progression. Inhibitors for growth factor receptors and pathways such as MAPK/ERK and PI3K/mTOR or cell cycle control were developed and could be adapted as GBM adjuvant therapies, as shown on Table 1.3 (Touat, Idbaih, Sanson, Ligon, & Ligon, 2017).

Table 1.3. Genomic alterations and example of targeted therapies, adapted from *Touat et al.*, *2017*

GENE	ALTERATION	CANDIDATE THERAPY
	Growth Factor Receptors:	
EGFR	Amplification	Rindopepimut (EGFRvIIi-specific peptide conjugated)
PDGFR	Amplification	Dasatinib (PDGFR inhibitor)
	MAPK and PI3K/mTOR pathways:	
PTEN	Delection	Voxtalisib (mTOR/PI3K inhibitor)
PIK3CA	Amplification	Buparlisib (PI3K inhibitor)
BRAF	Mutation (phosphomimic)	Trametinib (MEK inhibitor) or Vemurafenib (BRAF inhibitor)
	Cell Cycle pathways:	
MDM2	Amplification	AMG232 (MDM2 inhibitor)
CDK4/6	Amplification	Ribociclib (CDK4/6 inhibitor)
	Others:	
IDH1	Mutation	AG120 (IDH1 inhibitors)

In addition to these target pathways, in 2009 the Food and Drug Administration (FDA) approved provisionally an anti-angiogenic target drug called Bevacizumab for recurrent GBM treatment (Touat et al., 2017). Angiogenesis, the process of blood vessels growth from the existing vasculature, is a major hallmark of carcinogenesis and a very important feature in GBM invasion. Vascular Endothelial Growth Factor (VEGF) promotes proliferation and migration of vascular endothelial cells, as well as vascular permeability. It is consequently the main player of the angiogenic process. Bevacizumab is a monoclonal antibody that targets VEGF-A to inhibit its assembly with the respective receptor and so inhibits tumour vascularization (Keating, 2014).

Although it failed to prolong overall survival in newly diagnosed GBM and first recurrence, it is frequently used as a last-line treatment following temozolomide, carmustine and radiotherapy failure (K. J. Wenger et al., 2017).

1.2.3.4 Therapy resistance

GBM remains a therapeutic challenge being extremely difficult to prevent recurrence. Tumour regrowth typically occurs around the surgical cavity due to the failure of standard and targeted therapies, which do not comprise tumour heterogeneity. GBM cell subgroups are characterized by divergent expression profiles and genetic/epigenetic landscapes, derivative of differences in cell of origin and accumulation of mutations (Osuka & Meir, 2017). The clonal evolution theory states that cancers develop through a process of clonal expansion and selection in which tumours adapt to the surrounding environment. This leads to genetic diversification within the tumour architecture as shown in Figure 1.9 (Greaves & Maley, 2012).

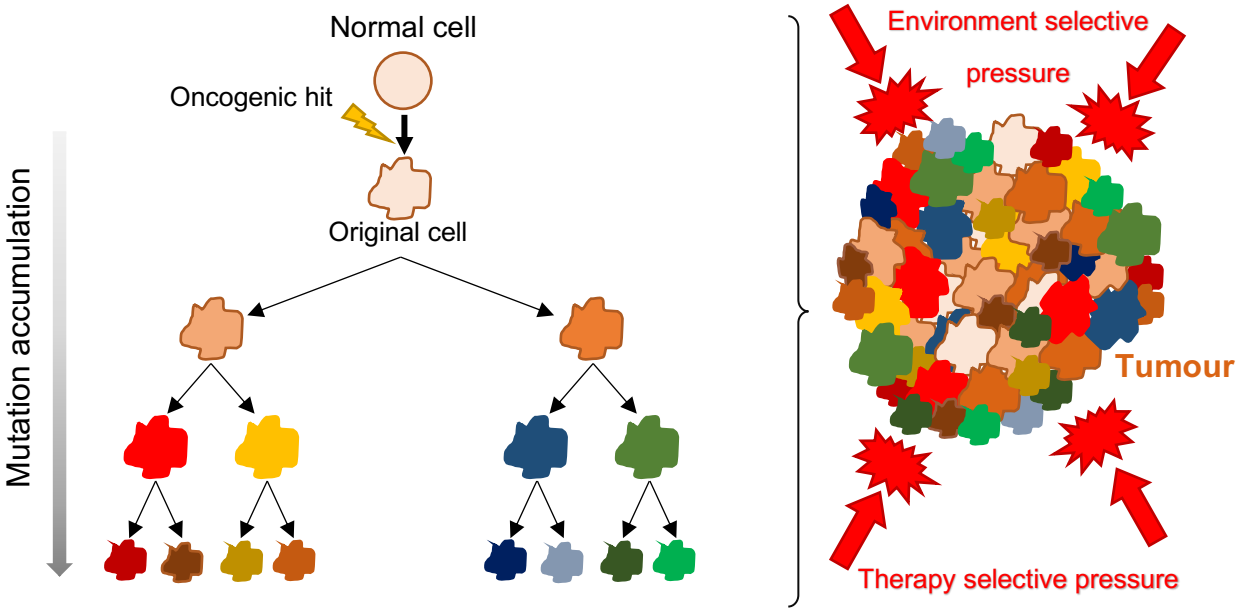

Figure 1.9. Clonal evolution theory: The clonal expansion leads to cell populations with different mutational landscapes (different colors) and different levels of mutational accumulation. Also, the tumour environment and external factors (therapy) contribute for the intratumoral heterogeneity.

Multiple study findings have shown that the higher the tumour heterogeneity levels, the lower the response of the patients to anticancer therapies (Dagogo-Jack & Shaw, 2017). Some of the tumour cell clones may evade from therapies due to their own 'resistant' genomic landscape. Indeed, drugs and radiation may artificially select resistant cell variants with increased malignant potential (Greaves & Maley, 2012). It has been further hypothesized that selection of resistant clones might occur through

surgery resection. Non-resected GBM cell populations with stem-like properties that through innate and adaptive resistance survive to treatments, repopulate the primary tumour site. These resistant cells will then initiate recurrence turning into recurrence-initiating stem-like cancer (RISC) cells (Osuka & Meir, 2017).

Besides external factors, some environmental features may also interfere with selection, introducing the surrounding cells with selection forces that lead to clonal assortment (Osuka & Meir, 2017). GBM is characterized by quite diverse histological hallmarks. These tumours are organized in specific niches with different features and functions within the tumour microenvironment. Three specific tumour niches have been identified as the most prominent for GBM regulation: The perivascular, vascular-invasive and hypoxic niches (Hambardzumyan & Bergers, 2015). The first refers to the tumours stem cell nest, where both tumour growth and differentiation are assured. In the vascular-invasive region, cells endorse tumour spreading into the brain parenchyma by promoting angiogenesis (Hambardzumyan & Bergers, 2015). Finally, the hypoxic niche, surrounds the necrotic core and its main feature is the low levels of oxygenation which derive from the absence of vasculature. This last precinct might be the most influential environment in terms of invasion and tumour spreading. Consequently, these cells activate mechanisms to evade from the hypoxic site and invade into brain's healthy tissue (Monteiro et al., 2017). In fact, these cells acquire such an invasive and migratory phenotype that the hypoxic field surroundings is characterized by palisading tumour cells, a well-known morphological hallmark of GBM (Hambardzumyan & Bergers, 2015). This feature constitutes a poor prognosis predictor and challenge in terms of therapy, however hypoxia may defy treatments through other individualities. Several studies have shown that hypoxia promotes stemness by increasing expression of cancer stem cell markers such as CD133, Sox2, Oct4, nestin and Klf4 (Hambardzumyan & Bergers, 2015). This may lead to recurrence through RISC cells as already reviewed (Osuka & Meir, 2017). Furthermore, it is also known that hypoxia constitutes a barrier to radiotherapy efficacy. Oxygen improves cancer cells sensitivity to irradiation and so, the effectiveness of radiotherapy. In oxygen privation, cells may survive to therapy to initiate recurrence later (Brown, 1999).

1.3 Hypoxia in Glioblastoma

As mentioned above, some tumour cells are exposed to hypoxic conditions, meaning that the cells demand of oxygen exceeds the supply. This is a natural consequence of tumour growth and expansion which leaves cells near the core distant from the oxygen supplier blood vessels. In such a critical environment, hypoxic cells activate pro-survival mechanisms such as metabolic changes, invasion pathways and tumour vascularization signaling. In order to do so, there is a family of transcription factors that play the most fundamental role in this hypoxic response: the Hypoxia inducible factors (HIFs). (Monteiro et al., 2017)

1.3.1 Hypoxia Inducible Factors

HIF transcription factors are, without a doubt, the master regulators of the hypoxia response. These transcription factors are heterodimeric complexes constituted by O_2 regulated α subunits (HIF1α, HIF2α and HIF3α) and the constitutively expressed β subunit (HIF1β). Within the complex, the α subunits are the determinant elements for these transcription factors action. HIF1α and HIF2α are considered the main regulators of the hypoxic response (Monteiro et al., 2017).

When the oxygen levels are normal, prolyl hydroxylases 1-3 (PHD1-3) hydroxylate two prolyl residues within the HIFα subunits allowing the binding of the von Hippel-Lindau (VHL) protein. This way, VHL protein recruits E3 ubiquitin ligases to target HIFα for proteasomal degradation, illustrated in Figure 1.10. However, in a hypoxic environment PHDs are inhibited which leads to the stabilization of the HIFα subunits. HIFα translocate into the nucleus to bind with HIF1β, forming the transcription factor complex which subsequently binds to co-activators and promoters of target genes orchestrating the response to hypoxia, Figure 1.10. Although both activated by a hypoxic setting, HIF1α and HIF2α are differentially expressed. While HIF1α is ubiquitously expressed, HIF2α is selectively expressed in distinct cell populations and both play different roles in tumorigenesis, having overlapping as well as distinct target genes (Monteiro et al., 2017).

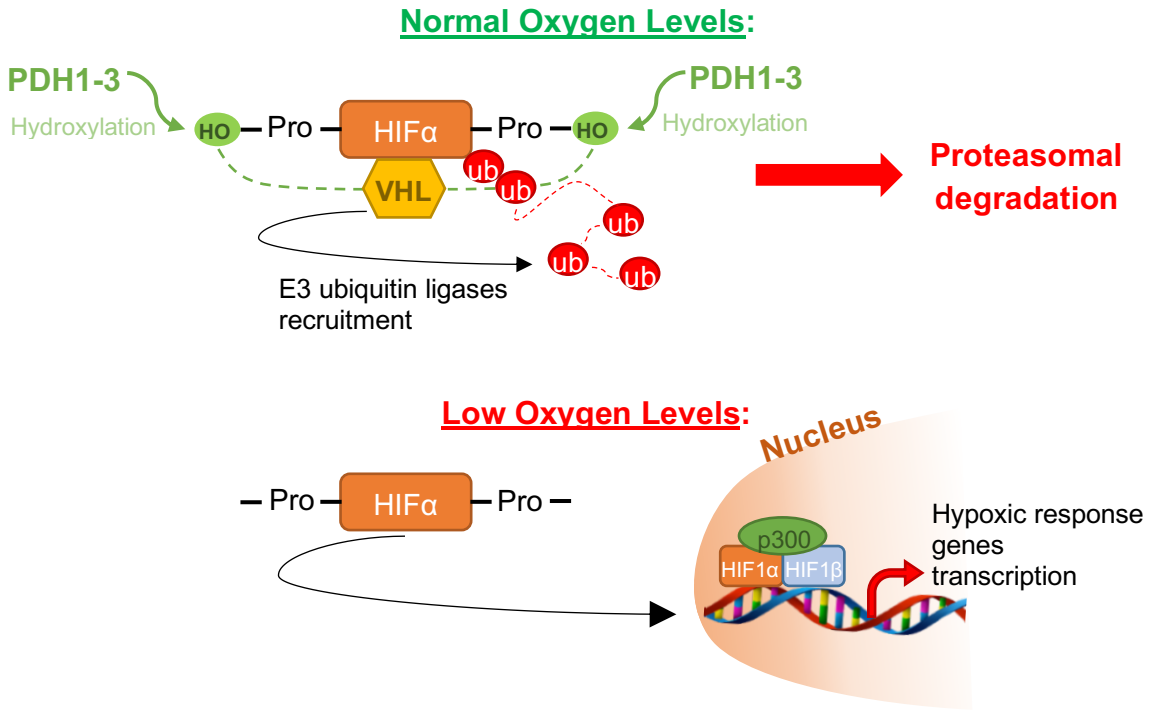

Figure 1.10. HIFα regulation in normoxia: Hydroxylation of HIF1α's proline residues promotes VHL anchorage, which will target HIF1α for proteasomal degradation; and in hypoxic conditions: HIF1α promotes gene transcription.

When hypoxia-triggered, HIF will induce the transcription of hundreds of genes that promote survival mechanisms, angiogenesis, metabolic reprogramming (glycolysis), invasion and metastasis. Hence, identifying and characterizing hypoxia upregulated pathways in GBM is crucial for the development of novel and more effective therapies against this deadly type of tumour (Monteiro et al., 2017).

1.3.2 Angiogenesis

Angiogenesis is the physiological feature in which new blood vessels are developed from pre-existing vessels. Angiogenesis is a well-organized and common event in adults (in the menstrual cycle and tissue repair/remodeling), as well in the embryonic and fetal development (Kaur, Tan, Brat, & Van meir, 2004). However, it is also a very important process for tumour survival and invasion since blood vessels are the cells suppliers of oxygen and nutrients (Keating, 2014). GBM is known to be among the most vascularized tumours and frequently depicted by microvascular hyperplasia (micro-aggregates of endothelial cells). In fact, the hyperbolic form of micro-aggregates, called glomeruloid body, is frequently reported in GBM (Kaur et al., 2004). It is not yet clear if this is a result of a dysfunctional cell proliferation or an

accelerated angiogenesis process, yet it is known to be the result of pro-angiogenic factors deregulation (Kaur et al., 2004).

During hypoxia, cells turn on the angiogenic switch by up-regulating the pro-angiogenic factors such as VEGF proteins, via HIF1α and HIF2α (Keating, 2014; Liao & Johnson, 2007). VEGFA is a potent angiogenic factor that appears to be particularly important for GBM, since its over-expression and release into the extracellular matrix (ECM) is commonly observed (Liang et al., 2002). In addition to the transcriptional regulation, hypoxia seems to result in increased stability of VEGFA mRNA. Both mechanisms result in a thriving of VEGF signal which is particularly predominant in the hypoxic zone (Kaur et al., 2004). When secreted by cells, VEGFA triggers angiogenesis by binding to the VEGF receptors 1 (VEGFR1) and 2 (VEGFR2) on the endothelial cell surface. These receptors will then signal for endothelial cell proliferation and migration, as well for the secretion of matrix metalloproteinases (MMPs) (Rundhaug, 2003). Besides these, the receptors neuropilin 1 (NRP1) and 2 (NRP2) expressed in neural and endothelial cells surface also play a role in angiogenesis (Kaur et al., 2004). Although not yet well-defined what is the role in angiogenesis, mice with targeted disruption of these receptors show severe vascular defects. Plus, it is known that NRP1 functions as a receptor for a specific isoform of VEGFA (VEGF 165), for VEGFB and PLGF, also pro-angiogenic factors (Kaur et al., 2004).

During hypoxia the VEGFC and VEGFD isoforms bind to the VEGFR3 receptor and are mostly involved in the formation and maintenance of lymphatic vessels, known as the lymphangiogenesis process (Chien et al., 2009; Christiansen & Detmar, 2011). Despite this process being inexistent in the brain, it has been hypothesized that VEGFC and VEGFD cleavage forms can interact with VEGFR2 and promote angiogenesis (Jenny et al., 2006). However, little is known about these two VEGF isoforms in GBM's hypoxia driven invasion.

The *placenta growth factor* (*PLGF*) is a frequently up-regulated gene in hypervascularized brain tumours, and its over-expression leads to tumour angiogenesis and growth (Kaur et al., 2004). Hence it is a pro-angiogenic protein that curiously shares 53% identity with VEGF. It has been shown that in the presence of

PLGF, VEGFA is released from VEGFR1 to bind VEGFR2, promoting endothelial cell proliferation. Plus, the activation of VEGFR1 by PLGF leads to inter-molecular trans-phosphorylation of VEGFR2. PLGF functions as an enhancing factor of VEGFA signal in GBM (Kaur et al., 2004).

1.3.3 Metabolic reprogramming

The most important feature in cancer cells metabolic reprogramming is the shift from aerobic respiration to anaerobic glycolysis. This reprogrammed mechanism allows the use of glucose to synthesize ATP without the need for oxidative phosphorylation. Besides being more time-effective and least energetically demanding than oxidative phosphorylation anaerobic glycolysis has the bonus of generating 'building-blocks' (nucleotides, lipids, etc.) and it is independent of oxygen levels which can vary dramatically during tumour growth. HIF activates the transcription of genes that encode for glucose-transporters and glycolytic enzymes, in order to maintain the cells energetic balance in an oxygen deprived environment (Labak et al., 2016a; Liberti & Locasale, 2016).

HIF1α activates the transcription of *GLUT1*, *GLUT3* and *GLUT4* genes, which encode for glucose-transporters. These are plasma-membrane proteins that promote the entry of glucose from the extracellular environment into the cell. GLUT1 and GLUT3 proteins are significantly up-regulated in glioma cells, since a large amount of glucose is needed to fulfil the high metabolic demands of these cancer cells (Zhang, Behrooz, & Ismail-Beigi, 1999).

Curiously, GLUT1 is either overexpressed or under-expressed in GBM, depending on the tumour area. Regularly, the overexpression zone correspond to the hypoxic foci, where HIF1α expression is highly predominant. In fact, GLUT1 is an established transcript target of HIF1α transcription factor. In addition to GLUT1, GLUT3 seems to have a role in GBM. First, GLUT3 is characterized as a brain tissue specific transporter, frequently found in neurons. Also, GLUT3 was shown to be over-expressed in hypoxic GBM cells and to correlate with clinical outcomes. Although not yet proven, some studies suggest a positive feedback loop between GLUT3 and OCT4 (a pluripotency marker), once their expressions are correlated (Labak et al., 2016).

Many glycolytic enzymes have been shown to be up-regulated during tumour hypoxia. Aldolase-A catalyzes the conversion of Fructose-1-6-bisphosphate into glyceraldehyde 3-phosphate. HIF1α activates the transcription of *aldolase-A* gene in response to hypoxia (Semenza et al., 1996). This protein is overexpressed in cancer cells not only for its importance in glycolysis, but also for being involved in vesicle trafficking, cell motility and epithelial to mesenchymal transition (EMT). In fact, aldolase A expression has been correlated with increased fibronectin and vimentin levels, as well as with down-regulation of E-cadherine and β-catenin levels (Lincet & Icard, 2015).

Lactate dehydrogenase A (LDHA) is a tetrameric enzyme which catalyzes the conversion of NADH to NAD+ and pyruvate to lactate. One of the key steps of glycolysis is the conversion of GADP to D-1,3-bisphosphoglycerate (1,3BPG) and NAD+ (LDH enzymatic product) is a fundamental participant of this process. In hypoxic conditions, due to the lack of oxidative phosphorylation which would otherwise regenerate NAD+, LDH enzymatic function is essential. Hence its significance in glycogenesis (Firth, Ebert, & Ratcliffe, 1995). LDHA synthesis has been shown to be upregulated in GBM tumour cells, especially in pseudopalisading cells and throughout the hypoxic area (Talasila et al., 2016).

Another mediator of glycolysis metabolism in cancer is Hexokinase 2 (HK2). This protein functions as a molecular switch from glycolysis to autophagy, in order to ensure the energy homeostasis in response to glucose deprivation (Tan & Miyamoto, 2015). In the healthy brain, HK2 is negligently expressed. However, in GBM there are several transcription and growth factors, such as myc, glucagon and cAMP, that regulate HK2 expression. Moreover HIF1α regulates the transcription of HK2 in GBM hypoxia cells (Wolf et al., 2011).

PFKB3 and PFKB4 are two isoenzymes from the PFK-2/FBPase-2 family which control the levels of fructose-2,6-biphosphate (Fru-2,6-P2). Both PFKB3 and PFKB4 are known to be upregulated by HIF1α during hypoxia and to promote cell survival through metabolic adaptation to this demanding environment (Ros & Schulze, 2013). In fact, PFKFB3 was suggested as the isoform that most likely contributes to the

glycolytic activity of cancer transformed cells. However, in GBM, PFKFB4 has been shown to play a main role in glycolysis (Ros & Schulze, 2013).

The SLC16A3 protein (also known as MCT4) has been shown as one of the most upregulated genes in GBM HSR-GBM1 and JHH-GBM10 hypoxic cell lines (Lim et al., 2014). This protein is a well-known lactate exporter and was hypothesized as a regulator of proliferation, survival and growth in GBM. In fact, knock down of MCT4 led to inhibition of proliferation, induction of apoptosis and suppression of HIF transcriptional activity. Associated with a poor prognosis and short survival, SLC16A3 seems to be correlated with a lower G-CIMP (methylation phenotype) typical in the most aggressive types of glioma (Lim et al., 2014).

1.3.4 Invasion

In order for tumour cells to be able to invade the surrounding environment they need to go through epithelial to mesenchymal transition (EMT) and promote extracellular matrix (ECM) degradation and remodeling. EMT is a feature of epithelial origin tumour cells in which the epithelial phenotype is lost in order to acquire a mesenchymal phenotype. Cells down regulate cell-cell adhesion molecules and lose polarity, leading to increased migration (Gialeli, Theocharis, & Karamanos, 2011). Naturally, to allow hypoxic cells to evade from the primary tumour site and invade other sites of the brain, HIF1α targets the transcription of genes involved in these steps (Martin, Ye, Sanders, Lane, & Jiang, 2013).

The plasmin system in cancer has been widely studied. There are two known forms of plasmin activators (PA): the urokinase type-PA (uPA) and the tissue PA (tPA). Both promote the enzymatic conversion of plasminogen into the active serine protease, plasmin (Zhai et al., 2011a). Capable of promoting the ECM degradation in a direct manner, plasmin has a key role in GBM invasion (Zhai et al., 2011a).

The plasminogen receptor annexin A2-S100A10 heterotetramer (AIIt) plays a key role in the regulation of plasmin at the cell surface. This complex is formed by a dimer of the S100A10 protein (also known as p11) which binds together two molecules of annexin A2 (or p36) (P. A. Madureira et al., 2011). When S100A10 is not bound in the AIIt, it is targeted for degradation via a proteasome-dependent mechanism.

However, when in the AIIt, S100A10 promotes the binding of plasminogen to the complex, increasing its affinity with tPA, as well the catalytic reaction efficiency (Patricia A Madureira, O'connell, Surette, Miller, & Waisman, 2012). Indeed, S100A10 activity has been linked to 50% of cellular plasmin generation (Patricia A Madureira et al., 2012). Plus, S100A10 expression is widely induced by several factors known to be overactivated in GBM, such as EGFR (Madureira P, O'Connell P, Surette A, et. al. 2012).

Studies have shown that annexin A2 knockdown leads to a decrease in the migration ability of GBM cells. Curiously, annexin A2 was reported as significantly more expressed in primary GBMs than in secondary tumours. This is due to a higher tumour methylation phenotype of secondary GBMs in which annexin A2 promotor is generally methylated, therefore inactivated (Kling et al., 2016). Consequently, annexin A2 expression often correlates with tumour grade. Indeed, patients with higher annexin A2 expression have a lower Overall Survival and Progression Free Survival than those with a lower expression (Maule et al., 2016). Due to its role in cancer, annexin A2 has become a protein of interest for GBM target therapy (Zhai et al., 2011). Overall, the AIIt heterotetramer leads to an increase in plasmin generation and therefore contributes to the breakdown of the basement membrane and ECM, crucial for tumour invasion (Madureira P, O'Connell P, Surette A, et. al. 2012).

Another plasminogen activation complex is the uPA system. When uPA binds to its receptor, the urokinase-type plasminogen receptor (uPAR), not only increases its enzymatic activity, but it also promotes a focal and directional proteolysis of the ECM. It is no surprise that uPARs are frequently co-localized with the hypoxic site (Mohanam et al., 1997). This system, often overexpressed in GBM, plays therefore an extremely important role in hypoxia induced invasion. In addition, the uPA-uPAR system also regulates cell motility, adhesion and proliferation, also crucial invasion steps (Chandrasekar et al., 2003). Interestingly, the uPA-uPAR complex co-localizes with S100A10 at the cell surface (Madureira P, O'Connell P, Surette A, et. al. 2012).

In addition to the direct breakdown of fibronectin, laminin and proteoglycans (ECM components), plasmin is also capable of activating MMPs which contribute to ECM degradation as well (Zhai et al., 2011a). MMPs are overexpressed in cancer

which leads to ECM remodeling, tumour invasion and metastasis and epithelial-mesenchymal transition (EMT) by modification of integrins (Radisky & Radisky, 2010). In GBM cells the MMP-2 and MMP-9 gelatinases, are frequently over-expressed and released into the ECM (Fujiwara et al., 2007). A unique feature of these gelatinases is the degradation of type IV collagen, gelatin and fibronectin which are major components of the ECM (Cathcart Jillian, Pulkoski-Gross Ashleigh, & Cao Jian, 2015). Studies led by *Li et. al.* have shown that via knockdown of HIF2-α, a decrease in MMP-2 expression was observed (N. Li, Wang, Zhang, & Zhao, 2016). In addition, MMPs 2 and 9 were both shown to be enhanced during hypoxia in GBM (Emara & Allalunis-Turner, 2014). Although known to be related with hypoxia, there are no references of gelatinases 2 and 9 expression by HIF1α.

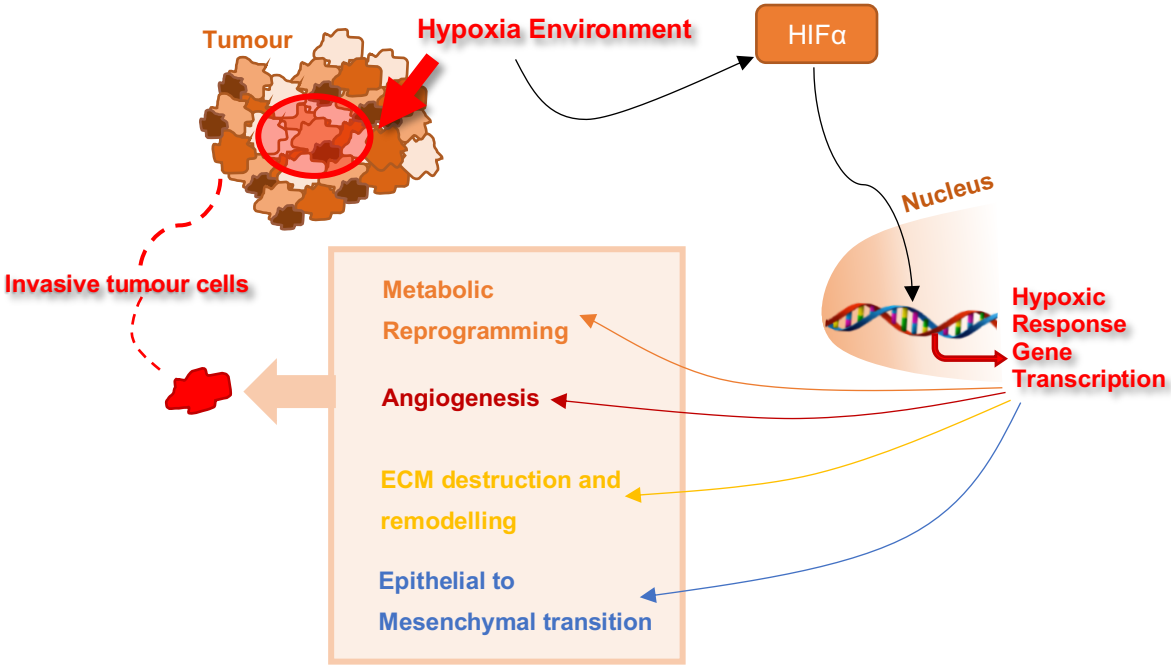

Figure 1.11. Hypoxia mediated invasion in Glioblastoma: HIF1α targets gene transcription to induce metabolic reprograming, angiogenesis, ECM destruction and remodeling and epithelial to mesenchymal transition.

During hypoxia, angiogenesis, metabolic reprogramming and invasion pathways cope as cell survival mechanisms in response to a "life-threatening" environment, as illustrated in Figure 1.11. By doing this, hypoxic GBM cells not only survive, but gain clonal advantage through an increased malignancy phenotype. These cells are prompt to migrate to other parts of the brain and colonize healthy tissue, which creates a therapeutic challenge. In conclusion, hypoxia benefits cancer

progression by activating malignancy pathways, which reflects into a bad prognosis in terms of treatment and patient survival. (Monteiro et al., 2017)

1.4 Study Objective

Glioblastoma multiforme is one of the deadliest, with a median survival of 14 months. GBM remains a therapeutic challenge due to these tumours aggressive phenotype and high rates of recurrence. Hence, it is essential to understand the molecular pathways in the core of GBM evolution.

One of the main features of GBM is hypoxia. Close to the tumour necrotic core, the hypoxic zone is characterized by low levels of oxygen. This harsh environment not only prompt cells with clonal selection forces, it activates pro-survival and malignancy mechanisms such as the metabolic switch, invasion and angiogenesis. Hence we proposed to investigate the expression of genes and proteins featuring these survival mechanisms in GBM hypoxia.

To do so, two GBM biopsy-derived cell lines (UP-029 and SEBTA-023) were used and cultured in hypoxic conditions for a selected set of time-points. We then investigated the hypoxic profile and landscape of these cells through microarrays performed for normoxia, six and 48 hypoxia hours of samples. We distinguished a panel of significant induction and validated through qRT-PCR assays. Lastly, we conducted protein detection assays and correlated with the previously obtained gene expression values.

CHAPTER II

MATERIALS AND METHODS

2. Materials and Methods

2.1 Ethical Statement

The patients' biopsies from which the cell lines used in this study were derived were obtained under the ethics permission within the Brain Tumour Research Centre, University of Portsmouth in compliance with the National Research Ethics Service (NRES). In addition, patients have concurred prior to surgery, to the use of biopsy material for purposes of research through the reading and signing of consent forms. This study was accepted by the ethics committees for the University of Portsmouth and SEBTA/BTR, reference number 11/SC/0048 of 19th June 2014.

2.2 Cell Lines and Cell Culture

The cell lines UP-029 and SEBTA-023, used in this study, were cultured at the University of Portsmouth and isolated via patient-derived ex-vivo GBM biopsies provided to the Brain Tumour Research Centre at University of Portsmouth, U.K. The human glioblastoma cell lines were maintained in high glucose (4500mg/l) Dulbecco's modified Eagle's medium (DMEM) (Sigma-Aldrich) supplemented with 10% Fetal Bovine Serum (FBS). Both cell lines were grown in a humidified incubator at 37ºC with an atmosphere of 5% CO_2. Cells were regularly tested for mycoplasma.

For experiments requiring cell counting, 10 µL of cells suspended in DMEM were mixed with 10 µL of trypan blue (Bio-Rad) and the number of live cells was determined using a Countess II FL Automated cell counted (ThermoFisher). For real hypoxia experiments the O_2 levels were regulated to 1% and cells were plated in 100mm plates with 10ml of complete DMEM medium per time point. 24 hours after platting, the cells were either not treated or treated (1% O_2) for different time points as described in the results section.

2.3 Western-Blotting

Western blotting is a widely used laboratory technique that permits the identification of individual proteins from a complex mixture. In this technique, proteins are separated by their molecular weight. Once denatured by heating, proteins migrate in the gel through which voltage is applied. Since these molecules have negative

charges, they will travel in direction to the cathode (positive electrode). This procedure is hence called gel electrophoresis. Smaller proteins travel faster and more easily through the gel pores, than larger proteins. By the end of the run, larger proteins will be closer to the top of the gel, while the small ones will be further away (Mahmood & Yang, 2012). In addition to protein detection, this is a semi-quantitative method that provides a relative comparison of proteins levels between samples. Hence, western-blot was used in this study to compare protein expression at different hypoxia hours.

2.3.1 Preparation of cell lysates for protein extraction

To obtain total protein extracts from both UP-029 and SEBTA-023 lines, cell lysates from different time points were prepared. Firstly, the medium of each plate was discarded and followed by a wash with approximately 2ml of Phosphate Buffered Saline (PBS) solution. The PBS was then removed and 200 to 300 μl of Lysis buffer (1x Protease Inhibitor cocktail [BIO-RAD], 2,5 mM EDTA, RIPA Buffer [*Pierce*™]; recipe in annex 1) was added to the plate. In this step, the plate was kept on ice to minimize the action of proteases and maintain proteins integrity as well. Also, in order to optimize the Lysis buffer action, with a spatula, mechanic lysis was induced by scrapping and spreading the solution through the plate. The follow-on solution (cell lysate) was then pipetted into a previously labeled and sterile 1.5 ml *Eppendorf* tube and left for 10 minutes on ice. These steps were repeated for all time-points of both cell-lines. After the 10 minutes incubation, the samples were centrifuged (VWR MiniStar silverline centrifuge) for 15 minutes at 15000 G, 4 ºC. This last step aimed to precipitate all non-soluble components so that the supernatant was merely the total protein extract. Subsequently, the supernatants were pipetted into new labelled and sterile *Eppendorf* tubes, to be kept at -80 ºC and so, preserved from degradation.

2.3.2 Protein Quantification

Afore preparing protein samples for western-blotting, the protein concentration of each sample was determined. To do so, the Thermo-Scientific's *Pierce*™ Bicinchoninic acid (BCA) Protein Assay Kit was used according to the manufacturer's instructions (annex 2). This assay consists on the biuret reaction: reduction of Cu^{2+} into Cu^{+} by protein in an alkaline medium. This is a method with high sensitivity and colorimetric detection selectivity of Cu^{+}. The stoichiometric reaction involves the

chelation of two molecules of BCA with each Cu^{+}, forming a purple water-soluble complex which exhibits a strong linear absorbance at 562 nm, directly proportional to protein concentrations.

The samples were prepared in a clear 96 well plate, for the BCA assay. First, 25 μl of each triplicate of unknown sample was added into a microplate well. Standard samples with known concentrations (Table 2.1) were added in triplicates in the plate as well, so that a calibration curve could be made. Then 200 μl of the Working reagent (50:1, BCA reagent A : BCA reagent B – annex 2) was pipetted into each well containing sample or standard solutions. Following, the plate was left in an incubator at 37 ºC for 30 minutes to be analyzed afterwards in a plate reader [Polar optima, BMG Labtech].

Table 2.1. Dilution Scheme of Diluted Albumin (BSA) standards. All standard solutions were diluted in ddH_2O. The Albumin standard stock solution provided with the kit was conserved at 4 ºC in 2 mg/ml ampules.

VIALS	VOLUME OF DILUENT (μl)	VOLUME AND SOURCE OF BSA (μl)	FINAL BSA CONCENTRATION (μg/ml)
A	0	300 of stock	2000
B	125	375 of stock	1500
C	325	325 of stock	1000
D	175	175 of vial B dilution	750
E	325	325 of vial C dilution	500
F	325	325 of vial E dilution	250
G	325	325 of vial F dilution	125
H	400	100 of vial G dilution	25
I	400	0	Blank

2.3.3 SDS-Page

In order to cast SDS-Page gels, a BIO-RAD Mini-PROTEAN Tetra Cell Casting Module was used. The first step was the assembly of a short glass and a glass spacer plate in a casting frame that will hold them in place as the gel polymerizes. The sodium dodecyl sulphate poly-acrylamide gel (SDS-PAGE) was then prepared. The

running/resolution gel was made up with the following stock solutions: 1M Tris (pH 8.8), 30% acrylamide:bisacrylamide solution, H2O, 10% Sodium Dodecyl Sulfate (SDS), 25% Ammonium Persulfate (APS) and N, N, N', N'-Tetramethylethylenediamine (TEMED), as shown on Table 2.2.

Table 2.2. Running gel formulation for different acrylamide percentages, for total volume of approximately 8 ml (1 gel).

	7%	**12%**	**15%**
1M Tris ph 8.8	3ml	3ml	3ml
30% Acrylamide:Bisacrylamide	1,9 ml	3,2 ml	4 ml
ddH_2O	3 ml	1,7 ml	0,9 ml
10% SDS	80 μl	80 μl	80 μl
25% APS	32 μl	32 μl	32 μl
TEMED	12 μl	12 μl	12 μl

After adding the TEMED, the solution was mixed and pipetted into the glass plates. Water was swiftly added to remove any potential bubbles and provide a smooth surface. Once the gel was polymerized, the water was discarded and the plate dried. The stacking gel was then prepared using the reagents and amounts shown on Table 2.3.

Table 2.3. Stacking Gel formulation for different gel quantities, being each gel equivalent to a total volume of approximately 3 ml.

	1 GEL	**2 GELS**	**3 GELS**	**4 GELS**	**5 GELS**	**6 GELS**
1M Tris ph 8.8	312.5 μl	625 μl	937.5 μl	1.25 ml	1.6 ml	1.9 ml
30% Acrylamide	550 μl	825 μl	1.2 ml	1.65 ml	2.1 ml	2.5 ml
ddH_2O	2.3 ml	3.5 ml	5.2 ml	6.9 ml	8.6 ml	10.4 μl
10% SDS	25 μl	50 μl	75 μl	100 μl	125 μl	150 μl
25% APS	12.5 μl	25 μl	37.5 μl	50 μl	62.5 μl	75 μl
TEMED	7.5 μl	15 μl	22.5 μl	30 μl	37.5 μl	45 μl

The stacking gel was pipetted into the plates immediately after adding the TEMED, once its polymerization is very fast and after checking that there were no air bubbles a comb was placed on the top until the gel was fully polymerized.

In order to prepare the samples to load in the gel, fractions containing 20 µg/20 µl of the extracted protein were mixed with 4x loading buffer [Bio-Rad] in final concentration of 1x. The samples were then boiled on a water bath or a Bio TDB-100 dry block thermostat (BioSan) for 5 minutes and centrifuged for 15 seconds at maximum speed. Meanwhile, when the samples were heating up, the already polymerized gels were placed in a Mini-PROTEAN ® Tetra Vertical Electrophoresis Cell and covered with 1x Running buffer (25 mM Tris base, 250 mM glycine, 0.1% SDS). Into the first well of each gel, 3 µl of Precision Plus Protein All Blue Standards (BIO-RAD) was loaded and in the following wells the 20 µg protein fractions prepared. The cell was then connected to a power supply and the gels ran at 140V for approximately 1 hour.

For the transfer, one sheet of nitrocellulose membrane and two sheets of thick blot filter paper were cut to the same size as the corresponding gel. They were then wetted in PierceTM 1-Step Transfer Buffer for a minimum of 15 minutes. After protein separation within the gel, the glass plates are separated and the gel retrieved. One sheet of thick blot filter paper was then placed on the Pierce™ G2 Fast Blotter cassette cathode, one nitrocellulose membrane was placed on top and the respective gel was arranged on top. One sheet of thick blot filter paper was added on top of the gel and any bubbles were removed with a blot roller. The anode plate was then gently pressed on top and the cassette slid into the control unit. The transfer then took place for 14 minutes at the high mW setting. Once complete, the membrane was placed in Licor Odyssey® Blocking Buffer and incubated for 1 hour at room temperature using a horizontal rocker. The blocking buffer was then removed and the primary antibody added. The membrane was then incubated overnight at 4ºC. The primary antibody was removed and the membrane was then washed 4 times for 5 minutes incubations using TBS-T solution (20 mM Tris pH7.5, 120 mM NaCl, 0.05% Tween-20) . The TBS-T was subsequently removed and the secondary antibody added. The membrane was then incubated for an hour at room temperature with shaking before removing the

secondary antibody. The membrane was washed using TBS-T for a further 4 times for 5 minutes each wash. A Licor Odyssey® CLx instrument was then used to visualize the membranes. Analysis of the bands was performed using the Image Studio Lite software.

2.3.4 Antibodies

The following primary antibodies listed on Table 2.4 were used for western blotting:

Table 2.4. List of primary antibodies used for western-blotting. All "SC" references refer to the Santa Cruz Biotechnology company.

ANTIBODY	REFERENCE
ACTIN (C-11)	SC-1615
ALDOLASE A	SC-12059
ANXA2	SC-1924
ANXA2 (D1/274.5)	Made in house
CAIX (H-11)	SC-365900
EGFR (A-10)	SC-373746
GADPH (FL-335)	SC-25778
GLUT1 (A-4)	SC-377228
HIF1A (H-206)	SC-10790
HIF2A	SC-46691
LDHA	SC-12059
MMP2 (8B4)	SC-13595
MMP9 (2C3)	SC-21733
NDRG1 (B-5)	SC-398291
PAI1 (C-9)	SC-5297
PDK1 (4A11F5)	SC-293160
PIGF (H-4)	SC-518003
S100A10 (4E7E10)	SC-81153
UPA (H77A10)	SC-59727
UPAR (E-3)	SC-376494
VEGFA	SC-152
VEGFC (E-6)	SC-374628
VEGFD	SC-13085

The following secondary antibodies listed on Table 2.5 used for western blotting:

Table 2.5. List of secondary antibodies used for western-blotting.

ANTIBODY	REFERENCE
ANTI-MOUSE	926-32210 (Li-COR)
ANTI-GOAT	926-32212 (Li-COR)
ANTI-RABBIT	926-32211 (Li-COR)

2.4 Polymerase Chain Reaction arrays

Real-time Reverse-Transcription Polymerase Chain Reaction (RT-PCR) is a highly sensitive and reliable method of gene expression analysis that quantify simultaneously genes of the same sample. It allows the measurement of gene amplification by means of RNA reverse-transcripts (cDNAs). For this investigation, PCR assays were made to quantify the gene expression levels during hypoxia comparing to normoxia.

2.4.1 RNA extraction

To obtain total RNA extractions from both UP-029 and SEBTA-023 cell lines for the different time-points, QIAGEN's RNeasy® Plus Mini Kit was used according the manufacturer's instructions (annex 3). First, each plate was washed with approximately 2 ml of Hank's Balanced Salted Solution (HBSS) [Thermo Fisher], followed by an incubation with 2 ml of TrypLE™ Express [Thermo Fisher] for 2-3 minutes at 37 ºC, to detach and suspend the cells. Next, the solutions with the suspended cells were pipetted into labelled 15 ml tubes with 3 ml of DMEM previously added to centrifuge for 5 minutes at 10 000 G. This centrifuging step meant to precipitate the cells in a pellet so that the supernatant with TrypLE™ Express and DMEM could be discarded. Right after this, 350 μl of the RTL buffer (lysis buffer provided with the kit) was added to each tube and lysis was mechanically instigated by pipetting up and down. The resultant RTL solutions were then transferred into gDNA Eliminator spin columns placed in previously labelled 2 ml collection tubes (all provided with the kit), to centrifuge for 30 seconds at 12000 G. Afterwards, the gDNA Eliminator spin columns were discarded and the flow-throughs saved in their respective columns to which 350 μl of ethanol 70% was directly added and mixed my pipetting up and down. Subsequently, the solutions were transferred into a RNeasy spin columns (delivered with the kit) placed in a new and labelled collection tubes to be centrifuged for 15 seconds at 12000 G. This step was repeated twice (350 μl each time), since the final volume of the previous step was 700μl and such volume could

not fit the column. The flow-throughs were then discarded and the columns saved in the same collection tubes, to be added 700 μl of the Kit's RW1 Buffer followed by a centrifuged of 15 seconds at 12000 G. Similarly to the former, this step was done twice, adding 350 μl of RW1 each time. The flow-throughs were again discarded and the columns saved in the same collection tubes so that 500 μl of the kit's RPE buffer could be added this time. The columns (in the respective tubes) were again centrifuged for 15 seconds at 12000 G and the flow-through discarded. This step was repeated, following the manufacturer's instructions, with a centrifugation time of 2 minutes, at the same speed. The flow throughs were discarded. Then, replacing the RNeasy spin columns in new and previously labelled 1,5 ml collection tubes, 30 μl of RNase-free water (also provided by the kit) was directly added into each of the column's membranes. This was followed by 1 minute centrifugation at 12000 G. Contrarily to the prior steps, this time the flow-through was saved, once it already contained the RNA extracts. Finally, repeating the last step, this time using 50 μl of RNase-free water, a total of 80μl of total RNA was extracted. This sample was then saved in the -80 ºC to avoid RNA degradation.

2.4.2 Hypoxia RT^2 profiler PCR array

The Hypoxia RT^2 profiler PCR array combines the technology of RT-PCRs with the multigene profiling capability of microarrays. To analyze the hypoxic profile of both UP-029 and SEBTA-023 cell lines, Hypoxia RT^2 profiler PCR array kit (QIAGEN) was used according to the manufacturer's instructions (annex 4). First, the concentration of the RNAs extracted was quantified and tested for integrity and quality through an Agilent 2100 Bioanalyzer machine. To do so, a gel-dye mix (1μl dye; 65 μl filtered gel) was prepared following the manufacturer's instructions (annex 5). Then, 9 μl of gel-dye mix was loaded at the bottom of the G-marked well of the Bioanalyzer RNA-chip which was settled up in the priming station (annex 5). Setting the timer to 30 seconds and making sure that the plunger was positioned at 1 ml, the chip priming station was closed to pressurize. The plunger of the syringe was pressed down until held by the clip and remained for 30 seconds, before releasing the mechanism. After 5 seconds, once the plunger moved back to at least the 0.3 ml mark, the plunger was gently pulled back to the 1 ml position. The chip priming station was finally opened once the pressurizing step was completed. Next, 9 μl of the gel-dye mix was pipetted into the

two respectively marked wells. To load the RNA 6000 Nano Marker, 5 μl of the solution was pipetted into the left wells. No wells were left empty since that could interfere with the run analysis. The ladder aliquots were defrosted and kept on ice to avoid extensive warming. Before loading and to minimize secondary structures, the samples were heated and denatured at 70 ºC for 2 minutes. Then, 1 μl of the sample was pipetted into each of the 12 sample wells. Also, 1 μl of the ladder was pipetted into the well marked with the ladder symbol. The timer was set for 60 seconds and the chip was placed horizontally in the adapter of the IKA vortex mixer to vortex with a speed of 2400 rpm. Lastly, the chip was inserted in the Agilent 2100 bioanalyzer to proceed with the analysis.

For the RNA reverse transcription into cDNA, the reagents provided with the RT^2 first strand kit (annex 4) were thaw and briefly centrifuged for 15 seconds to bring contents to the bottom of the tubes. The genomic DNA elimination mix was prepared according to Table 2.6. for each of the RNA samples.

Table 2.6. Genomic DNA elimination mix.

COMPONENT	AMOUNT
RNA	2 μg
Buffer GE	2 μl
RNase-free water	Up to 10 μl final volume

Then the mix was mixed with the samples by gently pipetting up and down, followed by a spin down. The samples were then incubated for 5 minutes at 42 ºC immediately followed by a second incubation of 1 minute on ice. The reverse-transcription mix was then prepared as shown on Table 2.7.

Table 2.7. Reverse-transcription mix. The amounts designated in the subsequent table refer to 1 reaction volume.

COMPONENT	AMOUNT
5x Buffer BC3	4 μl
Control P2	1 μl
RE3 Reverse Transcriptase Mix	2 μl
RNase-free water	3 μl
Total volume	**10 μl**

Once set, 10 μl of reverse-transcription mix was added to each tube containing the RNA samples and genomic DNA elimination mix. The solution was mixed by gently pipetting up and down, followed by an incubation at 42 ºC for 15 minutes. The reaction was then immediately stopped by incubating at 95 ºC for 5 minutes. Finally, each sample was supplemented with 91 μl of RNase-free water which was then mixed by pipetting up and down several times. The reaction tubes were kept on ice to proceed with the real-time PCR protocol.

For the real-time PCR, 4 plates of 96 wells each were provided with the kit. Each plate had 84 wells for hypoxia-related genes, 5 housekeeping genes, 1 well containing a genomic DNA control, 3 wells containing reverse transcription controls and lastly 3 wells with positive PCR controls, as shown on Figure 2.1

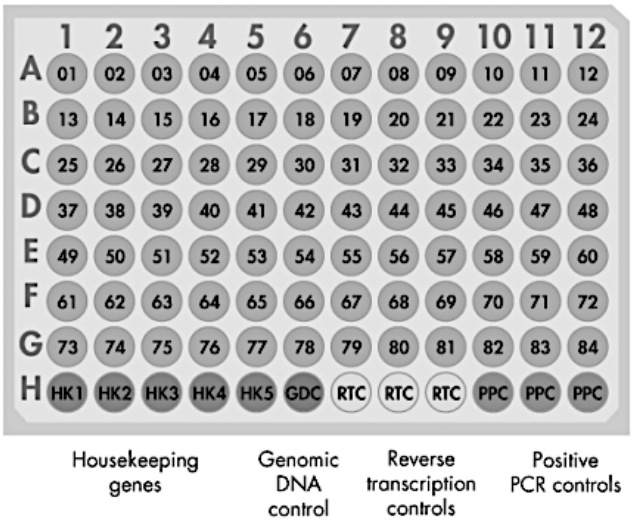

Figure 2.1. RT^2 Profiler PCR array plate format. Wells A1 to G12 contain the Hypoxia gene assays. Wells H1 to H5 contain the housekeeping genes panel (HKs), to normalize the array data. Well H6 contains a genomic DNA control (GDC). Wells H10 to H12 contain replicate positive PCR controls (PPC).

The genomic DNA control (GDC) is an assay that specifically detects non-transcribed genomic DNA. The reverse transcription control (RTC) is an assay that tests the efficiency of the reverse transcription reaction performed with the kit by detecting template synthesized from the kit's built-in external RNA control. The positive PCR control (PPC) tests the efficiency of the polymerase chain reaction itself. The catalogue of Hypoxia related and housekeeping genes is listed on Table 2.8.

Table 2.8. List of Hypoxia related and housekeeping genes analyzed by the RT^2 profiler array and respective plate position.

Position	Gene Name
A1	Adrenomedullin
A2	Adenosine A2b receptor
A3	Aldolase A, fructose-bisphosphate
A4	Angiopoietin-like 4
A5	Ankyrin repeat domain 37
A6	Annexin A2
A7	APEX nuclease (multifunctional DNA repair enzyme) 1
A8	Aryl hydrocarbon receptor nuclear translocator
A9	Ataxia telangiectasia and Rad3 related
A10	Basic helix-loop-helix family, member e40
A11	Bloom syndrome, RecQ helicase-like
A12	BCL2/adenovirus E1B 19 kDa interacting protein 3
B1	BCL2/ adenovirus E1B 19 kDa interacting protein 3-like
B2	B-cell translocation gene 1, anti-proliferative
B3	Carbonic anhydrase IX
B4	Cyclin G2
B5	COP9 constitutive photomorphogenic homolog subunit 5
B6	Cathepsin A
B7	DNA-damage-inducible transcript 4
B8	DnaJ (Hsp40) homolog, subfamily C, member 5
B9	Endothelin 1
B10	Egl nine homolog 1
B11	Egl nine homolog 2
B12	Early growth response 1
C1	Eukaryotic translation initiation factor 4E binding protein 1
C2	Enolase 1 (alpha)
C3	Erythropoietin
C4	ERO1-like
C5	Coagulation factor X
C6	Coagulation factor III
C7	FBJ murine osteosarcoma viral oncogene homolog
C8	Glucan (1,4-alpha-), branching enzyme 1
C9	Glucose-6-phosphate isomerase

C10	Glycogen synthase 1
C11	Hypoxia inducible factor 1, alpha subunit
C12	Hypoxia inducible factor 1, alpha subunit inhibitor
D1	Hypoxia inducible factor 3, alpha subunit
D2	Hexokinase 2
D3	Heme oxygenase 1
D4	Hepatocyte nuclear factor 4, alpha
D5	Immediate early response 3
D6	Insulin-like growth factor binding protein 3
D7	Jumonji domain containing 6
D8	Lactate dehydrogenase A
D9	Lectin, galactoside-binding, soluble, 3
D10	Lysyl oxidase
D11	Mitogen-activated protein kinase kinase kinase 1
D12	Met proto-oncogene
E1	Macrophage migration inhibitory factor
E2	Matrix Metalloproteinase 9
E3	Max interactor 1
E4	Nicotinamide phosphoribosyltransferase
E5	Nuclear receptor coactivator 1
E6	N-myc downstream regulated 1
E7	Nuclear factor kappa light polypeptide gene enhancer in B-cells 1
E8	Nitric oxidase synthase 3
E9	Ornithine decarboxylase 1
E10	Prolyl 4-hydroxylase, alpha polypeptide 1
E11	Prolyl 4-hydroxylase, beta polypeptide
E12	Pyruvate dehydrogenase kinase, isozyme 1
F1	Period homolog 1
F2	6-phosphofructo-2-kinase/fructose-2,6-biphosphotase 3
F3	6-phosphofructo-2-kinase/fructose-2,6-biphosphotase 4
F4	Phosphofructokinase, liver
F5	Phosphofructokinase, platelet
F6	Phosphoglycerate mutase 1, brain
F7	Placental growth factor
F8	Phosphoglycerate kinase 1
F9	Pim-1 oncogene

F10	Pyruvate kinase, muscle
F11	Plasminogen activator, urokinase
F12	Recombination signal binding protein for immunoglobulin kappa J region
G1	RuvB-like 2
G2	Serpin peptidase inhibitor, clade E, member 1
G3	Solute carrier family 16, member 3
G4	Solute carrier family 2, member 1
G5	Solute carrier family 2, member 3
G6	Transferrin receptor
G7	Tumour protein 53
G8	Triosephosphate isomerase 1
G9	Thioredoxin interacting protein
G10	Upstream transcription factor 2, c-fos interacting
G11	Voltage-dependent anion channel 1
G12	Vascular endothelial growth factor A
H1	Actin, beta
H2	Beta-2-microglobulin
H3	Glyceraldehyde-3-phosphate dehydrogenase
H4	Hypoxanthine phosphoribosyltransferase 1
H5	Ribossomal protein, large, P0

As for the real-time PCR protocol itself, first the RT^2 SYBR Green mastermix was briefly centrifuged for 10-15 seconds to bring the contents to the bottom of the tube. Then, the PCR components mix was prepared in a 5 ml tube, as demonstrated on Table 2.9.

Table 2.9. PCR components mix for 96 well array format. The total volume provides an excess amount of 300 μl to allow pipetting errors.

Array Format	**Amount**
2x RT^2 SYBR Green Mastermix	1350 μl
cDNA synthesis reaction	102 μl
RNase-free water	1248 μl
Total volume	**2700 μl**

The RT^2 profiler PCR plate was carefully removed from its sealed bag and 25 μl of PCR components mix was pipetted into each well of the plate. The pipette tip was swapped in between wells to avoid cross contaminations. Once concluded the

previous step, the plate was sealed with an optical adhesive film (provided by the kit). The plate was centrifuged at room temperature for 1 minute at 1000 G in order to remove any bubbles existent in the wells. Finally, the plate was inserted into the Lightcycler 96 SW qRT-PCR instrument (Roche) and programmed for a pre-incubation step of 1 cycle at 95 ºC (to activate the HotStart DNA Taq Polymerase), followed by 45 cycles of 15 seconds at 95 ºC and one minute at 60 ºC (to perform fluorescence data collection).

2.4.3 qRT-PCR assay

Real-time quantitative PCR quantifies the nucleic acids in a sensitive, specific and reproducible way. This technique generates copies of DNA template per cycle, resulting in a quantitative correlation between the initial and the accumulated amounts (Arya et al., 2005). Eventually the polymerase reaction ceases due to inhibitors found with the template, reaching the end of its exponential rate. In fact, qRT-PCR is such a powerful method that it is able to quantify gene expression of only 1 template (Arya et al., 2005).

For this study a method of relative quantification was used. This method analyzes the expression of a target gene relative to a reference group (Livak & Schmittgen, 2001). In this study, the target genes were analyzed in hypoxia time-points of 6, 24 and 48 hours and compared to normoxia (non-treated) samples.

For the quantitative real-time PCR assay (qRT-PCR), the One-step NZyRT supermix kit (Nzytech) was used. Nuclease-free water, One-step NZYSpeedy qPCR Green master mix, as well as NZyRT mix were provided with the kit. The One-step NZYspeedy qPCR Green master mix contains a green intercalating dye for detection, stabilizers, enhancers and dNTPs. The NZyRT mix is made up of Reverse transcriptase and Ribonuclease inhibitor.

The RNA concentration for this protocol was determined using a nanodrop spectrophotometer (Fisher Scientific). To prepare the mastermix for each set of primers, the reagents above listed and provided by the kit were mixed as shown on Table 2.10.

Table 2.10. NZyRT qRT-PCR Mastermix for 13 wells volume (1 well of excess volume to cover pipetting errors).

Reagent	Volume
One-step NZYspeedy qPCR Green master mix	65 μl
Forward primer	5,2 μl
Reverse primer	5,2 μl
NZyRT mix	5,2 μl
Nuclease-free water	36,4 μl
Total volume	**117 μl**

Once set, 9 μl of each mastermix was pipetted into the 12 wells of the respective gene/primers, as demonstrated in Figure 2.2.

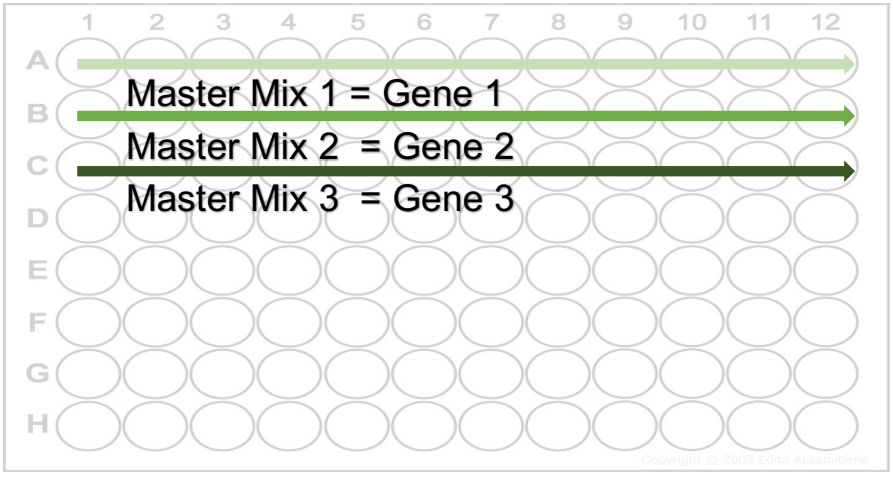

Figure 2.2. qRT-PCR array plate format. Demonstration of the mastermixes distribution through the plate.

Next, 1 μl of RNA sample (50 ng/μl) was added to each well, swapping pipette tips in between wells to avoid cross contaminations. There were 4 time-points (Non-treated, hypoxia: 6 hours, 24 hours and 48 hours) being analyzed for each gene, in triplicates. The RNA samples were distributed throughout the plates as shown in Figure 2.3.

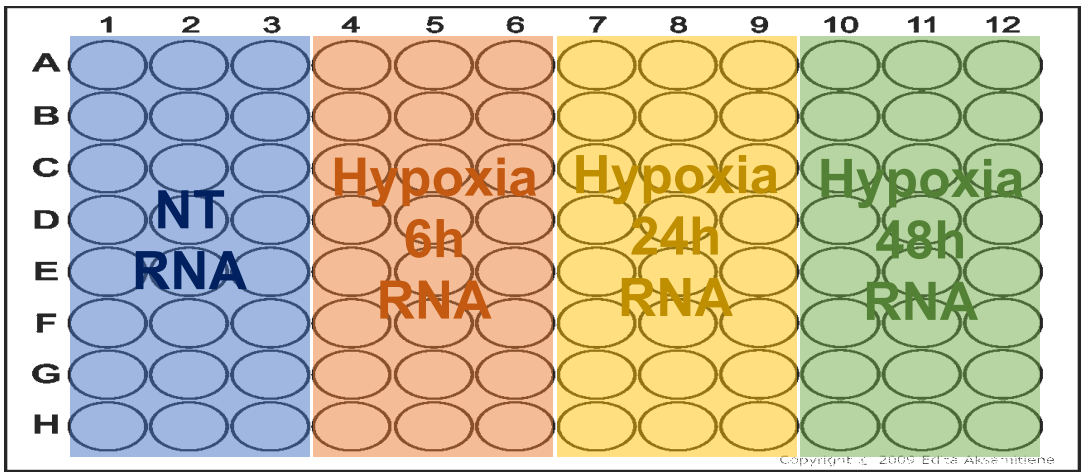

Figure 2.3. qRT-PCR assay plate format. Demonstration of the Non-treated (NT), hypoxia: 6 hours, 24 hours and 48 hours RNA samples distribution throughout the plate.

Once all the wells had their respective mastermix and RNA sample, the plate was sealed with a plastic adhesive (provided with the plate) and centrifuged at 1000 G for 1 minute. The plate was then placed into the Lightcycler 96 SW qRT-PCR instrument (Roche). The light cycler was programmed for a first step of pre-incubation and cDNA synthesis at 50ºC for 20 minutes (reverse transcription), followed by a gene amplification step at 95ºC for 5 minutes (polymerase activation), a denaturation step at 95ºC for 40 cycles of 5 seconds each and finally by an annealing/extension step of 40 cycles of 50 seconds each at 60ºC. After each annealing cycle the gene products were quantified.

2.4.2.1 Primers

The following primers were used for qRT-PCR:

GENE	FORWARD PRIMER	REVERSE PRIMER
GLUT1	CTCCTGCCCTGTTGTGTATAG	CAGGAGTGAGGTGGTGTATTT
LDHA	GCTGGTCATTATCACGGCTG	AGCAACTTGCAGTTCGGGCTG
VEGFA	GACCTTGCCTTGCTGCTCTA	CACCAGGGTCTCGATTGGATG
VEGFC	GAGGAGCAGTTACGGTCTGTG	TCCTTTCCTTAGCTGACACTTGT
VEGFD	ATGGACCAGTGAAGCGATCAT	GTTCCTCCAAACTAGAAGCAGC
HIF1α	ATCCATGTGACCATGAGGAAATG	TCGGCTAGTTAGGGTACACTTC
HIF2α	GTGCCATGACAAACATCTTCCAG	CTCGGGCTCTGTCTTCTTGCT
UPA	CAGGGCATCTCCTGTGCATG	AGCCCTGCCCTGAAGTCGTTA
UPAR	GCCTTACCGAGGTTGTGTGT	CATCCAGGCACTGTTCTTCA

ANXA2	CTCTACACCCCCAAGTGCAT	TCAGTGCTGATGCAAGTTCC
S100A10	AAATTCGCTGGGGATAAAGG	AGCCCACTTTGCCATCTCTA
PAI1	GGGCCATGGAACAAGGATGA	CTCCTTTCCCAAGCAAGTTG
MMP9	CGGACCAAGGATACAGTT	AGTGAAGCGGTACATAGG
MMP2	CGTCTGTCCCAGGATGACATC	ATGTCAGGAGAGGCCCCATA
ANGPTL4	GAGGTCCTTCACAGCCTGCA	TGGGCCACCTTGTGGAAGAG
BNIP3	CGCAGACACCACAAGATACCAAC	GCCAGCAAATGAGAGAGCAGC
SLC16A3	TGTGTGCGTGAACCGCTTT	AAACCCAACCCCGTGATGAC
CAIX	CTTGGAAGAAATCGCTGAGG	TGGAAGTAGCGGCTGAAGTC
DDIT4	GACAGCAGCAACAGTGGCTTCG	GCTGCATCAGGTTGGCACAC
EGR1	ACCGCAGAGTCTTTTCCTGACA	GGTGCAGGCTCCAGGGAAAA
HK2	GCCTTTCCGTCCCAGCCTTTAGCC	GGACTCCTGCGCCGGAGTTTCATG
NDRG1	CTGCACCTGTTCATCAATGC	AGAGAAGTGACGCTGGAACC
PDK1	CTGTGATACGGATCAGAAACCG	TCCACCAAACAATAAAGAGTGCT
PFKB3	AGTGCAGAGGAGATGCCCTA	TCAGTGTTTCCTGGAGGAGTCAGC
TFRC	ACTTGCCCAGATGTTCTCAG	GTATCCCTCTAGCCATTCAGTG
PFKB4	TTAATTTTGGAGAACAGAATGGC	CGTAGCCTCATCACTGTCGC
PIGF	TGCGGCGATGAGAATCTGC	AGCGAACGTGCTGAGAGAAC
RPL0	AGACAATGTGGGCTCCAAGCAGAT	GCATCATGGTGTTCTTGCCCATCA

The RPLP0 gene is a housekeeping gene therefore was used to normalize the data of the different samples and treatments.

2.4.4 Statistical analysis

2.4.4.1 Hypoxia RT^2 profiler PCR array

There is an integrated web-based software package for the RT2 Profiler PCR Array system that automatically performs all ΔΔCT based fold-change calculations from an uploaded raw threshold cycle (CT) data. The CT values refer to the cycle from each the amplification of the interest gene indeed started. This value is inversely proportional to the number of times the gene is transcript, meaning that the lower the CT, the higher the expression of that gene. To calculate the ΔΔCT, this values were normalized with housekeeping gene CTs. The web portal www.SABiosciences.com/pcrarraydataanalysis.php in which the excel-format data is

uploaded, delivers results in formats such as the tabular, scatter, volcano, cluster-gram and multi-group plots. This web portal also helps to correctly interpret the genomic DNA, reverse transcription efficiency, and positive PCR control well data.

The automatic selection from HKG panel was selected to conduct the RT2 Profiler PCR Array software-based analysis. This method automatically selects an optimal set of internal control / housekeeping / normalization genes for the analysis from the available housekeeping gene panel on the PCR Array. The software measures and identifies the genes with the most stable expression via a non-normalized calculation. The CT values for these genes are then geometrically averaged and used for the ΔΔCT calculations. The CT cut-off was set to 35 cycles.

Fold-Regulation represents fold-change results in a biologically meaningful way. Fold-change values greater than one indicate a positive- or an up-regulation, and the fold-regulation is equal to the fold-change. Fold-change values less than one indicate a negative or down-regulation, and the fold-regulation is the negative inverse of the fold-change. In order to calculate the fold-Change, the software used the $2^{-\Delta\Delta CT}$ formula which corresponds to: the normalized target gene expression $2^{-\Delta CT}$ in the test sample divided by the normalized gene expression $2^{-\Delta CT}$ in the control group (non-treated).

2.4.4.2 qRT-PCR arrays

The results obtained from the Lightcycler 96 SW qRT-PCR instrument were quantified using the $2^{-\Delta\Delta CT}$ method in order to calculate the relative gene induction (fold change) between different samples. Each gene expression was quantified through at least 3 different runs, in plate triplicates (3 wells per plate). To calculate the fold change of 1 run for each gene, the average of the 3 Cts was calculated. Next, the average Ct value of the housekeeping gene was then subtracted from the average Ct of each genes of interest to give the ΔCt value. For each gene, the ΔCt value of the control group (non-treated cells) was then subtracted from the ΔCt of the hypoxia treated samples to give the ΔΔCt value. Finally, the formula was used to calculate the fold change for each gene. Once all the fold change values were determined, the average of the $2^{-\Delta\Delta CT}$ values of at least three independent runs was calculated for each gene.

The standard deviation and P-value was calculated for each gene, using the software Microsoft® Excel Office 365 software. Explicitly, the statistical significance of gene expression (P-value) was evaluated for a N (nº runs) equal or higher than 3, using a type 2, two-tailed Student's t-test (Type 2, Tail 2). In every case a P-value of less than 0.05 (*), 0.01 (**) and 0.001 (***) were considered statistically meaningful in 3 different levels of significance.

CHAPTER III

RESULTS

3. Results

3.1 Investigating the expression of hypoxia genes in UP-029 and SEBTA-023 cell lines

The QUIAGEN's RT^2 hypoxia profiler assay was used in this study since it allows to quantify the expression of a broad panel of genes known to be implied in this cancer hallmark. Through these arrays, it was possible to generate a wide number of targets for validation and future studies.

The RT^2 hypoxia arrays experiments only RNA samples with A_{260}:A_{230} ratios greater than 1.7 and A_{260}:A_{280} ratios between 1.8 and 2.0 were considered for these studies. Both 18S and 28S ribosomal RNA bands and peaks were examined as signs of RNA integrity and no RNase degradation. The RNA Integrity Number (RIN) was also considered as a quality control parameter and only samples with a RIN higher than eight were pondered. The concentration and quality of the RNAs was performed using an Agilent 2100 Bioanalyzer machine.

For the RT^2 array quality control, the PCR array reproducibility, the RT efficiency and the genomic contamination parameters were considered. The Criteria for Genomic DNA Contamination (GDC) was the following**:** If C_T(GDC) was equal or higher than 35, then the GDC QC reports 'Pass'. If C_T(GDC) was inferior than 35, then the GDC QC reports 'Inquiry'.

The results of this section are displayed in scatter plots and heat maps in Figures 3.1 to 3.4. The scatter plot compares the normalized expression of all genes analyzed between the control and selected hypoxia time-point groups by plotting them against one another to quickly visualize large gene expression changes. The central line indicates unchanged gene expression. The dotted lines indicate the selected fold regulation threshold. Data points beyond the dotted lines in the upper left and lower right sections meet the selected fold regulation threshold. The Heat Map provides a visualization of the fold changes in expression between the selected groups (normoxia versus hypoxia) for every gene in the array in the context of the array layout. The heat map tables, provided in annex 6 (annex 6a UP-029, annex 6b SEBTA-023), specify

the fold regulation data used for the map as well as the comments associated with each one.

In the scatter plot, $\log_{10}$ (fold change) was calculated for each one of the analyzed genes to improve the symmetry of the data distribution and a simplified visualization. The same was considered for the heatmap, where the $\log_2$ (fold change) was calculated for each one of the analyzed genes. This last normalization was based in a $\log_2$ function and not a $\log_{10}$, to obtain a cleaner projection of the fold change in a larger scale. These results were then assessed by qRT-PCR analysis.

3.1.1 UP-029 RT^2 hypoxia array analysis

All samples from both 6 and 48 hours time-points passed the PCR array reproducibility and RT^2 efficiency quality control check-points. However, sample 1, equivalent to the *Adrenomedullin* (*ADM*) quantification well was reported as contaminated with genomic DNA. Due to its genomic contamination, ADM was not further analyzed in the qRT-PCR studies or considered in the following RT^2 hypoxia PCR arrays result's preliminary discussion.

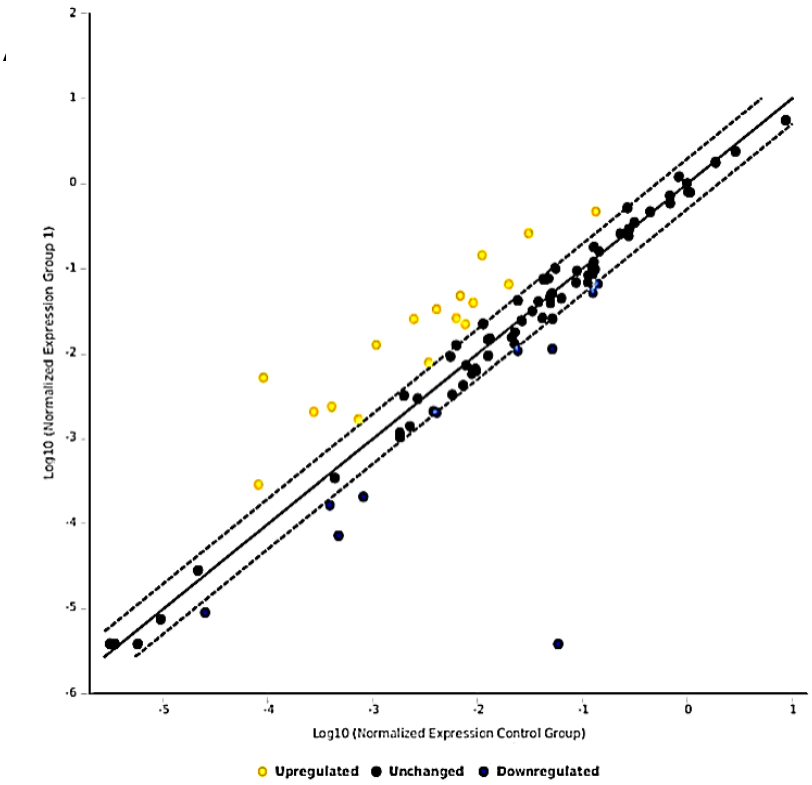

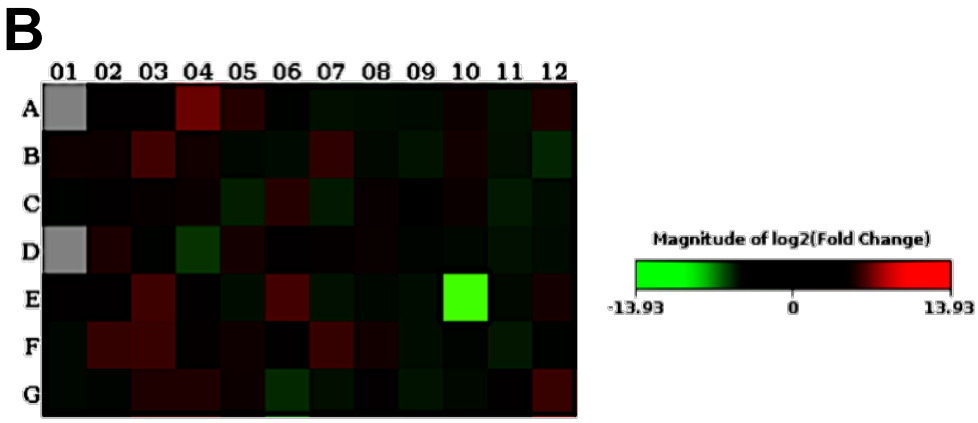

Figure 3.1. UP-029 6 hours (group 1) hypoxia time-point RT^2 profiler PCR array: **a. scatter plot**, the y axis corresponds to the $\log_{10}$ of the $2^{-\Delta CT}$ 6 hours time-point group genes and the x axis to the $\log_{10}$ of the $2^{-\Delta CT}$ non-treated group genes. The upregulated genes match the yellow dots above the threshold line and the downregulated genes the blue dots underneath the threshold line. The black dots in between the threshold lines (dotted lines) correspond to unchanged expression genes. **b. heat map**, $\log_2$ of the $2^{-\Delta\Delta CT}$ 6 hours time-point group genes heat map table. The expression magnitude was estimated as high when $\log_2$ (fold change) was higher than 0 and low when $\log_2$ (fold change) was lower than 0.

Analysis of Figure 3.1 shows that at 6 hours of hypoxia 17 genes were over-expressed, marked in yellow above the dotted threshold line and 10 genes were under-expressed, marked in blue underneath the dotted threshold line, compared to normoxia.

Three genes were highly down-regulated (Figure 3.1.b). Samples D4, G6 and B12, corresponding to the *Hepatocyte Nuclear Factor 4*α (*HNF4A*), *Transferrin Receptor* (*TFRC*) and *Early Growth Response 1* (*EGR1*) respectively, with fold values below -4. While, samples A4, B3, E3, E6, F2, F3, F7 and G12 are reported as upregulated. These correspond to *Angiopoietin Like 4* (*ADM*), *Carbonic Anhydrase IX* (*CAIX*), *Max Interactor 1* (*MXI1*), *N-myc Downstream Regulator 1* (*NDRG1*), *6-phosphofructo-2kinase/fructose-2,6-biphosphate 3* and *4* (*PFKB3* and *PFKB4*) and *Vascular Endothelial Growth Factor A* (*VEGFA*) genes, respectively. All fold-change values of these samples were relatively high (> 6). With the exception of *MXI1*, all genes were further investigated by qRT-PCR.

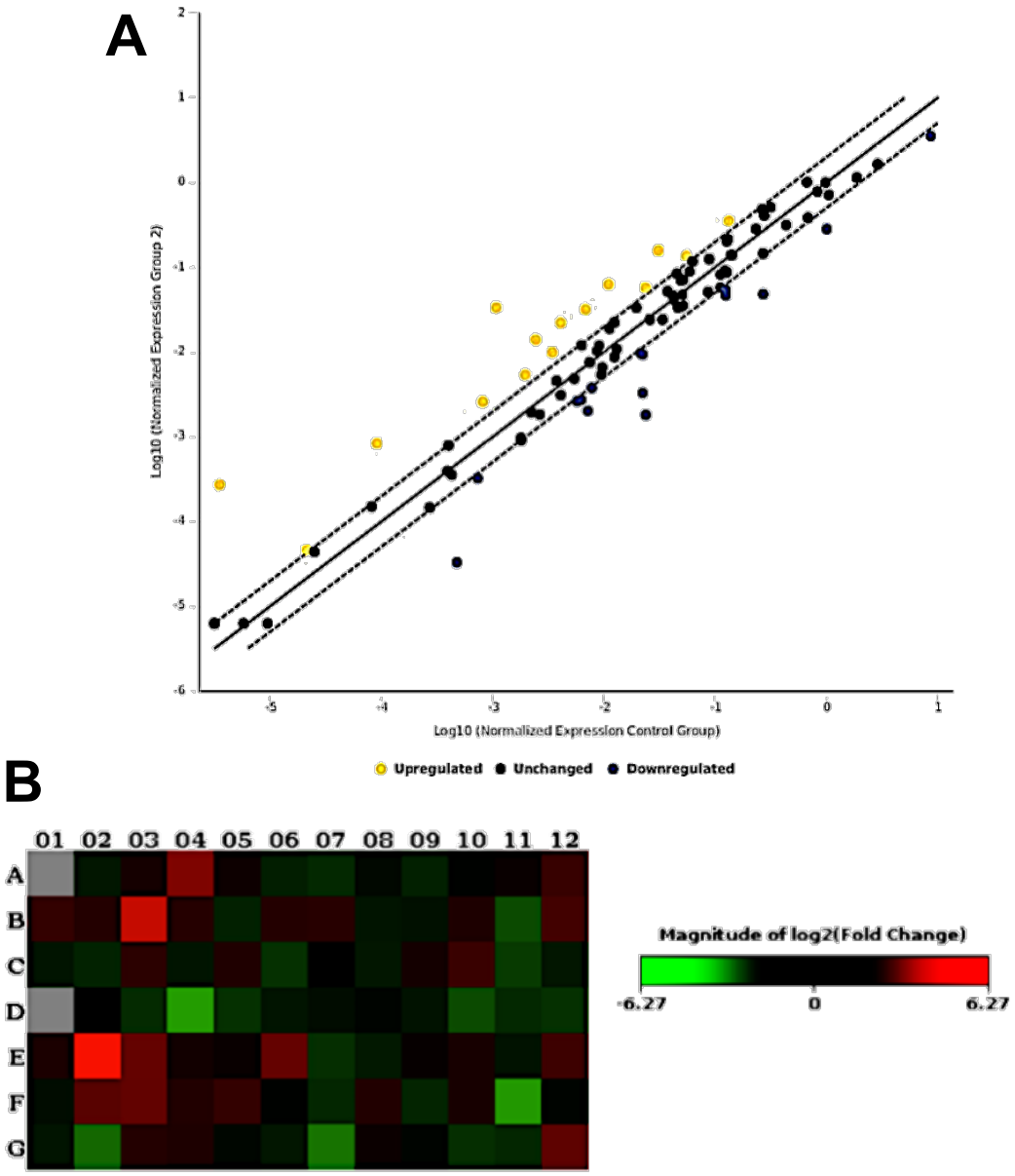

Figure 3.2. UP-029 48 hours (group 2) hypoxia time-point RT^2 profiler PCR array: **a. scatter plot**, the y axis corresponds to the $\log_{10}$ of the $2^{-\Delta CT}$ 48 hours time-point group genes and the xx axis to the $\log_{10}$ of the $2^{-\Delta CT}$ non-treated group genes. The upregulated genes match the yellow dots above the threshold line and the downregulated genes the blue dots underneath the threshold line. The black dots in between the threshold lines (dotted lines) correspond to unchanged expression genes. **b. heat map**, $\log_2$ of the $2^{-\Delta\Delta CT}$ 6 hours time-point group genes heat map's table. The expressions magnitude was estimated as high when $\log_2$ (fold change) was higher than 0 and low when $\log_2$ (fold change) was lower than 0.

Figure 3.2.a scatter plot distinguishes 15 over-expressed genes, marked in yellow above the dotted threshold line and 14 under-expressed genes, marked in blue underneath the dotted threshold line. The 6 hours time-point data revealed a wider variety of under-expressed genes than this group. Yet the amount of over-expressed samples was approximate. Focusing these data magnitudes, it is clear that discarding

relevant outliers, the heatmap turns out to be more sensitive. In fact, it is perceptible that samples B3 and E2 magnitudes are extremely high and close to the limit. he B3 gene (*CAIX*) was reported in the first time-point with a fold change of 11,55. In the 48 hours time-point *CAIX* recounted a fold change of 30,91. Also, the E2 sample, correspondent to the *Matrix Metalloproteinase 9* (*MMP9*), was not shown as over-expressed in the first time-point. Conversely, after 48 hours, *MMP9* sample represented a fold change of 77,17.

Likewise, samples A4 (*ANGPTL4*), E3 (*MXI1*), E6 (*NDRG1*), F3 (*PFKB4*), F2 (*PFKB3*) and G12 (*VEGFA*) were also considerably over-regulated with respective fold-change values of 9,19, 5,74, 5,66, 5,43, 4,66 and 5,13. These gene samples had, however, lower fold changes at 48 hours, compared to 6 hours of hypoxia.

Samples D4, F11, G2 and G7 were shown in Figure 3.2.b as under-expressed. These correspond respectively to the *Hepatocyte nuclear factor 4 alpha* (*HNF4A*), *Plasminogen Activator Urokinase* (*PLAU*), *Serpin Peptidase Inhibitor Clade E* (*SERPINE1*) and *Tumour Protein 53* (*TP53*). *HNF4A* and *PLAU* genes showed the most prominent magnitudes within the under-expressed samples with fold changes -14,52 and -13,18 correspondingly. *SERPINE1* and *TP53* also recounted significant fold changes of -5,66 and -6,87. Curiously, *SERPINE1* and *TP53* were not under-expressed in the 6 hours time-point. Both *HNF4A* and *PLAU*, although detected as down-regulated in the earliest time-point (with fold changes of -6,68 and -2,22), were unchanged at 48 hours.

3.1.2 SEBTA-023 RT^2 hypoxia array analysis

All SEBTA-023 samples from both 6 and 48 hours time-points passed the PCR array reproducibility and RT efficiency quality and Genomic DNA contamination control check-points.

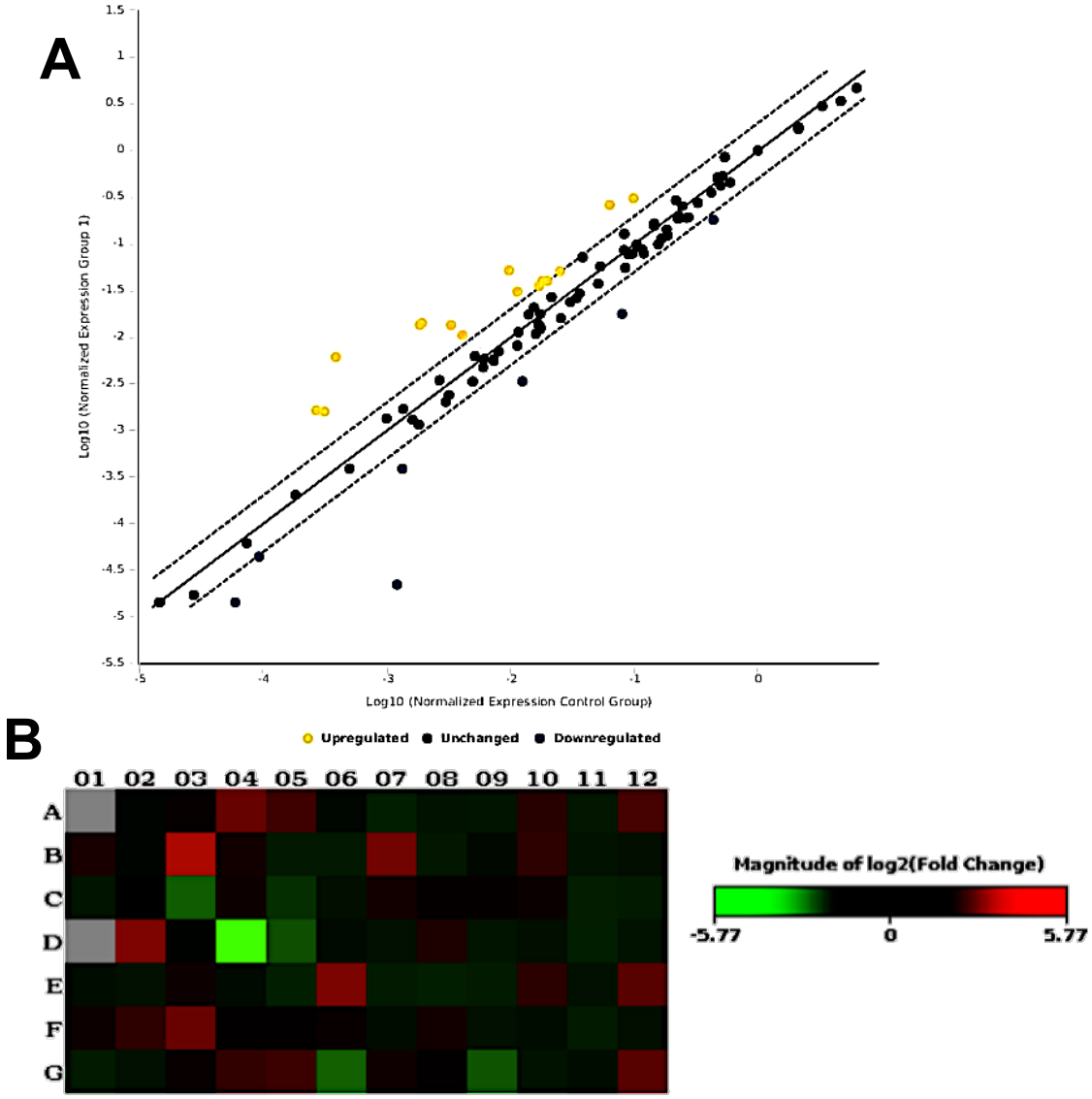

Figure 3.3. SEBTA-023 6 hours (group 1) hypoxia time-point RT^2 profiler PCR array: **a. scatter plot**, the y axis corresponds to the $\log_{10}$ of the $2^{-\Delta CT}$ 6 hours time-point group genes and the x axis to the $\log_{10}$ of the $2^{-\Delta CT}$ non-treated group genes. The upregulated genes match the yellow dots above the threshold line and the downregulated genes the blue dots underneath the threshold line. The black dots in between the threshold lines (dotted lines) correspond to unchanged expression genes. **b. heat map**, $\log_2$ of the $2^{-\Delta\Delta CT}$ 6 hours time-point group genes heat map's table. The expressions magnitude was estimated as high when $\log_2$ (fold change) was higher than 0 and low when $\log_2$ (fold change) was lower than 0.

Figure 3.3. shows 15 over-expressed genes, marked in yellow above the dotted threshold line and 6 under-expressed genes, marked in blue underneath the dotted threshold line.

The heatmap (Figure 3.3.b) shows that the genes *ANGPTL4* (A4), *CAIX* (B3), *DNA-Damage-Inducible Transcript 4* or *DDIT4* (B7), *Hexokinase 2* or *HK2* (D2), *NDRG1* (E6) and *PFKB4* (F3) were highly expressed with values between five and

eight fold. The B3 sample corresponds to the gene with the highest magnitude and, therefore, fold change (15,67).

Figure 3.3.b reported three samples meaningfully under-expressions. These samples were C3, D4, and G6 correspondent to the genes *Erythropoietin* (*EPO*), *HNF4A* and *TFRC*. The *HNF4A* gene had the highest magnitude and the lowest fold change value of -54,57. While *EPO* and *TFRC* had correspondent fold-changes of -4,17 and -4,53.

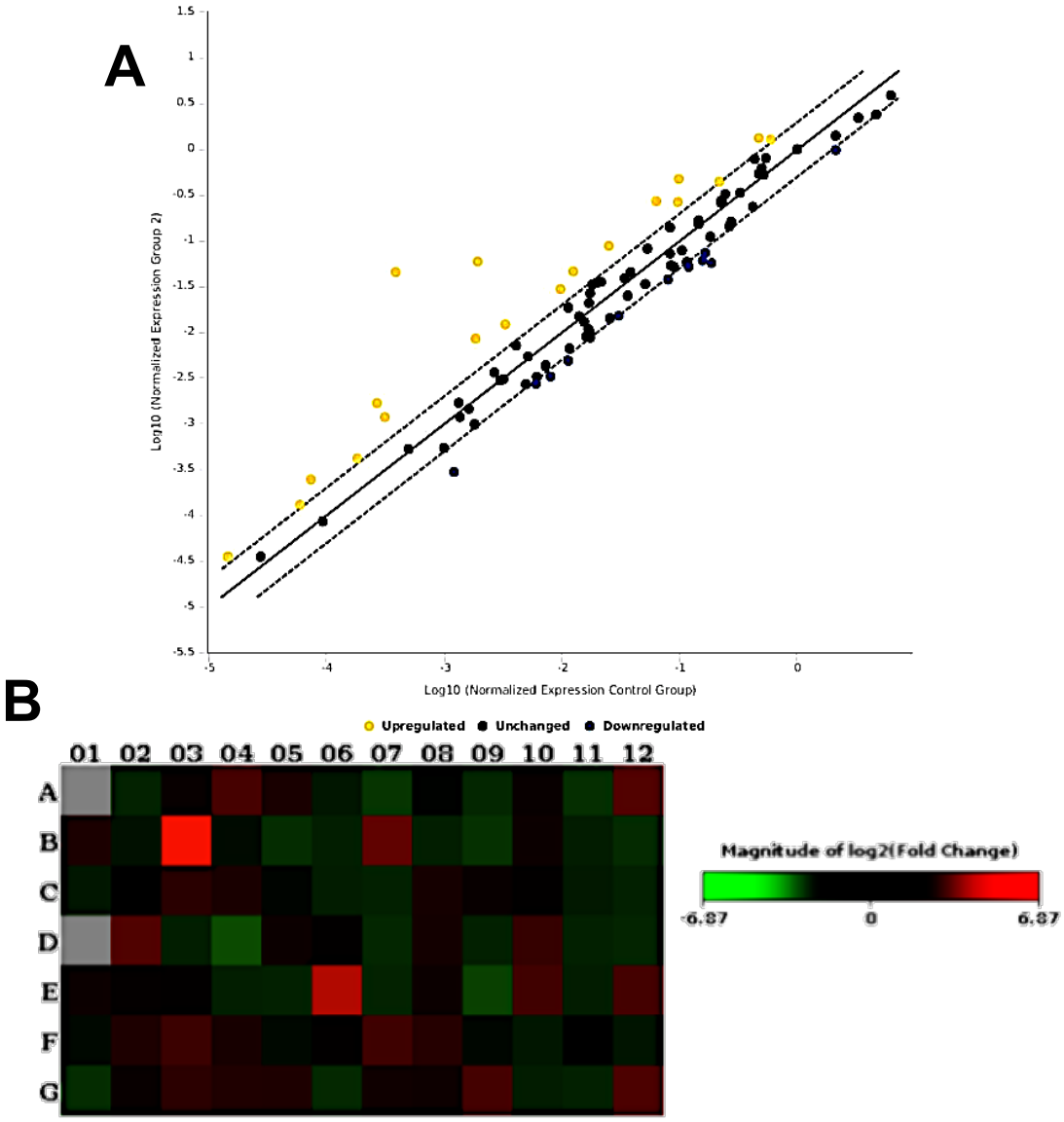

Figure 3.4. SEBTA-023 48 hours (group 2) hypoxia time-point RT^2 profiler PCR array: **a. scatter plot**, the y axis corresponds to the $\log_{10}$ of the $2^{-\Delta CT}$ 48 hours time-point group genes and the x axis to the $\log_{10}$ of the $2^{-\Delta CT}$ non-treated group genes. The upregulated genes match the yellow dots above the threshold line and the downregulated genes the blue dots underneath the threshold line. The black dots in between the threshold lines (dotted lines) correspond to unchanged expression genes. **b. heat map**, $\log_2$ of the $2^{-\Delta\Delta CT}$ 6 hours time-point group genes heat map's table. The expressions magnitude was estimated as high when $\log_2$ (fold change) was higher than 0 and low when $\log_2$ (fold change) was lower than 0.

The scatter plot exhibited in Figure 3.4.a confirms 21 over-expressed genes, marked in yellow above the dotted threshold line and seven under-expressed genes, marked in blue underneath the dotted threshold line.

Figure 3.4.b heatmap distinguishes at least eight samples with relatively noteworthy magnitudes. From these, *CAIX* (B3) and *NDRG1* (E6) are highly expressed. These genes respective fold changes were 116,97 and 30,48. Curiously, both genes were detected within the 6 hours time-point group with significant magnitudes and meaningful fold changes of 15,67 and 7,26 correspondingly.

The samples *ANGPTL4* (A4), *DDIT4* (B7), *HK2* (D2), *Pyruvate Dehydrogenase Kinase 1* or *PDK1* (E12), and *VEGFA* (G12) were also up-regulated. These genes fold-change values were 3,78, 6,28, 4,63, 3,68 and 4,23 fold, respectively. Except B7, that had a 0,17 lower fold-change in the 6 hours group, all other genes expression increased approximately 2 fold at 48 hours of hypoxia. In addition to these data, the *HNF4A* (D4) *gene* was meaningfully under-expressed, with a fold change of -4,06.

3.2 UP-029 and SEBTA-023 qRT-PCR arrays

The following qRT-PCR arrays were made in order to quantify and validate the expression of genes distinguished in the RT^2 profiler array. Each sample was ran at least 3 times, in order to increase significance of results.

Like the quality control parameters for the RT^2 array protocol, only RNA samples with the A_{260}:A_{230} ratio greater than 1.7 and the A_{260}:A_{280} ratio between 1.8 and 2.0 were considered as good quality to use in these experiments.

3.2.1 Hypoxia Inducible Factors 1α and 2α expression in GBM

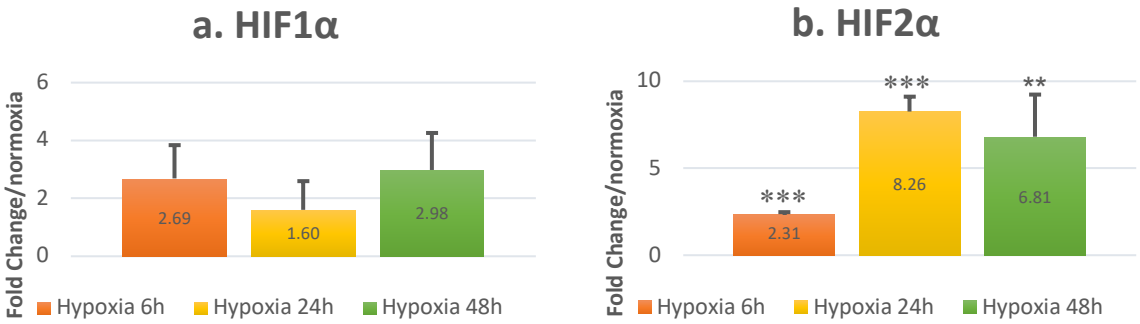

Figure 3.5. **UP-029 qRT-PCR assay**: **a**. *HIF1*α fold-change average; **b**. *HIF2*α fold-change average; 6 hours hypoxia time-point (orange), 24 hours hypoxia time-point (yellow) and 48 hours hypoxia time-point (green). Fold changes and significance levels are relative to the normoxia control (Fold-change = 1). P-values calculated with student t-test (Type 2, Tail 2) for significance levels of 0.05 (*), 0.01 (**) and 0.001 (***).

*HIF1*α expression in UP-029 cells was slightly up-regulated during hypoxia, as shown in Figure 3.5.a. However, these results were not significant (p-value > 0,05). Interestingly, the fold change of this gene at 24 hours was lower than both 6 and 48 hours.

Conversely to *HIF1*α, *HIF2*α expression in UP-029 cells was significant, as pictured in Figure 3.5.b. The highest over-expressions were detected in the 24 and 48 hours analysis, approximately 7 fold. Although up-regulated in the 6 hours analysis, *HIF2*α only increased 2 fold when compared to the control.

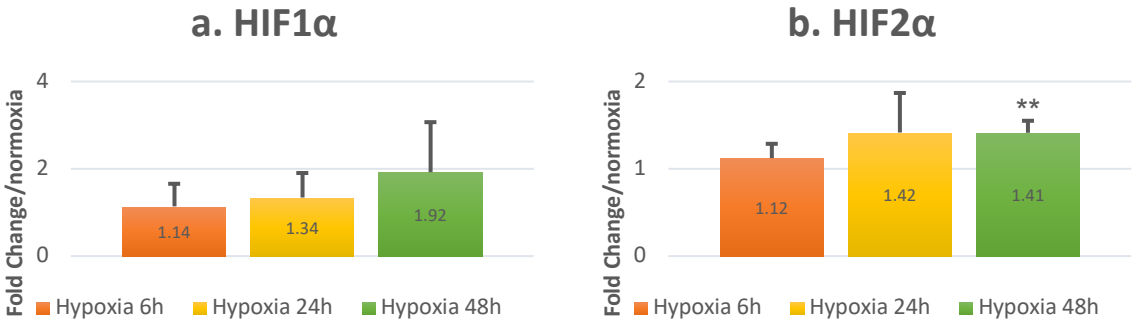

Figure 3.6. **SEBTA-023 qRT-PCR array**: **a**. *HIF1*α fold-change average; **b**. *HIF2*α fold-change average; 6 hours hypoxia time-point (orange), 24 hours hypoxia time-point (yellow) and 48 hours hypoxia time-point (green). Fold changes and significance levels are relative to the normoxia control (Fold-change = 1). P-values calculated with student t-test (Type 2, Tail 2) for significance levels of 0.05 (*), 0.01 (**) and 0.001 (***).

*HIF1*α was not significantly over-expressed in hypoxic SEBTA-023 cells compared to normoxic counterparts, as disclosed in Figure 3.6.a. Although our data

spotted an increase in *HIF1α* expression parallelly to the increase of hours in hypoxia, these values were not statistically significant.

The results in Figure 3.6.b, alike Figure 3.6.a, do not reveal any significant over-expression of *HIF2α* gene in SEBTA-023 cells. Again, the fold change values were all lower than 2 fold, for all hypoxia time-points.

3.2.2 Expression of angiogenic factors in hypoxic GBM cells

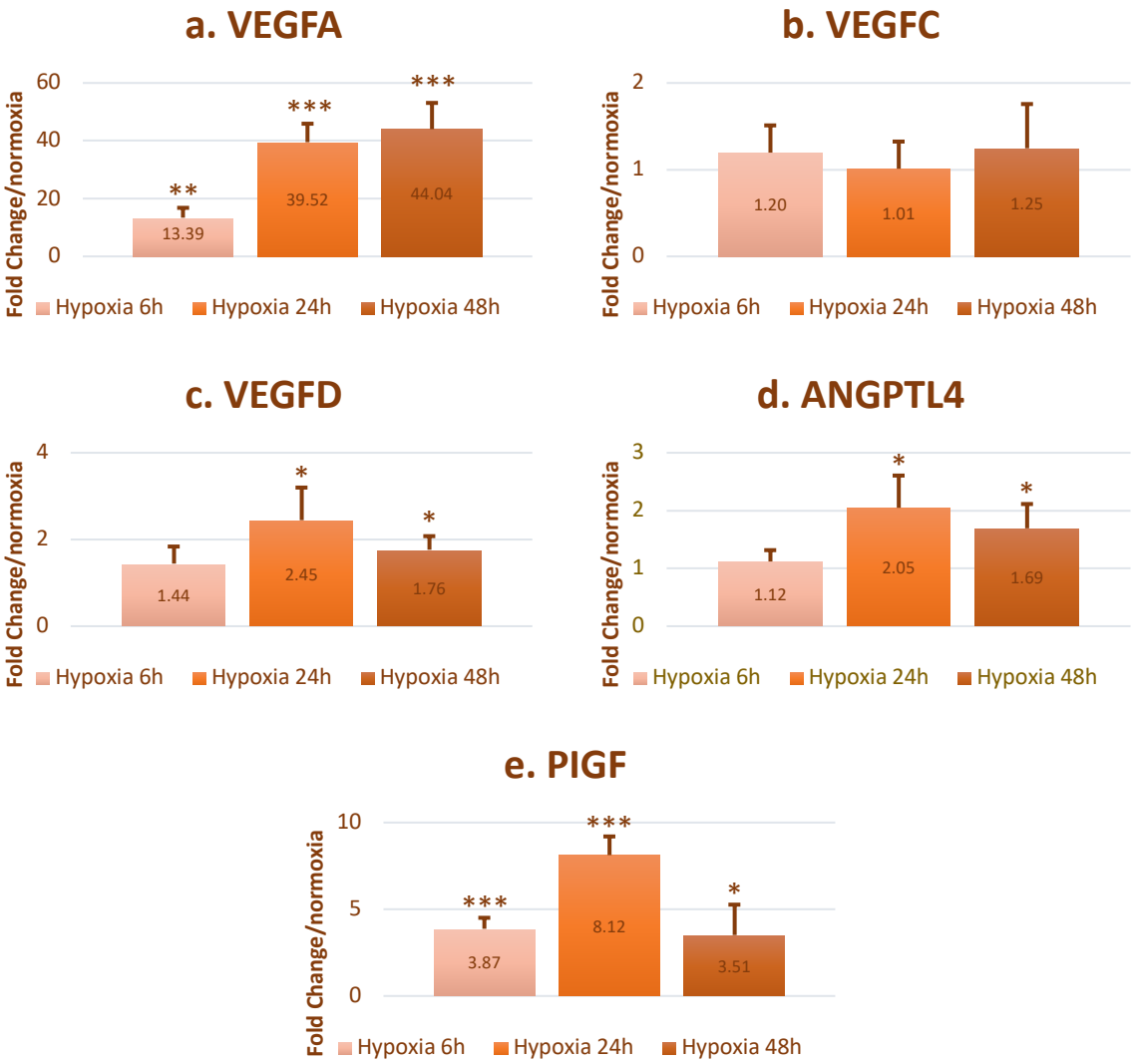

Figure 3.7. **UP-029 qRT-PCR array**: **a**. *VEGFA* fold-change average; **b**. *VEGFCA* fold-change average; **c.** *VEGFD* fold-change average; **d.** *ANGPTL4* fold-change average; **e.** *PIGF* fold-change average; fold change for 6 hours hypoxia (light orange), 24 hours (orange) and 48 hours (dark orange). Fold changes and significance levels are relative to the normoxia control (Fold-change = 1). P-values calculated with student t-test (Type 2, Tail 2) for significance levels of 0.05 (*), 0.01 (**) and 0.001 (***).

Figure 3.7.a shows a time dependent up-regulation of *VEGFA* in UP-029 cells during hypoxia. The fold-change values were 13,39, 39,52 and 44,04 for the 6, 24 and

48 hours of hypoxia, respectively. The expression of *VEGFC, VEGFD* and *ANGPTL4* did not change under hypoxic conditions (Figures 3.7.b-d). Contrarily, *PIGF* was over-expressed approximately 4 fold at both 6 and 48 hours of hypoxia (3.7.e). Still, the most impressive and significant result was at 24 hours hypoxia with an induction of approximately 8 fold.

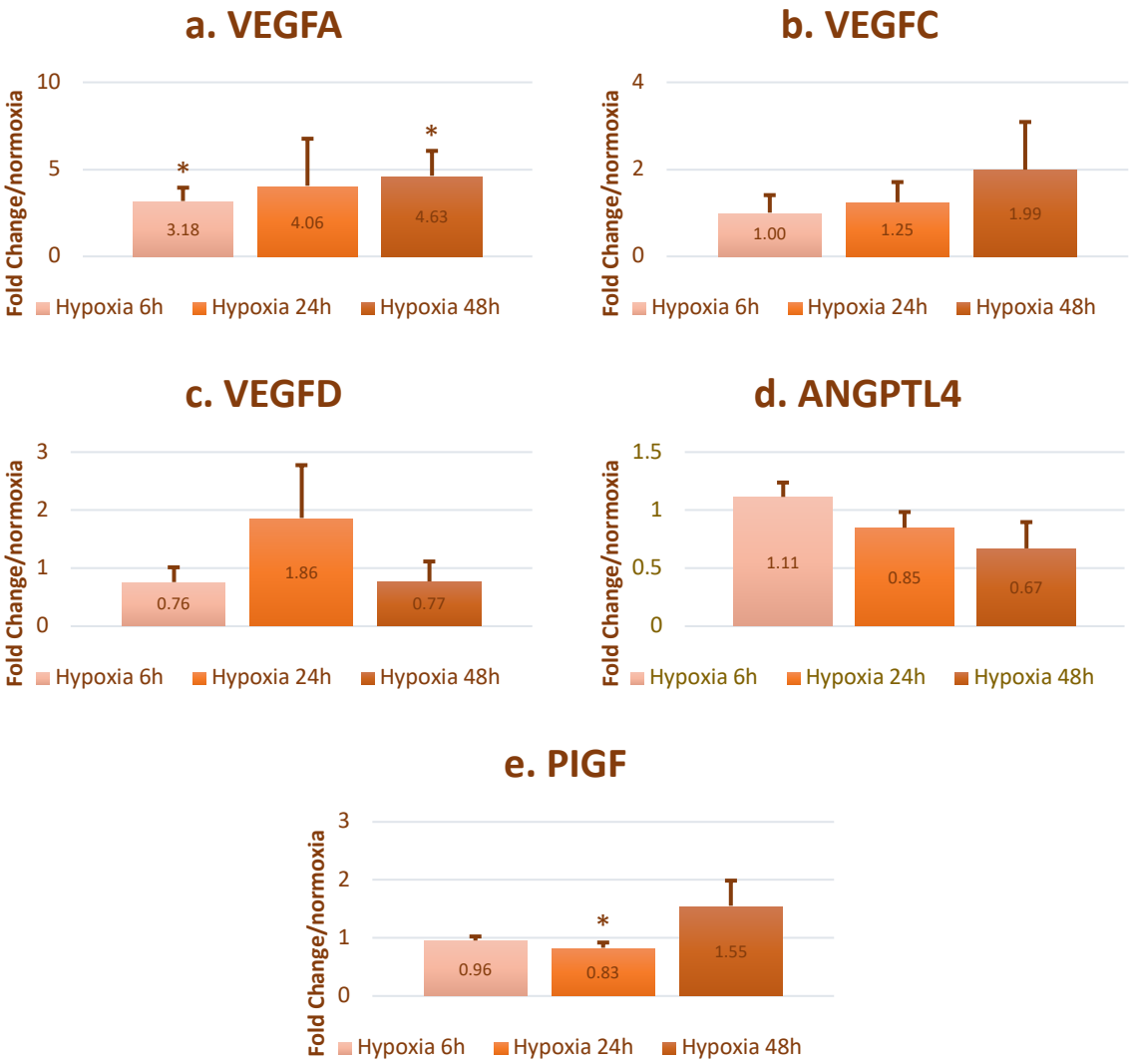

Figure 3.8. **SEBTA023 qRT-PCR array**: **a**. *VEGFA* fold-change average; **b**. *VEGFC* fold-change average; **c.** *VEGFD* fold-change average; **d.** *ANGPTL4* fold-change average; **e.** *PIGF* fold-change average; for 6 hours hypoxia (light orange), 24 hours (orange) and 48 hours (dark orange). Fold changes and significance levels are relative to the normoxia control (Fold-change = 1). P-values calculated with student t-test (Type 2, Tail 2) for significance levels of 0.05 (*), 0.01 (**) and 0.001 (***).

Figure 3.8.a refers to the *VEGFA* expression in the SEBTA-023 cell line. This gene was significantly induced, in a time-dependent manner, with fold change expression values of 3,18, 4,06 and 4,63 fold for the 6, 24 and 48 hours of hypoxia,

respectively. Expression of *VEGFC, VEGFD, ANGPTL4* and *PIGF* fold-expressions, did not significantly change (3.8.b-e).

3.2.3 Expression of Metabolic factors in hypoxic Glioblastoma

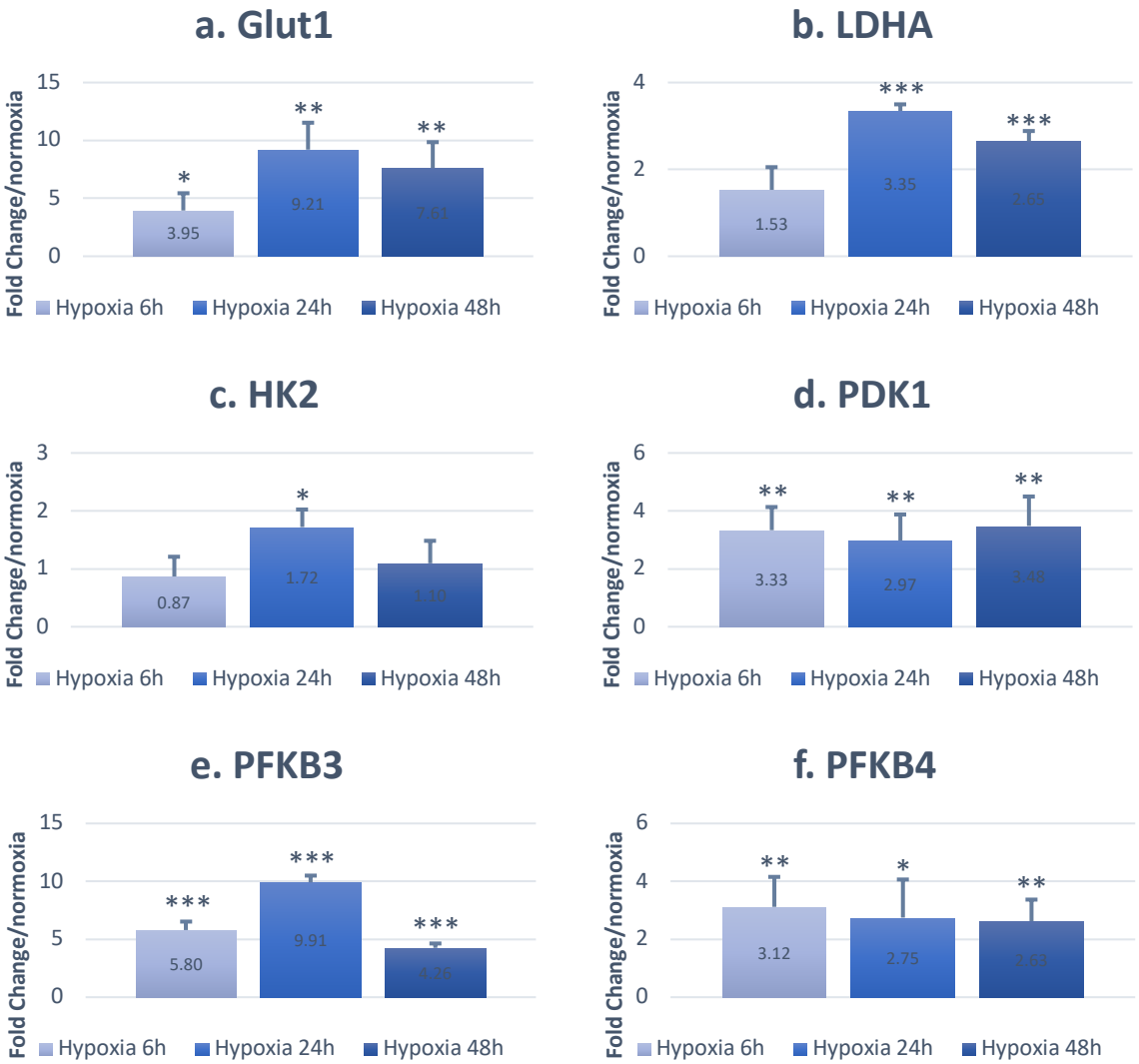

Figure 3.9. **UP0-29 qRT-PCR array**: **a**. *Glut1* fold-change average; **b**. *LDHA* fold-change average; **c.** *HK2* fold-change average; **d.** *PDK1* fold-change average; **e.** *PFKB3* fold-change average; **f.** *PFKB4* fold-change average; fold change for 6 hours hypoxia (light blue), 24 hours (blue) and 48 hours (dark blue). Fold changes and significance levels are relative to the normoxia control (Fold-change = 1). P-values calculated with student t-test (Type 2, Tail 2) for significance levels of 0.05 (*), 0.01 (**) and 0.001 (***).

GLUT1 gene (Figure 3.9.a), is significantly over-expressed in UP-029 cells, with correspondent fold-changes of 3,95, 9,21 and 7,61 for 6, 24 and 48 hours of hypoxia. *GLUT1* highest induction was concomitant with the 24 hours hypoxia. Likewise, *PFKB3* highest over-expression was at 24 hours of hypoxia (Figure 3.9.e). *PFKB3* gene is significantly induced in UP-029 cells with fold-change values of 5,80, 9,91 and 4,26 at 6, 24 and 48 hours of hypoxia. *LDHA* and *HK2* genes were not significantly

induced (Figures 3.9.b and 3.9.c). Contrarily, *PDK1* and *PFKB4* genes, were slightly over-expressed (Figures 3.9.d and 3.9.f). These genes reported fold change values at 6, 24 and 48 hours hypoxia were 3,33, 2,97 and 3,48 for *PDK1* and 3,12, 2,75 and 2,63 for *PFKB4.*

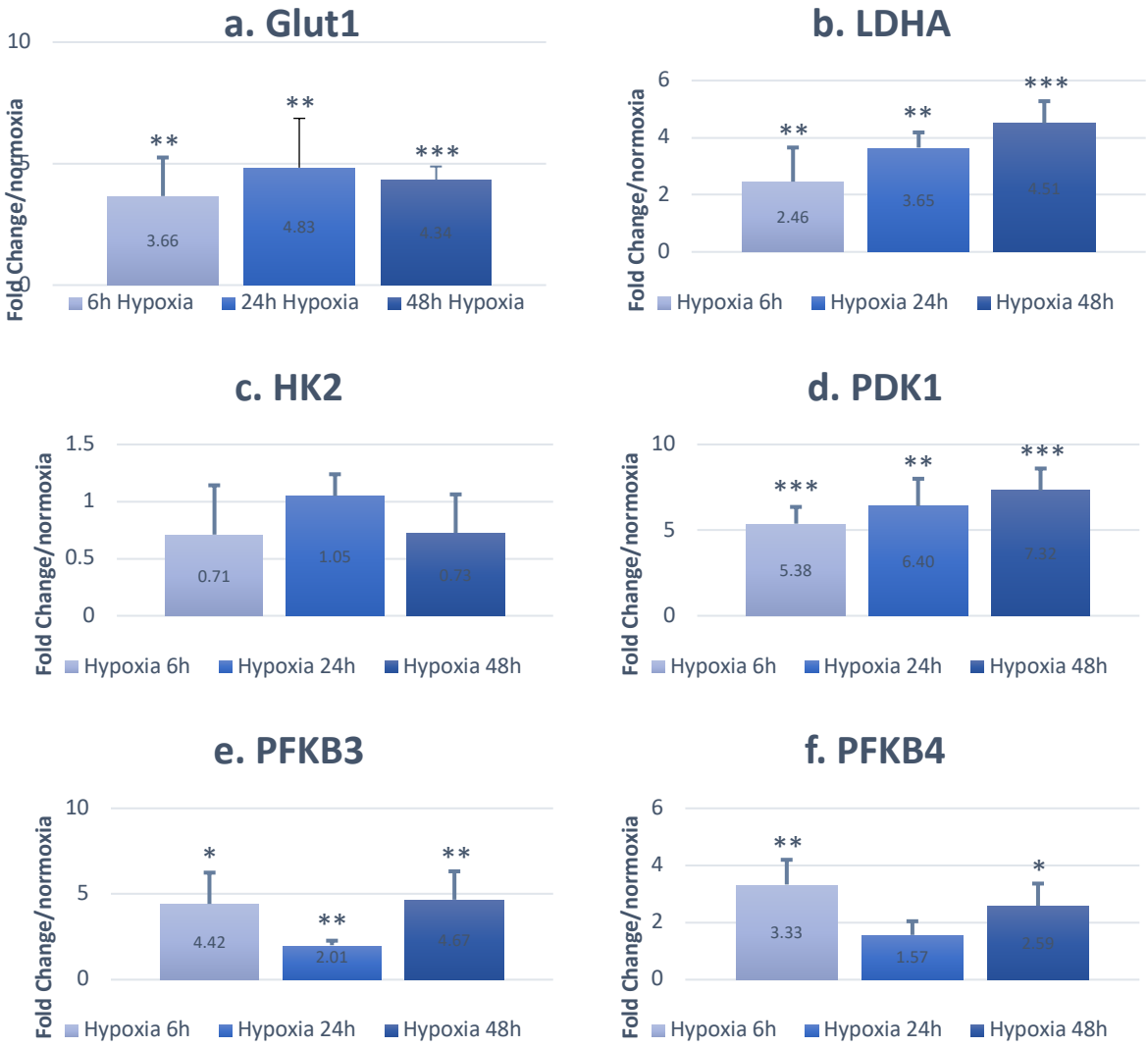

Figure 3.10. **SEBTA-023 qRT-PCR array**: **a**. *Glut1* fold-change average; **b**. *LDHA* fold-change average; **c.** *HK2* fold-change average; **d.** *PDK1* fold-change average; **e.** *PFKB3* fold-change average; **f.** *PFKB4* fold-change average; fold change for 6 hours hypoxia (light blue), 24h (blue) and 48h (dark blue). Fold changes and significance levels are relative to the normoxia control (Fold-change = 1). P-values calculated with student t-test (Type 2, Tail 2) for significance levels of 0.05 (*), 0.01 (**) and 0.001 (***).

Figure 3.10.a shows that *GLUT1* gene is induced in SEBTA-023 cells during hypoxia, with the highest expression at 24 hours. *GLUT1* fold change values were 3,66, 4,83 and 4,34 at the 6, 24 and 48 hours of hypoxia. *LDHA* was relatively over-expressed in a time-dependent manner (Figure 3.10.b). Starting with 2,46 fold at 6 hours hypoxia, this gene expression increased to 3,65 and 4,51 fold at 24 and 48

hours of hypoxia, respectively. Similarly, *PDK1* was more over-expressed with the hypoxia time increment (Figure 3.10.d). *PDK1* fold change values were 5,38, 6,40 and 7,32 for 6, 24 and 48 hours of hypoxia. *PFKB3* was significantly induced, especially at 6 and 48 hours, with correspondent fold change values of 4,42 and 4,67 fold (Figures 3.10.e).

Both *HK2* (Figure 3.10.c) and *PFKB4* (Figure 3.10.f) genes did not report major fold changes. *PFKB4* was only significantly induced at 6 and 48 hours with fold values of 3,33 and 2,59, respectively.

3.2.4 Expression of Invasion factors in hypoxic Glioblastoma

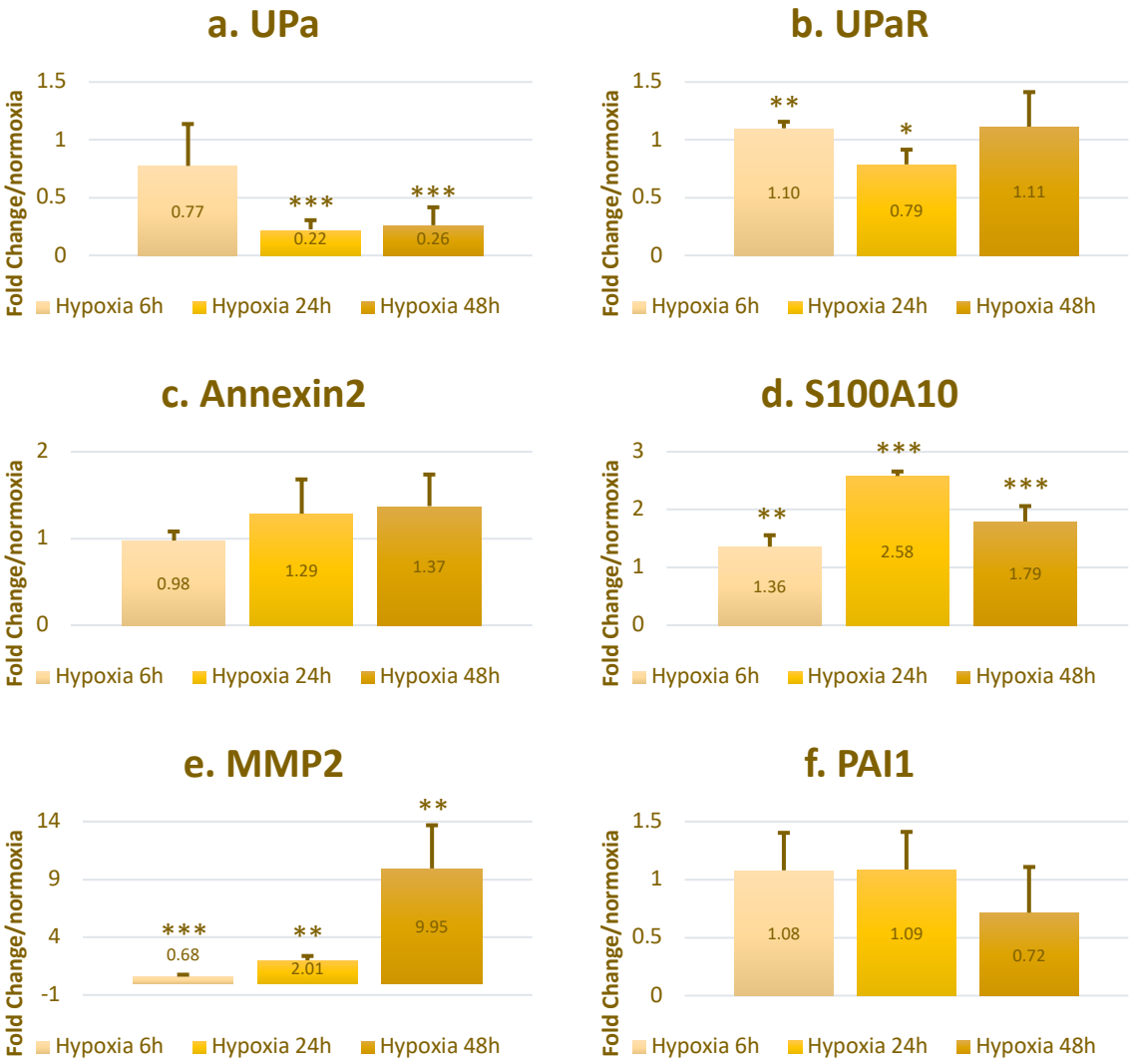

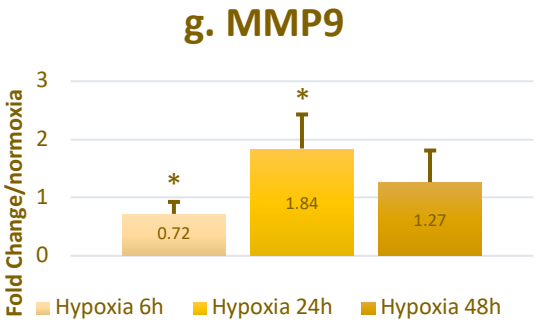

Figure 3.11. **UP-029 qRT-PCR array**: **a**. *UPa* fold-change average; **b**. *UPaR* fold-change average; **c.** *Annexin2* fold-change average; **d.** *S100A10* fold-change average; **e.** *MMP2* fold-change average; **f.** *PAI1* fold-change average; **g.** *MMP9* fold-change average; fold change for 6 hours hypoxia (light yellow), 24h (yellow) and 48h (dark yellow). Fold changes and significance levels are relative to the normoxia control (Fold-change = 1). P-values calculated with student t-test (Type 2, Tail 2) for significance levels of 0.05 (*), 0.01 (**) and 0.001 (***).

Figure 3.11 characterizes the expression of different invasion factors in UP-029 cells. It is observable that most of these genes did not change significantly. In fact, *Upa* and *PAI1* genes, charted in Figures 3.11.a and 3.11.f seemed to be down-regulated in a time-dependent fashion. *Upa* is significantly under-expressed in UP-029 GBM cells, with fold change values of 0,77, 0,22 and 0,26 at 6, 24 and 48 hours of hypoxia. The *UpaR*, *Annexin2*, *S100A10* and *MMP9* genes did not change significantly (3.11.b-d and 3.11.g). Interestingly, Figure 3.11.e, referent to *MMP2*, reported indeed a significant under-expression of 0,68 fold at 6 hours of hypoxia and an over-expression of 9,95 fold at 48 hours of hypoxia.

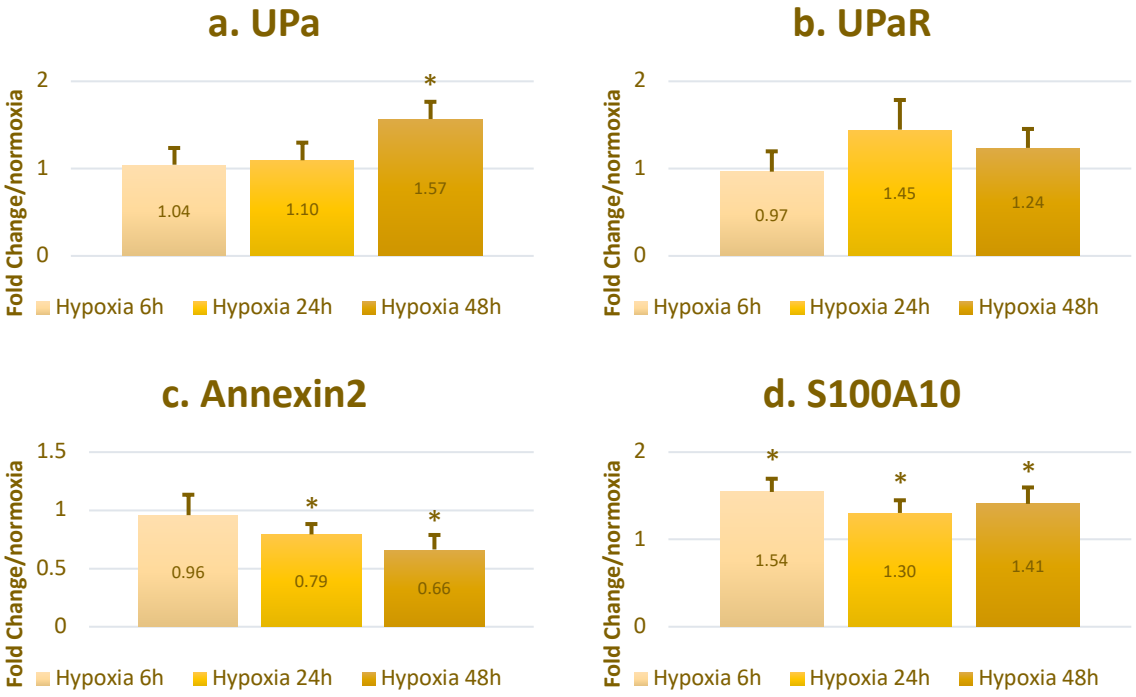

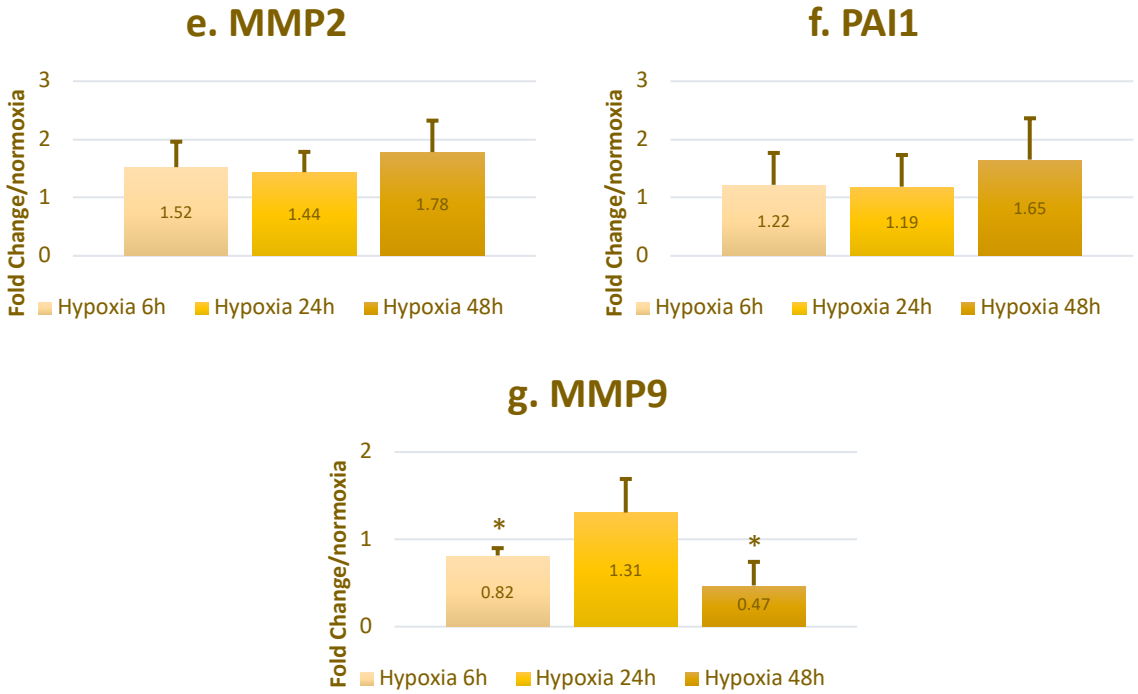

Figure 3.12. **SEBTA-023 qRT-PCR array**: **a**. *UPa* fold-change average; **b**. *UPaR* fold-change average; **c.** *Annexin2* fold-change average; **d.** *S100A10* fold-change average; **e.** *MMP2* fold-change average; **f.** *PAI1* fold-change average; **g.** *MMP9* fold-change average; fold change for 6 hours hypoxia (light yellow), 24h (yellow) and 48h (dark yellow). Fold changes and significance levels are relative to the normoxia control (Fold-change = 1). P-values calculated with student t-test (Type 2, Tail 2) for significance levels of 0.05 (*), 0.01 (**) and 0.001 (***).

No invasion genes analyzed were significantly up-regulated in SEBTA-023 cells undergoing hypoxia (Figure 3.12). Yet, *Annexin2* and *MMP9* were significantly under-expressed. *Annexin2* under-regulation followed a hypoxia time-dependent fashion, with fold values of 0,96, 0,79 and 0,56 fold at 6, 24 and 48 hours hypoxia. Also, *MMP9* was under-expressed at 6 and 48 hours of hypoxia with fold-changes of 0,82 and 0,47 fold.

3.2.5 Expression of other factors in hypoxic Glioblastoma

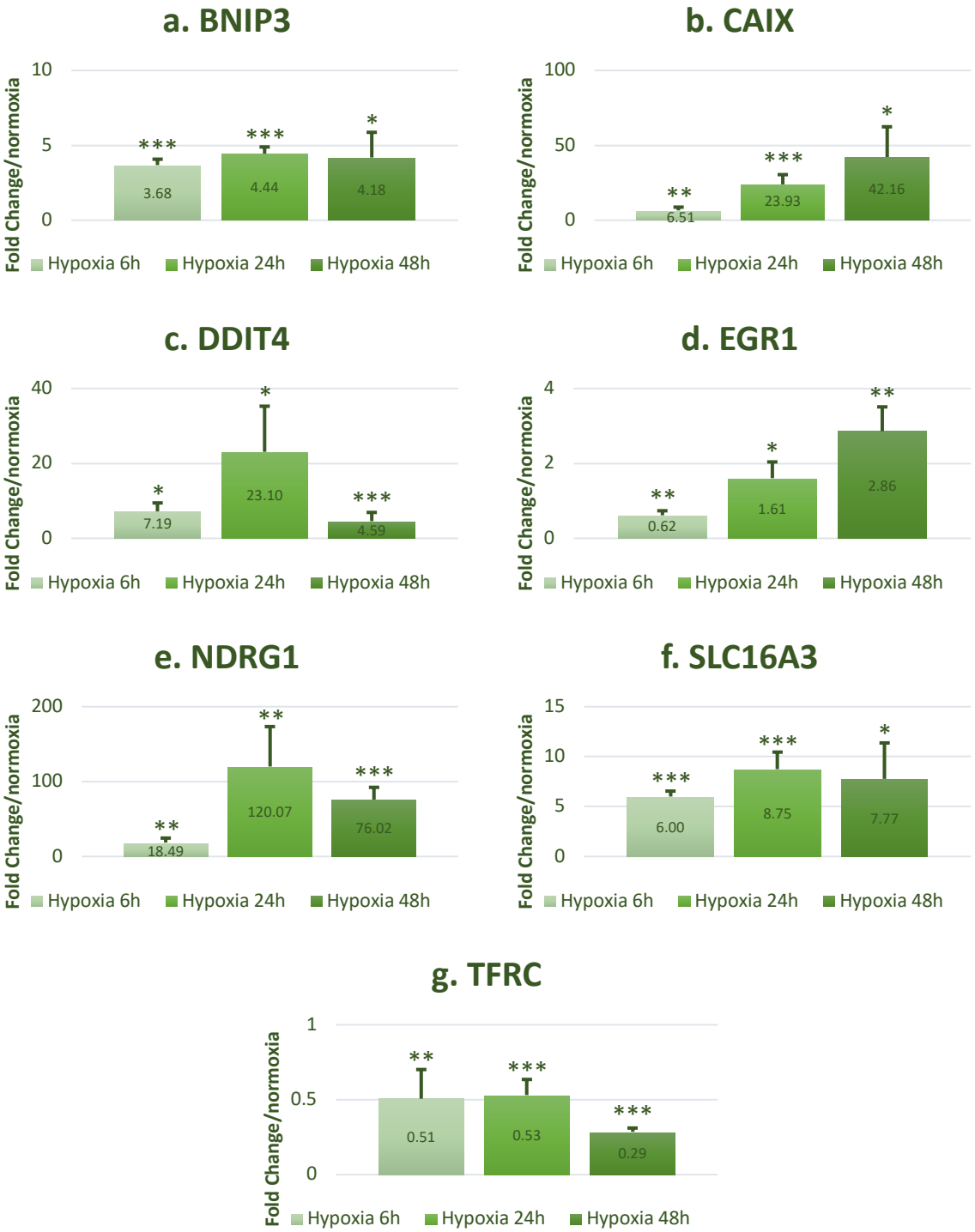

Figure 3.13. **UP-029 qRT-PCR array**: **a**. *BNIP3* fold-change average; **b**. *CAIX* fold-change average; **c.** *DDIT4* fold-change average; **d.** *EGR1* fold-change average; **e.** *NDRG1* fold-change average; **f.** *SLC16A3* fold-change average; **g.** *TFRC* fold-change average; fold change for 6 hours hypoxia (light green), 24 hours (green) and 48 hours (dark green). Fold changes and significance levels are relative to the normoxia control (Fold-change = 1). P-values calculated with student t-test (Type 2, Tail 2) for significance levels of 0.05 (*), 0.01 (**) and 0.001 (***).

Several factors were significantly induced in UP-029 cells. Figure 3.13.a shows *BNIP3* gene significantly induced by approximately 4 fold during hypoxia. *CAIX* is also

induced with significance in a hypoxia time dependent manner, as shown in Figure 3.13.b. This gene fold change values were 6,51, 23,93 and 42,16 at 6, 24 and 48 hours. Figure 3.13.c shows that *DDIT4* is significantly induced, especially at the 24 hours with a fold value of 23,10. *DDIT4 over*-expression values at 6 and 48 hours were 7,19 and 4,59, respectively. The same is verified for *NDRG1* and *SLC16A3* genes in Figures 3.13.e and 3.13.f. *NDRG1* pick of induction was at 24 hours with a fold value of 120,07, while at 6 and 48 hours was 18,49 and 76,02. *SLC16A3* reported fold-change values of 6,00, 8,75 and 7,77 at 6, 24 and 48 hours of hypoxia. *EGR1* was not significantly over-expressed in SEBTA-023 cells (Figure 3.13.d). *TFRC* gene, however, was significantly under-regulates with fold change values of 0,51, 0,53, and 0,29 at 6, 24 and 48 hours hypoxia (Figure 3.13.g)

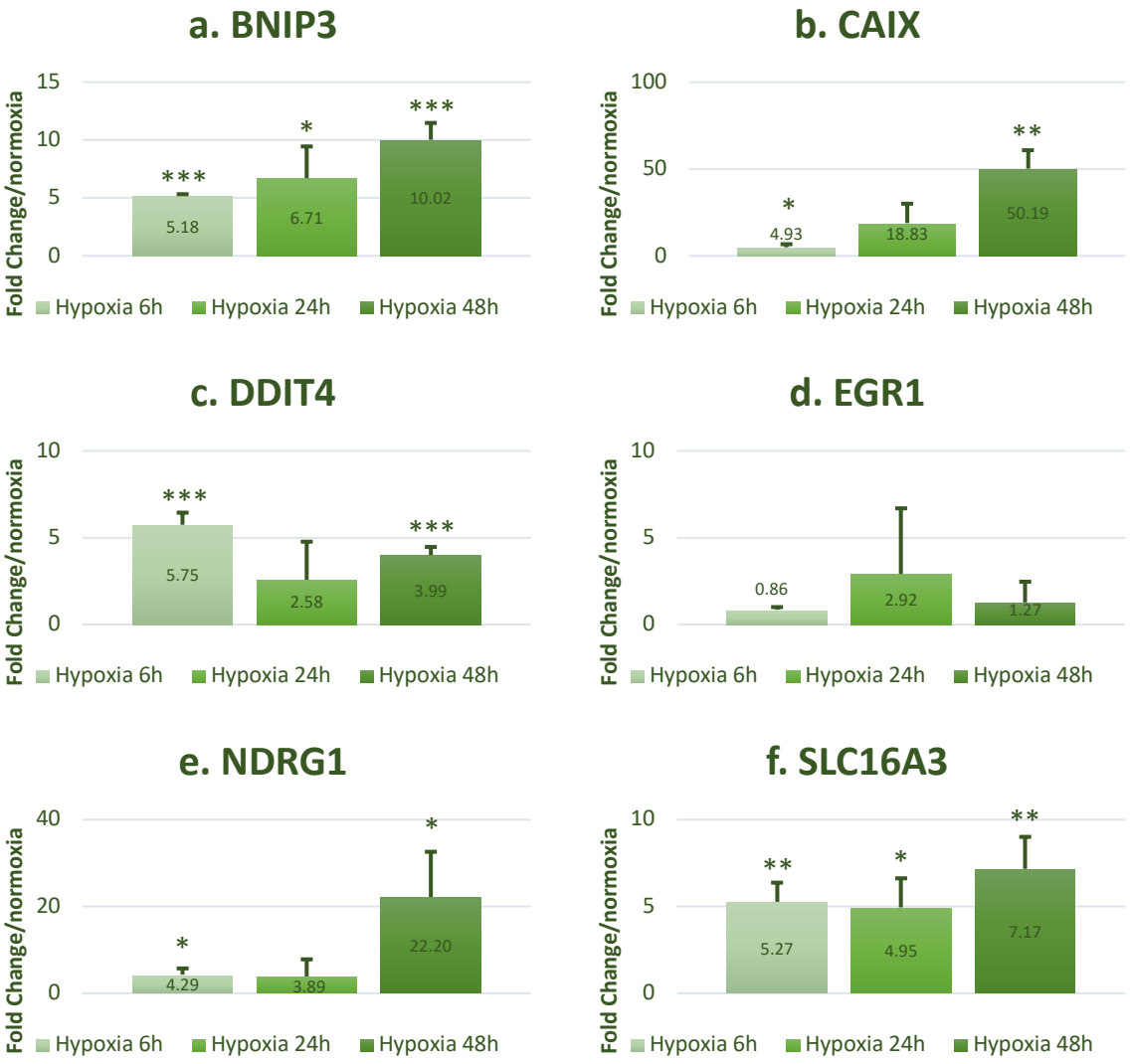

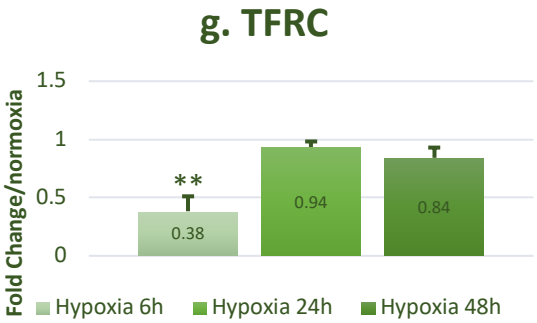

Figure 3.14. **SEBTA-023 qRT-PCR array**: *BNIP3* fold-change average; **b**. *CAIX* fold-change average; **c.** *DDIT4* fold-change average; **d.** *EGR1* fold-change average; **e.** *NDRG1* fold-change average; **f.** *SLC16A3* fold-change average; **g.** *TFRC* fold-change average; fold change for 6 hours hypoxia (light green), 24 hours (green) and 48 hours (dark green). Fold changes and significance levels are relative to the normoxia control (Fold-change = 1). P-values calculated with student t-test (Type 2, Tail 2) for significance levels of 0.05 (*), 0.01 (**) and 0.001 (***).

BNIP3 is significantly over-expressed in a time-dependent fashion in SEBTA-023 cells with fold change values of 5,18, 6,71 and 10,02 at 6, 24 and 48 hours of hypoxia (Figure 3.14.a). Analogously, *SLC16A3* gene expression, also seemed to follow similar induction, with 5,27, 4,95 and 7,17 fold at 6, 24 and 48 hours of hypoxia (Figure 3.14.f). *DDIT4* reported a significant over-expression as well, with fold values of 5,75, 2,58 and 3,99 during hypoxia (Figure 3.14.c). *CAIX* and *NDRG1* genes were highly over-expressed with significance in this cell line (Figures 3.14.b and 3.14.e). Both genes expression increased during hypoxia in a time-dependent manner. Indeed, at 6, 24 and 48 hours *CAIX* gene reported induction values of 4,93,18,83 and 50,19 fold, and *NDRG1* 4,29, 3,89 and 22,20 fold. *EGR1* gene was not over-expressed with significance in SEBTA-023 cells (Figure 3.14.d). *TFRC* was significantly under-regulated in this cell-line, with fold-values of 0,51, 0,53 and 0,29 fold at 6, 24 and 48 hours of hypoxia (Figure 3.14.g).

3.3 Protein expression analysis

Following the gene expression analysis, western-blot assays were performed in order to investigate how the differentially gene expressions were affecting protein expression.

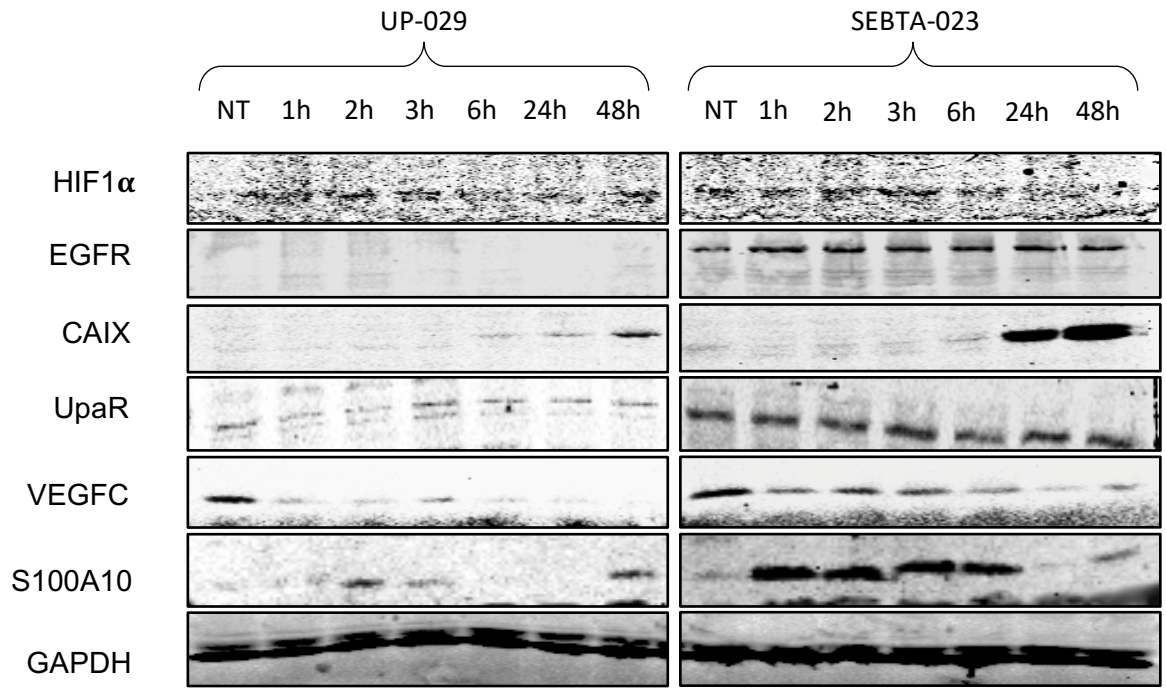

Figure 3.15. **UP-029 and SEBTA-023 western-blots** for Non-treated cells (NT) and 1, 2, 3, 6, 24 and 48 hours real hypoxia treatment. GAPDH blot for loading control.

Figure 3.15 reports the western-blot analysis made for HIF1α, EGFR, CAIX, UpaR, VEGFC, S100A10 and GAPDH proteins. The GAPDH blot in this analysis was performed as a loading control, to assure the equal loading of protein in each well of the eletrophoresis gel. This is indeed validated by the similar intensity of the bands pictured.

HIF1α blot was performed in order to validate the hypoxia treatment apllied to the cell lines. Yet, it is visible that the correspondent bands are quite fade. This may be the result of an inefficiency in the protein extraction protocol done outside the hypoxic chamber, since HIF1α protein is rapidily degradated in normoxia. This fact may have affected the interpretation of the protein transdution levels.

The CAIX blot was implemented, since the corresponding gene was reported as extremelly upregulated in the qRT-PCR analysis. EGFR protein detection was included in this section, since it is commonly up-regulated in GBM. Curiously, EGFR protein was not detected in the UP-029 samples. Yet, it was observed in the SEBTA-023 samples, inclusively in normoxia (NT). Additionaly, CAIX was also detecatable at 6, 24 and 48 hours in both cell lines. The expression of this protein seemed to increase

in a time-depend manner. Moreover, SEBTA-023 cell line had a higher protein signal than UP-029, during hypoxia.

Although UpaR, VEGFC and S100A10 proteins did not correspond to highly over-expressed genes in both cell lines, blots for these proteins were performed. The UpaR protein was detectable in both UP-029 and SEBTA-023 in all samples (inclusevely normoxia). However, SEBTA-023 showed an higher expression of this protein than UP-029. Similiarly, S100A10 protein was detectable in both cell lines. In SEBTA-023, S100A10 was extremely expressed at 1, 2, 3 and 6 hours of hypoxia. In UP-029 cell line, S100A10 was only detected in the 2, 3 and 48 hours of hypoxia, in a much lower level of expression. Curiously, VEGFC protein was fairly detectable in both UP-029 and SEBTA-023 cells in normoxia and its detection was slightly reduced concomitantly with the increment in time of hypoxia.

CHAPTER IV

DISCUSSION

4. Discussion

4.1 Hypoxia gene profile of the UP-029 and SEBTA-023 Glioblastoma cell lines

Through the RT^2 Hypoxia Profiler PCR array, the UP-029 and SEBTA-023 cell lines were analyzed for their hypoxic response panorama. The expression values were quantified for two different experimental groups (hypoxia 6 hours and hypoxia 48 hours) and then plotted against the respective non-treated control, as seen in Figures 3.1-3.4.

Overall, UP-029 cells were slightly more affected by the hypoxia treatments than SEBTA-023, once the first had a total of 56 differentially regulated genes while SEBTA-023 had 49. Summing both time-points, the UP-029 cell line had more differentially expressed genes than SEBTA-023, with a total of 24 repressed genes against 13. Despite this, SEBTA-023 reported more over-expressed genes (36 total) than the UP-029 cell line (32 total). For the graphical construction a cut off of two was used, however for the data interpretation only genes above 4 fold for over-expressed and -4 fold for under-expressed were considered, as to highlight the categorically evocative values.

Focusing in the UP-029 data, the number of induced genes at 6 and 48 hours of hypoxia was approximate, with 17 and 15 over-expressed genes respectively. Accordingly, the analysis of Figures 3.1.b and 3.2.b both time-points disclosed eight noteworthy over-expressed genes, with fold-change values above four fold. In the first experimental cohort, *ANGPTL4*, *CAIX*, *MXI1*, *PFKB3*, *PFKB4, NDRG1* and *PIGF* genes were substantially induced. With the exception of *PIGF*, all these genes maintained over-expressed in the 48 hours time-point. Plus, in this later time-set we detected an over-expression of *MMP9*'s gene, which was not reported at 6 hours of hypoxia.

Still in the UP-029 hypoxia time-point cohorts, it was clear an elevated gene repression in the 48 hours group. Comparing both time-course sets, 48 hours hypoxia reported 14 under-expressed genes, while at six hour's showed only eight (excluding the outlier). In the first data set, the *TFRC*, *HNF4A* and *EGR1*, genes were identified

as meaningfully under-regulated. From these, only *TFRC* gene was repressed in the 48 hours time-point. In addition to these, PLAU, *TP53*, *SERPINE1*, *EGLN2* (*Egl nine homolog two*), *LOX* (*Lysil Oxidase*), *HPRT* (*Hypoxanthine Phosphoribosyltransferase one*), *F3* (*Coagulation Factor III*), *MET* (*Hepatocyte Growth Factor Receptor*), *IER2* (*Immediate Early Response two*), *USF2* (*Upstream Transcription Factor two*), *NFKB1* and *HMOX1* (*Heme Oxygenase one*) were also down-regulated in the 48 hours hypoxia group.

In the SEBTA-023 hypoxia profiling data from Figures 3.3 and 3.4, it is noticeable an inferior number of over-expressed genes in the 6 hours cohort (15) than in the 48 hours (21). Observing the heatmaps data from Figures 3.3.b and 3.4.b, the previous number of genes considered indeed meaningful reduced drastically to 6 and 8 in the 6 and 48 hours time-points. At 6 hours of hypoxia *CAIX*, *ANGPTL4*, *NDRG1*, *PFKB4*, *HK2* and *DDIT4* genes were significantly over-expressed. All these were again reported as induced in the 48 hours cohort with addition of *PDK1* and *VEGFA*.

Hypoxia did not seem to have a broad repression influence in SEBTA-023 cell line. In fact, the sum of the two time-point analysis only reckoned a total of three meaningfully repressed genes. In the 6 hours time-point, *HNF4A*, *TFRC* and *EGR1* were repressed below minus four fold. Curiously, *HNF4A* reported -54,57 fold expression in the 6 hours cohort and was the only gene with a meaningful fold change in the 48 hours group.

Gathering these UP-029 and SEBTA-023 enquiries, the genes *ANGPTL4, NDRG1, CAIX, PFKB4* and *VEGFA* appear to be the most relevant induced genes. As for the repressed factors, both cell lines under-expressed the *HNF4A* and *TFRC* genes. Overall these induced and repressed genes seemed to be key factors in these cell lines hypoxia response and were further studied through qRT-PCR analysis, conjointly with other cell-line specific induced and repressed factors.

4.2 Validation of hypoxia differentially expressed genes in UP-029 and SEBTA-023 Glioblastoma cell lines

By means of qRT-PCR assays, an effort was made to validate common and specific differentially expressed genes in UP-029 and SEBTA-023 cell lines. To do so, each gene's PCR analysis was performed at least three times ($n > 3$).

4.2.1 Hypoxia Inducible Factors 1α and 2α expression in SEBTA-023 and UP-029 Glioblastoma cell lines

The major hypoxia regulators *HIF1α* and *HIF2α* were firstly investigated in order to evaluate how hypoxic response was induced in the studied time-points.

HIF1α is known and described in the literature as a main driver of the hypoxia adaptive response (Monteiro et al., 2017). The RT^2 profiler microarray reported *HIF1α* gene as under-regulated in UP-029 and not differentially expressed in SEBTA-023. This data was subsequently corroborated in both cell lines by the qRT-PCR analysis which did not report a significant *HIF1α*'s over-expression, with fold-changes below three fold (Figures 3.5.a and 3.6.a). Nonetheless, high fold-expression values were not expected, since this protein is not regulated at transcriptional level, but at protein level (R. H. Wenger, Kvietiko, Rolfs, Gassmann, & Marti, 1997). Furthermore, it has been shown that in normoxia, the levels of *HIF1α* mRNA are rapidly reduced (Gorlach, 2009). The fact that the RNA extraction was performed in normoxia may have affected this gene's mRNA levels.

The performed profiler array did not report any over- or under- expression of *HIF2α* gene in both cell lines during hypoxia. This is not a startling outcome since *HIF2α,* which is selectively expressed, is not as key in GBM hypoxic response as *HIF1α* (Monteiro et al., 2017). Moreover, it has been shown that *HIF2α* is preferentially expressed in Glioblastoma stem cells (GSCs) (Z. Li et al., 2009). Intriguingly, the CD44 stem cell marker was disclosed to interact specifically with *HIF2α* gene in order to stabilize its transcripts in both hypoxia and normoxia environments (Johansson et al., 2017). Through the qRT-PCR analysis, it was demonstrated that *HIF2α* gene was indeed up-regulated in UP-029 cells during hypoxia (Figures 3.5.b and 3.6.b). The SEBTA-023 cell line did not report any significant expression increment in *HIF2α*, with

its highest fold-change being 1,42 fold. Notwithstanding, the UP-029 cell line reported significantly high fold-change values for the 6 and 48 hours hypoxia time-points. It would be interesting to investigate if this cell-line expresses stem-markers such as CD44 to elucidate whether this cell line was originated from GSCs.

4.2.2 Angiogenic factors expression in SEBTA-023 and UP-029 Glioblastoma cell lines

In this section, we will analyze the expression of angiogenic factors in both UP-029 and SEBTA-023 cell lines. In this cohort, we verified the expression *ANGPTL4* and *VEGFA* genes previously distinguished in the RT^2 array. In addition, *PIGF* results are also reviewed in this segment due to its relevant results in the UP-029 qRT-PCR.

VEGFA reported as induced in both cell lines qRT-PCR (Figures 3.7.a and 3.8.a). Yet, in the UP-029 cell line *VEGFA* did not report such a high over-expression in the RT^2 array as in the qRT-PCR. Moreover, while in the RT^2 array the fold-expression decreased at 48 hours of hypoxia, in the qRT-PCR it was almost triplicated in a time-dependent fashion. The fact that UP-029 broadly over-expressed *VEGFA* more than the SEBTA-023 cell line, hints for a more aggressive phenotype (Chen et al., 2015). In the other hand, this observation may also suggest that this tumour cell line had origin in an astrocytoma precursor. Astrocytes naturally have *VEGFA* upregulated and in cancer this induction is even farther enhanced (Stefanik, 2013).

The *ANGPTL4* gene codes for a protein that has been implicated in GBM progression through the activation of Erk1/2 kinase (Brunckhorst, Wang, Lu, & Yu, 2010). Furthermore, *ANGPTL4* was recently reported as induced during GBM hypoxia (Beig et al., 2018). Agreeably with the literature, this factor was indeed induced, especially in the first 6 hours of hypoxia in the RT^2 hypoxia profiler array. Yet, the Figures 3.7.d and 3.8.d qRT-PCR analysis did not confirm the magnitude of the microarrays fold-inductions. Oppositely, the fold-change values were below the designated cut-off of relevance (2 fold) in both studied cell-lines. *ANGPTL4*'s induction has been associated with chronic hypoxia (Olbryt et al., 2014). Therefore, a possible explanation for the fact that *ANGPTL4* was not highly over-expressed in the qRT-PCRs may be that 48 hours was not enough for a fully chronic response.

PIGF was not meaningfully over-expressed in the SEBTA-023 RT^2 profiler and qRT-PCRs arrays. Yet, in the UP-029 cell line *PIGF* was significantly induced in the six and 24 hours time-points. In fact, *PIGF* highest expression in the qRT-PCR analysis occurred at 24 hours of hypoxia and in the microarray analysis was only reported in the 6 hours cohort. Curiously, PIGF was demonstrated to regulate *HIF1*α transcription in epithelial cells (Patel & Kalra, 2010).

The PIGF protein is known to enhance VEGFA mediated signaling and increase angiogenesis in GBM during hypoxia (Kaur et al., 2004). As denoted above, VEGFA was highly induced in the UP-029 cell line as well. The fact that both of these angiogenic factors are expressively induced not only suggests a synergist role between factors.

4.2.3 Expression of metabolic factors in SEBTA-023 and UP-029 Glioblastoma cell lines

This section will discuss and analyze the expression of metabolic factors in both UP-029 and SEBTA-023 cell lines.

In both studied cell lines, *GLUT1* and *LDHA* genes were not reported as differentially expressed in the RT^2 profiler array. However, both genes were reported as relevantly over-expressed in the qRT-PCRs, as shown in Figures 3.9.a and 3.10.a (*GLUT1*) and 3.9.b and 3.10.b (*LDHA*). In the UP-029 cell line both genes had their fold-induction peak at the 24 hours of hypoxia. Whereas in the SEBTA-023 cells the fold change of *GLUT1* and *LDHA* were higher at 24 and 48 hours of hypoxia respectively. Interestingly, *GLUT1* has been shown to be up-regulated in GSCs through VEGFA (Labak et al., 2016b). Studies regarding this interaction in GBM should be considered in the future.

The *PDK1* was fairly induced and maintained through the hypoxic time course in both cell lines, as shown in Figures 3.9.d and 3.10.d. The protein encoded by this gene is key in the ATP synthesis via glycolysis and is commonly up-regulated in cancer due to the tumour cells energy uptake (Labak et al., 2016b).

Similarly, to PDK1, PFKB3 and PFKB4 are central effectors of the glycolytic metabolism. In addition, PFKB4 has been found to be required in GSCs (Chesney et al., 2014). The fact that *PFKB4* was so noteworthy induced in both cell lines and detected in both arrays, hints once again for a stem-like phenotype. Interestingly, *PFKB3* was described in the literature as less induced than *PFKB4* (Chesney et al., 2014). This was indeed seen in Figures 3.10.e and f which correspond to the SEBTA-023 cell line. Yet, in Figures 3.10.e and f the opposite was reported, being *PFKB3* significantly more expressed than *PFKB4* in UP-029 cells. Interestingly, *PFKB3* was described as a resistance factor to radiotherapy (Gustafsson et al., 2018). According to the available information, the patients from whom this studies' cell lines were derived went through the standard therapy (which includes radiotherapy), previously to the biopsy extraction. The fact that only UP-029 up-regulated *PFKB3* instead of *PFKB4*, may infer for a more aggressive phenotype and an adaptive resistance mechanism of this cell line.

4.2.4 Expression of invasion factors in SEBTA-023 and UP-029 Glioblastoma cell lines

This section will disclose the differentially expression of invasion factors in both UP-029 and SEBTA-023 cell lines. Unexpectedly, none of the invasion genes analyzed through both cell lines qRT-PCR assays, were indeed significantly over-expressed. Furthermore, only *MMP9* was reported as over-expressed in the RT^2 profiler array.

Both *UPA* and *UPAR* genes are normally over-expressed in GBM normoxia (Brat et al., 2004). Therefore, it was not expected great fold-increments of these genes. Also, AnnexinA2 reported low fold-change values, however we extrapolate that it might be an later event in hypoxic response. Furthermore, *S100A10*, which was not significantly over-expressed, is ubiquitously expressed and regulated at protein levels (Madureira P, O'Connell P, Surette A, et. al. 2012).

PAI1 is an inhibitor of the tPA and uPA plasminogen activation systems and is described as up-regulated during hypoxia (Kaur et al., 2005). However, *PAI1* was not significantly over-expressed in the qRT-PCR assays of both cell lines.

Since *MMP2* and *MMP9* are known to be regulated by HIF2α, an increase of these gene's expression was not expected in the SEBTA-023 cell line (Li N, Whang H, Zhang J, Zhao E, 2016). Conversely, the UP-029 reported an over-expression of *HIF2*α gene. Indeed, MMP9 was over-expressed in the 48 hours cohort of the RT^2 array. Yet, *MMP2* was not relevantly induced in the qRT-PCR. Curiously, *MMP9* is reported in the literature as more induced than *MMP2* in primary GBM's (Choe et al., 2002).

4.2.5 Expression of other hypoxia related genes in SEBTA-023 and UP-029 Glioblastoma cell lines

This last gene expression analysis section will focus in varied factors, non-specifically integrated in a hypoxic feature such as the above nominated.

The *BNIP3* gene codes for a pro-apoptotic protein of the Bcl-2 family. In normal conditions its expression is low in brain. In GBM, BNIP3 expression in highly induced during hypoxia. Nevertheless, BNIP3 protein has been reported to be sequestered in the nucleus of GBM cells to block their ability of association with the mitochondria and inducing cellular death (Burton, Henson, Baijal, Eisenstat, & Gibson, 2006). Accordingly, BNIP3 was indeed reported as over-expressed in the RT^2 profiler and qRT-PCR arrays.

The *DDIT4* gene codes for a protein which functions as an mTOR inhibitor. Yet, in GBM over-expression of this protein is associated with poor prognosis (Pinto et al., 2017). *DDIT4* gene was indeed already reported as up-regulated during hypoxia in GBM (Mongiardi et al., 2016). However, the mechanisms through which DDIT4 promotes GBM are poorly understood. Although relatively upregulated in the SEBTA-023 cell line, the most prominent *DDIT4* induction was reported in UP-029 at 6 hours of hypoxia. This result validates *DDIT4* as a hypoxia-induced factor in GBM.

SLC16A3 has been reported as a poor outcome marker and as over-expressed in astrocytes and GSCs during hypoxia. High expression levels of this gene were found especially in the non C-GIMP than any other subtype of GBM. Curiously, the protein coded by this gene is known to involved in the glycolytic cycle in non-

neoplastic neural stem-cells (Lim et al., 2014). The significant over-expression of this gene in both cell lines suggests an non C-GIMP phenotype, as well as astroglial characteristics.

TFRC protein functions as an iron transporter and is normally up-regulated in cancer stem cells (Schonberg et al., 2015). Curiously, this gene was reported with under-expression values in the RT^2 profiler array. Accordingly, *TFRC* was also under-expressed in its qRT-PCRs analysis. Yet, there is no reference in the literature of the repression of this gene in GBM hypoxia, pointing it out as a novel marker in need of further studies.

Both *NDRG1* and *CAIX* genes were the leading over-expressed factors of the present section. In fact, both these genes are described in GBM hypoxia literature. *CAIX* gene is related with the acid/base homeostasis (Monteiro et al., 2017). Indeed, this gene is a known marker of previous or current chronic hypoxia (Harun M. Said et al., 2008). Concurrent with the literature, *CAIX* was indeed over-expressed in the RT^2 profiler and qRT-PCR arrays and its inducement was directly proportional to the increment of hypoxia hours in both cell lines. Additionally, *CAIX* is a known biomarker of chemo- and radiotherapy resistance (Monteiro et al., 2017). Knowing that the patients from whom the cell-lines were derived went through standard therapy, we may extrapolate that the high levels of *CAIX* as early as 6 hours of hypoxia may be derived from an adaptive resistance. Also, *NDRG1* seems to have a meaningful role as a tumour suppressor in cancer and is transcriptional regulated by *HIF1*α in acute hypoxia (Harun M. Said et al., 2008; Harun Muayad Said et al., 2017). Indeed, we observed significant over-expression of this gene at 24 hours in UP-029 cells with concomitant decrease at 48 h of hypoxia. This was previously reported in other studies (Harun Muayad Said et al., 2017). Nevertheless, in the SEBTA-023 cell line, the *NDRG1* gene suffered an over-expression increment throughout the hypoxia time-course. A possible justification for this result could be that the SEBTA-023 suffered a delayed acute hypoxia response.

4.3 Protein levels analysis in SEBTA-023 and UP-029 Glioblastoma cell lines

In this section we will analyze the levels of expression of proteins in both UP-029 and SEBTA-023 GBM cell lines, during hypoxia.

HIF1α expression was detectable throughout both cell line's hypoxia time-points. HIF1α signal was not extremely high due to the fast protein degradation. Yet, despite the correspondent gene fold-change values were not significant, there is an increase of the protein levels. Once more, it is confirmed that *HIF1α* is regulated not at transcriptional, but protein level.

EGFR was added to this experiment since it is commonly up-regulated in GBM, especially in the primary subtype (HONGSHENG et al., 2017). Curiously, this protein was only detectable in SEBTA-023 samples. From these results, we query whether SEBTA-023 may be an primary GBM.

CAIX protein signal was detected in both cell lines at 6, 24 and 48 hours of hypoxia. This results are in concordance with the correspondent gene expression values obtained through qRT-PCR. Once more, the detection of CAIX at 6 hours of hypoxia may be a result of an adaptive resistance mechanism. Curiously, this protein was more predominant in the SEBTA-023 cell line.

UPAR gene was not significantly over-expressed in UP-029 and SEBTA-023 cells during hypoxia in opposite to what was expected. However, we detected UPAR protein in both cell lines, especially in the SEBTA-023 samples. We extrapolate that the induction of the uPA system in the this specific cell line may be an later event and more time-points should be added to this experiment in order to verify this.

VEGFC was highly detectable in both cell lines during both normoxia and hypoxia. Peculiarly, this protein levels seem to decrease in a time-depend manner, during hypoxia. However, there is no reports in the literature of this fact or VEGFC role in GBM hypoxia.

S100A10 was detectable in both cell lines. In the UP-029, protein levels could be seen at 2, 3 and 48 hours of hypoxia, while in SEBTA-023 it could be seen at 1, 2, 3, 4 and 48 hours of hypoxia. This shows that S100A10 is indeed regulated at protein level, since it gene expression values were maintained. In addition, it demonstrates that the protein levels of AnnexinA2 were increased in these time-points, since without the bonding to annexin, S100A10 is immediately degraded.

Overall, we extrapolate that the low detection of invasion proteins in these cell lines may be a late event. The activation of metabolic and angiogenic mechanisms seem to be an earlier event in the hypoxic response. Reaching the a critical stage of survival, in which these signaling features are not enough, cells finally activate invasion as a chronic response. Therefore, more time-points such as 72 and 48 hours of hypoxia should be added in future studies. Furthermore, the low protein signal in the UP-029 cells, especially in the uPAR blot, may be derived of complications in the protein extraction or even western-blot sample preparation protocols.

CHAPTER V

CONCLUSION

5. Conclusion

The relevance of this research work relies especially in the poor prognosis and low overall-survival of GBM patients. Glioblastoma is highly characterized by a hypoxic phenotype which leads to invasion, angiogenesis and metabolic shift, all crucial steps of carcinogenesis. Understanding the molecular mechanisms underlying hypoxia in GBM is therefore of the highest relevance.

In the present study SEBTA-023 and UP-029 biopsy-derived cell lines were used in order to identify and validate hypoxia-triggered factors that may be contributing to GBM progression and relapse. In addition, an approach to characterize the studied cell lines was made throughout this study. Our results distinguished several genes related with specific hypoxia-features, such as angiogenesis and the metabolic switch. This study identified, *ANGPTL4, NDRG1, CAIX, PFKB4*, *VEGFA*, *PIGF*, *PDK1*, *PFKB3*, *PFKB4*, *BNIP3*, *CAIX*, *DDIT4*, *NDRG1* and *SLC16A3* as genes that were up-regulated and *HNF4A* and *TFRC* as down-regulated genes during hypoxia in GBM cells. Indicating that these genes might be important for hypoxia induced GBM pathogenesis. Moreover, revising the panel of differentially expressed genes, our data suggested a stem-like phenotype of the investigated cell lines. This should be confirmed by immune-staining with specific stem cell markers, such as CD44. Additionally, we detected low invasion genes and proteins expressions in both cell lines. We hypothesize that these factors might be regulated in response to chronic hypoxia. Curiously, our findings suggest PFKB3 as a possible novel resistance biomarker in GBM. Additionally, we hypothesize TFRC as having an important role as a tumour suppressor.

CHAPTER VI

FUTURE PERSPECTIVES

6. Future perspectives

In the future, it would be interesting to repeat this research with more GBM cellular types. Since GBM tumours are highly heterogeneous, elevating the number of lines in this study would bring more selectivity in targeting novel markers of hypoxia invasion from wide panels. Also, both RT^2 profiler arrays and qRT-PCRs should be performed for a higher n, in order to increase the results significance and avoid fold regulations miss-interpretations. Moreover, more hypoxia time-point should be considered in order to fully evaluate chronic hypoxic response, especially in invasion genes and proteins.

To confirm and validate the role of each one of the supposed novel markers, functional assays in hypoxia should be performed. Studies should be conducted in order to understand how standard treatment affects the expression of *PFKB3*. For example, studies regarding the detection of this protein in biopsies pre- and post-standard treatment, as well functional studies in GBM cell lines. In addition, *TFRC* knock-out assays should be done in order to understand the relevance of this gene's repression.

CHAPTER VII

BIBLIOGRAPHY

7. Bibliography

Alcantara Llaguno, S. R., & Parada, L. F. (2016). Cell of origin of glioma: biological and clinical implications. *British Journal of Cancer* , *115*, 1445–1450. https://doi.org/10.1038/bjc.2016.354

Amador-Arjona, A., Cimadamore, F., Huang, C.-T., Wright, R., Lewis, S., Gage, F. H., & Terskikh, A. V. (2015). SOX2 primes the epigenetic landscape in neural precursors enabling proper gene activation during hippocampal neurogenesis. *PNAS* , 1936–1945. https://doi.org/10.1073/pnas.1421480112

Arif, S. H., Arshad, A. P., Abdul, R. B., Altaf, U. R., Malik, N. K., Chibber, S. S., … Kirmani, A. (2015). EGFR and PTEN Gene Mutation Status in Glioblastoma Patients and their Prognostic Impact on Patient's Survival. *Journal of Carcinogenesis and Mutagenesis*, *6*(2). https://doi.org/10.4172/2157-2518.1000218

Arya, M., Shergill, I. S., Williamson, M., Gommersall, L., Arya, N., & Patel, H. R. (2005). Basic principles of real-time quantitative PCR. *Expert Review of Molecular Diagnostics*, *5*(2), 209–219. https://doi.org/10.1586/14737159.5.2.209

Balesaria, S., Brock, C., Bower, M., Clark, J., Nicholson, S., Lewis, P., … Fisher, R. (1999). Loss of chromosome 10 is an independent prognostic factor in high-grade gliomas. *British Journal of Cancer*, *81*(8), 1371–1377. Retrieved from https://www.ncbi.nlm.nih.gov/pmc/articles/PMC2362970/pdf/81-6693403a.pdf

Barani, I. J., & Larson, D. A. (2015). Radiation Therapy of Glioblastoma. *Cancer Treatment and Research*, *163*, 49–73. https://doi.org/10.1007/978-3-319-12048-5_4

Beig, N., Patel, J., Prasanna, P., Hill, V., Gupta, A., Correa, R., … Tiwari, P. (2018). Radiogenomic analysis of hypoxia pathway is predictive of overall survival in Glioblastoma. *Scientific Reports*, *8*(1), 7. https://doi.org/10.1038/s41598-017-18310-0

Brat, D. J., Castellano-Sanchez, A. A., Hunter, S. B., Pecot, M., Cohen, C., Hammond, E. H., … Van Meir, E. G. (2004). Pseudopalisades in glioblastoma are hypoxic, express extracellular matrix proteases, and are formed by an actively migrating cell population. *Cancer Research*, *64*(3), 920–927. Retrieved from http://www.ncbi.nlm.nih.gov/pubmed/14871821

Brown, M. J. (1999). The Hypoxic Cell. *Cancer Research*, *59*(23), 5863–5870. Retrieved from http://www.ncbi.nlm.nih.gov/pubmed/8402639

Brunckhorst, M. K., Wang, H., Lu, R., & Yu, Q. (2010). Angiopoietin-4 Promotes Glioblastoma Progression by Enhancing Tumor Cell Viability and Angiogenesis. *Cancer Research*, *70*(18), 7283–7293. https://doi.org/10.1158/0008-5472.CAN-09-4125

Burnet, N. G., Thomas, S. J., Burton, K. E., & Jefferies, S. J. (2004). Defining the tumour and target volumes for radiotherapy. *Cancer Imaging*, *4*, 153–161. https://doi.org/10.1102/1470-7330.2004.0054

Burton, T. R., Henson, E. S., Baijal, P., Eisenstat, D. D., & Gibson, S. B. (2006). The pro-cell death Bcl-2 family member, BNIP3, is localized to the nucleus of human glial cells: Implications for glioblastoma multiforme tumor cell survival under hypoxia. *International Journal of Cancer*, *118*(7), 1660–1669. https://doi.org/10.1002/ijc.21547

Cabrera, A. R., Kirkpatrick, J. P., Fiveash, J. B., Shih, H. A., Koay, E. J., Lutz, S., … Chang, E. (2016). Radiation therapy for glioblastoma: Executive summary of an

American Society for Radiation Oncology Evidence-Based Clinical Practice Guideline. *Practical Radiation Oncology*, *6*(4), 217–225. https://doi.org/10.1016/J.PRRO.2016.03.007

Castaldo, S. A., Freitas, J. R., Conchinha, N. V., & Madureira, P. A. (2016). The Tumorigenic Roles of the Cellular REDOX Regulatory Systems. *Oxidative Medicine and Cellular Longevity*, *2016*, 1–17. https://doi.org/10.1155/2016/8413032

Cathcart Jillian, Pulkoski-Gross Ashleigh, & Cao Jian. (2015). Targeting matrix metalloproteinases in cancer: Bringing new life to old ideas. *Genes & Diseases*, *2*(1), 26–34. https://doi.org/10.1016/J.GENDIS.2014.12.002

Chalhoub, N., & Baker, S. J. (2009). PTEN and the PI3-Kinase Pathway in Cancer. *Annual Review of Pathology: Mechanisms of Disease*, *4*, 127–150. https://doi.org/10.1146/annurev.pathol.4.110807.092311

Chandrasekar, N., Mohanam, S., Gujrati, M., Olivero, W. C., Dinh, D. H., & Rao, J. S. (2003). Downregulation of uPA inhibits migration and PI3k/Akt signaling in glioblastoma cells. *Oncogene*, *22*(3), 392–400. https://doi.org/10.1038/sj.onc.1206164

Chen, W., He, D., Li, Z., Zhang, X., Pan, D., & Chen, G. (2015). Overexpression of vascular endothelial growth factor indicates poor outcomes of glioma: a systematic review and meta-analysis. *International Journal of Clinical and Experimental Medicine*, *8*(6), 8709–8719. Retrieved from http://www.ncbi.nlm.nih.gov/pubmed/26309522

Chesney, J., Clark, J., Klarer, A. C., Imbert-Fernandez, Y., Lane, A. N., & Telang, S. (2014). Fructose-2,6-bisphosphate synthesis by 6-phosphofructo-2-kinase/fructose-2,6-bisphosphatase 4 (PFKFB4) is required for the glycolytic response to hypoxia and tumor growth. *Oncotarget*, *5*(16), 6670–6686. https://doi.org/10.18632/oncotarget.2213

Chien, M.-H., Ku, C.-C., Johansson, G., Chen, M.-W., Hsiao, M., Su, J.-L., … Kuo, M.-L. (2009). Vascular endothelial growth factor-C (VEGF-C) promotes angiogenesis by induction of COX-2 in leukemic cells via the VEGF-R3/JNK/ AP-1 pathway. *Carcinogenesis*, *30*(12), 2005–2013. https://doi.org/10.1093/carcin/bgp244

Choe, G., Park, J. K., Jouben-Steele, L., Kremen, T. J., Liau, L. M., Vinters, H. V, … Henry Singleton Brain Tumor Program T J K, the E. (2002). Active Matrix Metalloproteinase 9 Expression Is Associated with Primary Glioblastoma Subtype 1. *Clinical Cancer Research*, *8*, 2894–2901. Retrieved from http://home.clara.net/sisa/index.htm.

Chowdhary, S. A., Ryken, T., & Newton, H. B. (2015). Survival outcomes and safety of carmustine wafers in the treatment of high-grade gliomas: a meta-analysis. *J Neurooncol*, *122*, 367–382. https://doi.org/10.1007/s11060-015-1724-2

Christiansen, A., & Detmar, M. (2011). Lymphangiogenesis and Cancer. *Genes & Cancer*, *2*(12), 1146–1158. https://doi.org/10.1177/1947601911423028

Cohen, A., Holmen, S., & Colman, H. (n.d.). IDH1 and IDH2 Mutations in Gliomas. https://doi.org/10.1007/s11910-013-0345-4

Dagogo-Jack, I., & Shaw, A. T. (2017). Tumour heterogeneity and resistance to cancer therapies. *Nature Reviews Clinical Oncology*, *15*(2), 81–94. https://doi.org/10.1038/nrclinonc.2017.166

Das, K. K., & Kumar, R. (2017). Pediatric Glioblastoma. In De Vleeschouwer S (Ed.), *Glioblastoma* (1st ed.). Brisbane: Codon Publications. https://doi.org/10.15586/CODON.GLIOBLASTOMA.2017.CH15

Davis, M. E. (2016). Glioblastoma: Overview of Disease and Treatment. *Clinical*

Journal of Oncology Nursing, *20*(5), S2–S8. https://doi.org/10.1188/16.CJON.S1.2-8
De Bonis, P., Anile, C., Pompucci, A., Fiorentino, A., Balducci, M., Chiesa, S., … Mangiola, A. (2012). Safety and efficacy of Gliadel wafers for newly diagnosed and recurrent glioblastoma. *Acta Neurochirurgica*, *154*(8), 1371–1378. https://doi.org/10.1007/s00701-012-1413-2
Delgado-López, P. D., & Corrales-García, E. M. (2016). Survival in glioblastoma: a review on the impact of treatment modalities. *Clinical and Translational Oncology*, *18*. https://doi.org/10.1007/s12094-016-1497-x
DrugBank Database. (2005a). Carmustine. Retrieved June 13, 2018, from https://www.drugbank.ca/drugs/DB00262
DrugBank Database. (2005b). TEMOZOLOMIDE. Retrieved June 13, 2018, from https://www.drugbank.ca/drugs/DB00853
Dunn, G. P., Rinne, M. L., Wykosky, J., Genovese, G., Quayle, S. N., Dunn, I. F., … Hahn, W. C. (2012). Emerging insights into the molecular and cellular basis of glioblastoma. *Genes & Development*, *26*(8), 756–784. https://doi.org/10.1101/gad.187922.112
Emara, M., & Allalunis-Turner, J. (2014). Effect of hypoxia on angiogenesis related factors in glioblastoma cells. *Oncology Reports*, *31*, 1947–1953. https://doi.org/10.3892/or.2014.3037
Feng, H., Rong, H., Hua, Y., Jian, L., Jianmei, S., Xin, X., … Shibin, S. (2016). PTEN gene mutations correlate to poor prognosis in glioma patients: a meta-analysis. *OncoTargets and Therapy*, *9*, 3485–3492. https://doi.org/10.2147/OTT.S99942
Fernandes, C., Costa, A., Osório, L., Lago, R. C., Linhares, P., Carvalho, B., & Caeiro, C. (2017). Current Standards of Care in Glioblastoma Therapy. In Steven De vleeS chouwer (Ed.), *Glioblastoma* (1st ed., pp. 197–262). Brisbane, Australia: Codon Puclications. Retrieved from https://www.ncbi.nlm.nih.gov/books/NBK469998/pdf/Bookshelf_NBK469998.pdf
Firth, J. D., Ebert, B. L., & Ratcliffe, P. J. (1995). Hypoxic Regulation of Lactate Dehydrogenase A. *Journal of Biological Chemistry*, *270*(36), 21021–21027. https://doi.org/10.1074/jbc.270.36.21021
Fujiwara, S., Nakagawa, K., Harada, H., Nagato, S., Furukawa, K., Teraoka, M., … Ohnishi, T. (2007). Silencing hypoxia-inducible factor-1alpha inhibits cell migration and invasion under hypoxic environment in malignant gliomas. *International Journal of Oncology*, *30*(4), 793–802. Retrieved from http://www.ncbi.nlm.nih.gov/pubmed/17332917
Gialeli, C., Theocharis, A. D., & Karamanos, N. K. (2011). Roles of matrix metalloproteinases in cancer progression and their pharmacological targeting. *FEBS Journal*, *278*(1), 16–27. https://doi.org/10.1111/j.1742-4658.2010.07919.x
Gorlach, A. (2009). Regulation of HIF-1α at the Transcriptional Level. *Current Pharmaceutical Design*, *15*(33), 3844–3852. https://doi.org/10.2174/138161209789649420
Greaves, M., & Maley, C. C. (2012). Clonal evolution in cancer. *Nature*, *481*(7381), 306–313. https://doi.org/10.1038/nature10762
Gupta, A., & Dwivedi, T. (2017). A Simplified Overview of World Health Organization Classification Update of Central Nervous System Tumors 2016. *Journal of Neurosciences in Rural Practice*, *8*(4), 629–641. https://doi.org/10.4103/jnrp.jnrp_168_17
Gustafsson, N. M. S., Färnegårdh, K., Bonagas, N., Ninou, A. H., Groth, P., Wiita, E., … Helleday, T. (2018). Targeting PFKFB3 radiosensitizes cancer cells and

suppresses homologous recombination. *Nature Communications*, *9*(1), 3872. https://doi.org/10.1038/s41467-018-06287-x

Hambardzumyan, D., & Bergers, G. (2015). Glioblastoma: Defining Tumor Niches. *Trends Cancer*, *1*(4), 252–265. https://doi.org/10.1016/j.trecan.2015.10.009

Haupt Susan, Berger Michael, Goldberg Zehavit, & Haupt Ygal. (2003). Apoptosis – the p53 network. *Journal of Cell Science*, *116*, 4077–4085. https://doi.org/10.1242/jcs.00739

Hoelper, D., Huang, H., Jain, A. Y., Patel, D. J., & Lewis, P. W. (2017). Structural and mechanistic insights into ATRX- dependent and -independent functions of the histone chaperone DAXX. *Nature Communications*, *8*(1193). https://doi.org/10.1038/s41467-017-01206-y

HONGSHENG, X., HAILIANG, Z., CHONG, M., XING, M., MING, S., KAI, L., … LEI, C. (2017). Epidermal growth factor receptor in glioblastoma. *ONCOLOGY LETTERS*, *14*, 512–516. https://doi.org/10.3892/ol.2017.6221

Jenny, B., Harrison, J., Baetens, D., Tille, J.-C., Burkhardt, K., Mottaz, H., … Pepper, M. (2006). Expression and localization of VEGF-C and VEGFR-3 in glioblastomas and haemangioblastomas. *The Journal of Pathology*, *209*(1), 34–43. https://doi.org/10.1002/path.1943

Johansson, E., Grassi, E. S., Pantazopoulou, V., Tong, B., Lindgren, D., Berg, T. J., … Pietras, A. (2017). CD44 Interacts with HIF-2α to Modulate the Hypoxic Phenotype of Perinecrotic and Perivascular Glioma Cells. *Cell Reports*, *20*(7), 1641–1653. https://doi.org/10.1016/J.CELREP.2017.07.049

Jones, P. S., Puliyappadamba, V., Han, S. J., Das, S., Nandakumar, P., & Mansouri, A. (2017). The Role of ATRX in Glioma Biology. *Front. Oncol*, *7*(7). https://doi.org/10.3389/fonc.2017.00236

Kaur, B., Khwaja, F. W., Severson, E. A., Matheny, S. L., Brat, D. J., & Van Meir, E. G. (2005). Hypoxia and the hypoxia-inducible-factor pathway in glioma growth and angiogenesis 1. *Neuro-Oncology*. https://doi.org/10.1215/S1152851704001115

Kaur, B., Tan, C., Brat, D. J., & Van meir, E. G. (2004). Genetic and hypoxic regulation of angiogenesis in gliomas. *Journal of Neuro-Oncology*, *70*(2), 229–243. https://doi.org/10.1007/s11060-004-2752-5

Keating, G. M. (2014). Bevacizumab: A review of its use in advanced cancer. *Drugs*, *74*, 1891–1925. https://doi.org/10.1007/s40265-014-0302-9

Killela, P. J., Pirozzi, C. J., Reitman, Z. J., Jones, S., Rasheed, B. A., Lipp, E., … Yan, H. (2013). The genetic landscape of anaplastic astrocytoma. *Oncotarget*, *5*(6). Retrieved from www.impactjournals.com/oncotarget

Kling, T., Ferrarese, R., Hailín, D. Ó., Johansson, P., Heiland, D. H., Dai, F., … Nelander, S. (2016). Integrative Modeling Reveals Annexin A2-mediated Epigenetic Control of Mesenchymal Glioblastoma. *EBIOM*, *12*, 72–85. https://doi.org/10.1016/j.ebiom.2016.08.050

Kostaras, X., Cusano, F., Kline, G. A., Roa, W., & Easaw, J. (2014). Use of dexamethasone in patients with high-grade glioma: a clinical practice guideline. *Current OnCOlOgy—VOlume*, *21*(3), 493–503. https://doi.org/10.3747/co.21.1769

Labak, C. M., Wang, P. Y., Arora, R., Guda, M. R., Asuthkar, S., Tsung, A. J., & Velpula, K. K. (2016a). Glucose transport: meeting the metabolic demands of cancer, and applications in glioblastoma treatment. *American Journal of Cancer Research*, *6*(8), 1599–1608. Retrieved from http://www.ncbi.nlm.nih.gov/pubmed/27648352

Labak, C. M., Wang, P. Y., Arora, R., Guda, M. R., Asuthkar, S., Tsung, A. J., & Velpula, K. K. (2016b). Glucose transport: meeting the metabolic demands of cancer, and applications in glioblastoma treatment. *Am J Cancer Res*, *6*(8), 1599–1608. Retrieved from www.ajcr.us

Li, N., Wang, H., Zhang, J., & Zhao, E. (2016). Knockdown of hypoxia inducible factor-2α inhibits cell invasion via the downregulation of MMP-2 expression in breast cancer cells. *Oncology Letters*, *11*(6), 3743–3748. https://doi.org/10.3892/ol.2016.4471

Li, X., Wu, C., Chen, N., Gu, H., Yen, A., Cao, L., … Wang, L. (2016). PI3K/Akt/mTOR signaling pathway and targeted therapy for glioblastoma. *Oncotarget*, *7*(22). Retrieved from www.impactjournals.com/oncotarget

Li, Z., Bao, S., Wu, Q., Wang, H., Eyler, C., Sathornsumetee, S., … Robert, P. (2009). Hypoxia-Inducible Factors Regulate Tumorigenic Capacity of Glioma Stem Cells. *Cancer Cell*, *15*(6), 501–513. https://doi.org/10.1016/j.ccr.2009.03.018

Liang, Y., Li, X.-Y., Rebar, E. J., Li, P., Zhou, Y., Chen, B., … Case, C. C. (2002). Activation of vascular endothelial growth factor A transcription in tumorigenic glioblastoma cell lines by an enhancer with cell type-specific DNase I accessibility. *The Journal of Biological Chemistry*, *277*(22), 20087–20094. https://doi.org/10.1074/jbc.M201766200

Liao, D., & Johnson, R. S. (2007). Hypoxia: A key regulator of angiogenesis in cancer. *Cancer Metastasis*, *26*, 281–290. https://doi.org/10.1007/s10555-007-9066-y

Liberti, M. V, & Locasale, J. W. (2016). The Warburg Effect: How Does it Benefit Cancer Cells? *Trends Biochem Sci.*, *41*(3), 211–218. https://doi.org/10.1016/j.tibs.2015.12.001

Lim, K. S., Lim, K. J., Price, A. C., Orr, B. A., Eberhart, C. G., & Bar, E. E. (2014). Inhibition of monocarboxylate transporter-4 depletes stem-like glioblastoma cells and inhibits HIF transcriptional response in a lactate-independent manner. *Oncogene*, *33*(35), 4433–4441. https://doi.org/10.1038/onc.2013.390

Lin, S. H., & Kleinberg, L. R. (2008). Carmustine wafers: localized delivery of chemotherapeutic agents in CNS malignancies. *Expert Review of Anticancer Therapy*, *8*(3), 343–359. https://doi.org/10.1586/14737140.8.3.343

Lincet, H., & Icard, P. (2015). How do glycolytic enzymes favour cancer cell proliferation by nonmetabolic functions? *Oncogene*, *34*(29), 3751–3759. https://doi.org/10.1038/onc.2014.320

Livak, K. J., & Schmittgen, T. D. (2001). Analysis of Relative Gene Expression Data Using Real-Time Quantitative PCR and the 2 C T Method. *METHODS*, *25*, 402–408. https://doi.org/10.1006/meth.2001.1262

Lombardi, M. Y., & Assem, M. (2017). Glioblastoma Genomics: A Very Complicated Story. In Steven De Vleeschouwer (Ed.), *Glioblastoma* (1st ed., pp. 3–25). Brisbane, Australia: Codon Publications. https://doi.org/10.15586/CODON.GLIOBLASTOMA.2017.CH1

Long term side effects of radiotherapy | Brain tumour (primary). (2015). Retrieved May 30, 2018, from http://www.cancerresearchuk.org/about-cancer/brain-tumours/treatment/radiotherapy/long-term-side-effects

Madureira, P. A., O'connell, P. A., Surette, A. P., Miller, V. A., & Waisman, D. M. (2012). The Biochemistry and Regulation of S100A10: A Multifunctional Plasminogen Receptor Involved in Oncogenesis. *Journal of Biomedicine and Biotechnology*, *2012*. https://doi.org/10.1155/2012/353687

Madureira, P. A., Surette, A. P., Phipps, K. D., Taboski, M. A. S., Miller, V. A., & Waisman, D. M. (2011). The role of the annexin A2 heterotetramer in vascular

fibrinolysis. *Blood*, *118*(18), 4789–4797. https://doi.org/10.1182/blood-2011-06-334672

Mahmood, T., & Yang, P.-C. (2012). Western blot: technique, theory, and trouble shooting. *North American Journal of Medical Sciences*, *4*(9), 429–434. https://doi.org/10.4103/1947-2714.100998

Malta, T. M., Souza, C. F. de, Sabedot, T. S., Silva, T. C., Mosella, M. S., Kalkanis, S. N., … Noushmehr, H. (2017). Glioma CpG island methylator phenotype (G-CIMP): biological and clinical implications. *Neuro-Oncology*, *20*(5), 608–620. https://doi.org/10.1093/neuonc/nox183

Mansouri, A., Karamchandani, J., & Das, S. (2017a). Molecular Genetics of Secondary Glioblastoma. In *Glioblastoma*. Retrieved from http://www.ncbi.nlm.nih.gov/pubmed/29251857

Mansouri, A., Karamchandani, J., & Das, S. (2017b). *Molecular Genetics of Secondary Glioblastoma*. *Glioblastoma*. Codon Publications. https://doi.org/10.15586/CODON.GLIOBLASTOMA.2017.CH2

Marina, O., Suh, J. H., Reddy, C. A., Barnett, G. H., Vogelbaum, M. A., Peereboom, D. M., … Chao, S. T. (2011). Treatment outcomes for patients with glioblastoma multiforme and a low Karnofsky Performance Scale score on presentation to a tertiary care institution. *Journal of Neurosurgery*, *115*(2), 220–229. https://doi.org/10.3171/2011.3.JNS10495

Martin, vTracey A., Ye, L., Sanders, A. J., Lane, J., & Jiang, W. G. (2013). Cancer Invasion and Metastasis: Molecular and Cellular Perspective. Landes Bioscience.

Maule, F., Bresolin, S., Rampazzo, E., Boso, D., Puppa, A. Della, Esposito, G., … Persano, L. (2016). Annexin 2A sustains glioblastoma cell dissemination and proliferation. *Oncotarget*, *7*(34), 54632–54649. Retrieved from www.impactjournals.com/oncotarget

Maus, A., & Godefridus, J. P. (2017). Glutamate and α-ketoglutarate: key players in glioma metabolism. *Amino Acids*, *49*, 21–32. https://doi.org/10.1007/s00726-016-2342-9

Minniti, G., Muni, R., Lanzetta, G., & Enrici, R. M. (2009). Chemotherapy for Glioblastoma: Current Treatment and Future Perspectives for Cytotoxic and Targeted Agents. *Anticancer Research*, *29*, 5171–5184. Retrieved from http://ar.iiarjournals.org/content/29/12/5171.full.pdf

Modrek, A. S., Golub, D., Khan, T., Bready, D., Prado, J., Bowman, C., … Placantonakis, D. G. (2017). Low-grade astrocytoma mutations in IDH1, P53 and ATRX cooperate to block differentiation of human neural stem cells via repression of SOX2. *Cell Reports*, *21*(5), 1267–1280. https://doi.org/10.1016/j.celrep.2017.10.009

Mohanam, S., Chintala, S. K., Go, Y., Bhattacharya, A., Venkaiah, B., Boyd, D., … Rao, J. S. (1997). In vitro inhibition of human glioblastoma cell line invasiveness by antisense uPA receptor. *Oncogene*, *14*, 1351–1359. Retrieved from https://www.nature.com/articles/1200963.pdf?origin=ppub

Mongiardi, M. P., Savino, M., Falchetti, M. L., Illi, B., Bozzo, F., Valle, C., … Levi, A. (2016). c-MYC inhibition impairs hypoxia response in glioblastoma multiforme. *Oncotarget*, *7*(22), 33257–33271. https://doi.org/10.18632/oncotarget.8921

Monteiro, A., Hill, R., Pilkington, G., & Madureira, P. (2017). The Role of Hypoxia in Glioblastoma Invasion. *Cells*, *6*(4), 45. https://doi.org/10.3390/cells6040045

Morokoff, A., Ng, W., Gogos, A., & Kaye, A. H. (2015). Molecular subtypes, stem cells and heterogeneity: Implications for personalised therapy in glioma. *Journal of Clinical Neuroscience*, *22*, 1219–1226. https://doi.org/10.1016/j.jocn.2015.02.008

Nakano, K., & Vousden, K. H. (2001). PUMA, a Novel Proapoptotic Gene, Is Induced by p53. *Molecular Cell*, *7*, 683–694. Retrieved from https://ac.els-cdn.com/S1097276501002143/1-s2.0-S1097276501002143-main.pdf?_tid=74ab16b0-07bb-40b7-8557-92076abcd7fb&acdnat=1524227068_59363d505aeb9ba362a061adc125de8b

Newlands, E. S., Stevenst, M. F. G., Wedge, S. R., Wheelhouse, R. T., & Brock, C. (1997). Temozolomide: a review of its discovery, chemical properties, pre-clinical development and clinical trials. *Cancer Treatment Reviews*, *23*, 35–61. Retrieved from https://www.cancertreatmentreviews.com/article/S0305-7372(97)90019-0/pdf

Ohgaki, H., & Kleihues, P. (2007). Genetic Pathways to Primary and Secondary Glioblastoma. *American Journal of Pathology*, *170*. Retrieved from https://www.ncbi.nlm.nih.gov/pmc/articles/PMC1854940/pdf/JPATH170001445.pdf

Ohgaki, H., & Kleihues, P. (2013). The Definition of Primary and Secondary Glioblastoma. *Clin Cancer Res*, *19*(4), 764–772. https://doi.org/10.1158/1078-0432.CCR-12-3002

Olbryt, M., Habryka, A., Student, S., Jarząb, M., Tyszkiewicz, T., & Lisowska, K. M. (2014). Global gene expression profiling in three tumor cell lines subjected to experimental cycling and chronic hypoxia. *PloS One*, *9*(8), e105104. https://doi.org/10.1371/journal.pone.0105104

Ooi, H. K., & Ma, L. (2013). Modeling heterogeneous responsiveness of intrinsic apoptosis pathway. *BMC Systems Biology*, *7*(65). Retrieved from http://www.biomedcentral.com/1752-0509/7/65

Osuka, S., & Meir, E. G. Van. (2017). Overcoming therapeutic resistance in glioblastoma: the way forward. *The Journal of Clinical Investigation*, *127*(2), 415–426. https://doi.org/10.1172/JCI89587

Pandey, V., Bhaskara, V. K., & Babu, P. P. (2016). Implications of mitogen-activated protein kinase signaling in glioma. *Journal of Neuroscience Research*, *94*(2), 114–127. https://doi.org/10.1002/jnr.23687

Paolillo, M., Boselli, C., & Schinelli, S. (2018). Glioblastoma under Siege: An Overview of Current Therapeutic Strategies. *Brain Sciences*, *8*(1), 15. https://doi.org/10.3390/brainsci8010015

Patel, N., & Kalra, V. K. (2010). Placenta Growth Factor-induced Early Growth Response 1 (Egr-1) Regulates Hypoxia-inducible Factor-1α (HIF-1α) in Endothelial Cells. *Journal of Biological Chemistry*, *285*(27), 20570–20579. https://doi.org/10.1074/jbc.M110.119495

Pinto, J. A., Rolfo, C., Raez, L. E., Prado, A., Araujo, J. M., Bravo, L., … Gomez, H. L. (2017). In silico evaluation of DNA Damage Inducible Transcript 4 gene (DDIT4) as prognostic biomarker in several malignancies. *Scientific Reports*, *7*(1), 1526. https://doi.org/10.1038/s41598-017-01207-3

Radisky, E. S., & Radisky, D. C. (2010). Matrix Metalloproteinase-Induced Epithelial-Mesenchymal Transition in Breast Cancer. *Journal of Mammary Gland Biology and Neoplasia*, *15*(2), 201–212. https://doi.org/10.1007/s10911-010-9177-x

Reifenberger, G., & Louis, D. N. (2003). Oligodendroglioma: Toward Molecular Definitions in Diagnostic Neuro-Oncology. *Journal of Neuropathology and Experimental Neurology*, *62*(2). Retrieved from https://watermark.silverchair.com/62-2-111.pdf?token=AQECAHi208BE49Ooan9kkhW_Ercy7Dm3ZL_9Cf3qfKAc485ysgAAAcUwggHBBgkqhkiG9w0BBwagggGyMIIBrgIBADCCAacGCSqGSIb3DQE

HATAeBglghkgBZQMEAS4wEQQMDzAOBDyAaIZRopTQAgEQgIIBeKJ5aLjt5z6kIzzZlyvqIOTY82ca2mXK5K2WE2EtYcuz16

Ros, S., & Schulze, A. (2013). Balancing glycolytic flux: the role of 6-phosphofructo-2-kinase/fructose 2,6-bisphosphatases in cancer metabolism. *Cancer & Metabolism*, *1*(8). https://doi.org/10.1186/2049-3002-1-8

Rundhaug, J. E. (2003). Matrix metalloproteinases, angiogenesis, and cancer: commentary re: A. C. Lockhart et al., Reduction of wound angiogenesis in patients treated with BMS-275291, a broad spectrum matrix metalloproteinase inhibitor. Clin. Cancer Res., 9: 00-00, 2003. *Clinical Cancer Research : An Official Journal of the American Association for Cancer Research*, *9*(2), 551–554. Retrieved from http://www.ncbi.nlm.nih.gov/pubmed/12576417

Said, H. M., Polat, B., Staab, A., Hagemann, C., Stein, S., Flentje, M., … Vordermark, D. (2008). Rapid detection of the hypoxia-regulated CA-IX and NDRG1 gene expression in different glioblastoma cells in vitro. *Oncology Reports*, *20*(2), 413–419. https://doi.org/10.3892/or_00000023

Said, H. M., Safari, R., Al-Kafaji, G., Ernestus, R.-I., Löhr, M., Katzer, A., … Hagemann, C. (2017). Time- and oxygen-dependent expression and regulation of NDRG1 in human brain cancer cells. *Oncology Reports*, *37*(6), 3625–3634. https://doi.org/10.3892/or.2017.5620

Schonberg, D. L., Miller, T. E., Wu, Q., Flavahan, W. A., Das, N. K., Hale, J. S., … Rich, J. N. (2015). Preferential Iron Trafficking Characterizes Glioblastoma Stem-like Cells. *Cancer Cell*, *28*(4), 441–455. https://doi.org/10.1016/j.ccell.2015.09.002

Semenza, G. L., Jiang, B. H., Leung, S. W., Passantino, R., Concordet, J. P., Maire, P., & Giallongo, A. (1996). Hypoxia response elements in the aldolase A, enolase 1, and lactate dehydrogenase A gene promoters contain essential binding sites for hypoxia-inducible factor 1. *The Journal of Biological Chemistry*, *271*(51), 32529–32537. https://doi.org/10.1074/JBC.271.51.32529

Shibue, T., Takeda, K., Oda, E., Tanaka, H., Murasawa, H., Takaoka, A., … Tanaka, N. (2003). Integral role of Noxa in p53-mediated apoptotic response. *Genes & Development*, *17*, 2233–2238. https://doi.org/10.1101/gad.1103603

Side effects of radiotherapy | Brain tumour (primary). (2015). Retrieved May 30, 2018, from http://www.cancerresearchuk.org/about-cancer/brain-tumours/treatment/radiotherapy/side-effects

Sionov, R. V., & Haupt, Y. (1999). The cellular response to p53: the decision between life and death. *Oncogene*, *18*, 6145–6157. Retrieved from https://www.nature.com/articles/1203130.pdf

Stefanik, D. (2013). *Vascular Endothelial Growth Factor in Malignant Disease of the Central Nervous System*. Landes Bioscience. Retrieved from https://www.ncbi.nlm.nih.gov/books/NBK6434/?report=reader

Talasila, K. M., Røsland, G. V., Hagland, H. R., Eskilsson, E., Flønes, I. H., Fritah, S., … Miletic, H. (2016). The angiogenic switch leads to a metabolic shift in human glioblastoma. *Neuro-Oncology*, *19*(3), now175. https://doi.org/10.1093/neuonc/now175

Tan, V. P., & Miyamoto, S. (2015). HK2/hexokinase-II integrates glycolysis and autophagy to confer cellular protection. *Autophagy*, *11*(6), 963–964. https://doi.org/10.1080/15548627.2015.1042195

Touat, M., Idbaih, A., Sanson, M., Ligon, K. L., & Ligon, K. L. (2017). Glioblastoma targeted therapy: updated approaches from recent biological insights. *Annals of Oncology*, *28*, 1457–1472. https://doi.org/10.1093/annonc/mdx106

van Lith, S. A. M., Navis, A. C., Verrijp, K., Niclou, S. P., Bjerkvig, R., Wesseling, P., … Leenders, W. P. J. (2014). Glutamate as chemotactic fuel for diffuse glioma cells: Are they glutamate suckers? *Biochimica et Biophysica Acta - Reviews on Cancer*. https://doi.org/10.1016/j.bbcan.2014.04.004

Verhaak, R. G., Hoadley, K. A., Purdom, E., Wang, V., Qi, Y., Wilkerson, M. D., … Neil Hayes, D. (2010). Integrated Genomic Analysis Identifies Clinically Relevant Subtypes of Glioblastoma Characterized by Abnormalities in PDGFRA, IDH1, EGFR, and NF1. *Cancer Cell*, *17*, 98–110. https://doi.org/10.1016/j.ccr.2009.12.020

Wenger, K. J., Wagner, M., You, S.-J., Franz, K., Harter, P. N., Burger, M. C., … Bahr, O. (2017). Bevacizumab as a last-line treatment for glioblastoma following failure of radiotherapy, temozolomide and lomustine. *ONCOLOGY LETTERS*, *14*, 1141–1146. https://doi.org/10.3892/ol.2017.6251

Wenger, R. H., Kvietiko, I., Rolfs, A., Gassmann, M., & Marti, H. H. (1997). Hypoxia-inducible factor-1α is regulated at the post-mRNA level. *Kidney International*, *51*(2), 560–563. https://doi.org/10.1038/ki.1997.79

Wesseling, P., Van Den Bent, M., & Perry, A. (2015). Oligodendroglioma: pathology, molecular mechanisms and markers. *Acta Neuropathol*, *129*, 809–827. https://doi.org/10.1007/s00401-015-1424-1

Wolf, A., Agnihotri, S., Micallef, J., Mukherjee, J., Sabha, N., Cairns, R., … Guha, A. (2011). Hexokinase 2 is a key mediator of aerobic glycolysis and promotes tumor growth in human glioblastoma multiforme. *The Journal of Experimental Medicine*, *208*(2), 313–326. https://doi.org/10.1084/jem.20101470

Yang, H., Ye, D., Guan, K.-L., & Xiong, Y. (2012). IDH1 and IDH2 mutations in tumorigenesis: mechanistic insights and clinical perspectives. *Clinical Cancer Research*, *18*(20), 5562–5571. https://doi.org/10.1158/1078-0432.CCR-12-1773

Young, R. M., Jamshidi, A., Davis, G., & Sherman, J. H. (2015). Current trends in the surgical management and treatment of adult glioblastoma. *Annals of Translational Medicine*, *3*(9). https://doi.org/10.3978/j.issn.2305-5839.2015.05.10

Zhai, H., Acharya, S., Gravanis, I., Mehmood, S., Seidman, R. J., Shroyer, K. R., … Tsirka, S. E. (2011a). Annexin A2 Promotes Glioma Cell Invasion and Tumor Progression. *Journal of Neuroscience*, *31*(40), 14346–14360. https://doi.org/10.1523/JNEUROSCI.3299-11.2011

Zhai, H., Acharya, S., Gravanis, I., Mehmood, S., Seidman, R. J., Shroyer, K. R., … Tsirka, S. E. (2011b). Annexin A2 Promotes Glioma Cell Invasion and Tumor Progression. *Journal of Neuroscience*, *31*(40), 14346–14360. https://doi.org/10.1523/JNEUROSCI.3299-11.2011

Zhang, J. Z., Behrooz, A., & Ismail-Beigi, F. (1999). Regulation of glucose transport by hypoxia. *American Journal of Kidney Diseases : The Official Journal of the National Kidney Foundation*, *34*(1), 189–202. https://doi.org/10.1053/AJKD03400189

CHAPTER VIII

APPENDIX

8. Appendix

8.1 Annex 1: Lysis Buffer preparation protocol

- First, prepare a box with Ice.
- Prepare buffer solution as established in the following table (ALWAYS keep the Lysis Buffer solution on ice; Don't save any lysis buffer, always prepare a fresh solution for the protocol):

Volume	RIPA PIERCE buffer	Proteases inhibitor (100x)	MEBTA solution (0,5 M)
0,5 ml	500 µl	5µl	2,5µl
1 ml	1000 µl	10µl	5µl
2 ml	2000 µl	20µl	10µl
3ml	3000 µl	30µl	15µl

8.2 Annex 2: BCA assay protocol

(Provided in informatic support)

8.3 Annex 3: QIAGEN: Rneasy^{R} Plus Mini Kit Protocol

- Discard the media and wash with HBSS (~2ml).
- Incubate for 2-3 minutes, at 37ºC with Trypsin.
- Pass the cells into a 15ml tube with 3ml of growth medium.
- Centrifugate for 5 min. and discard medium.
- Add 350 µl of RLT Buffer (lysis buffer) to the tube and mechanically instigate the lysis process by pipetting.
- Transfer the RLT solution with cells to the gDNA Eliminator spin column (purple) placed in a 2ml collection tube.
- Centrifuge 30s at ≥10'000 rpm (p.e. 10'500 rpm) and discard the column. SAVE THE FLOW-THROUGH.

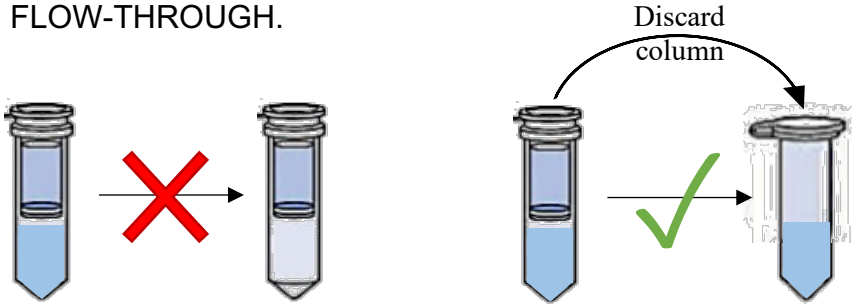

- Add 350 µl of ethanol 70% directly to the flow-through and mix it by pipetting.
- Transfer all solution (~700 µl) to a RNeasy spin column (pink) placed in a 2ml collection tube. Close lid and centrifuge for 15s at ≥10'000 rpm (p.e. 10'500 rpm). Discard the flow-through.
- Add 700 µl of RW1 Buffer to the same RNeasy spin column (pink) and centrifuge for 15s at ≥10'000 rpm (p.e. 10'500 rpm). Discard the flow-through.

- Add 500 µl RPE Buffer to the same RNeasy spin column (pink) and centrifuge for 15s at ≥10'000 rpm (p.e. 10'500 rpm). Discard the flow-through.

- Add 500 µl RPE Buffer to the same RNeasy spin column (pink) and centrifuge for 2 minutes at ≥10'000 rpm (p.e. 10'500 rpm). Discard the flow-through.

- Place the RNeasy spin column (pink) in a new 1,5ml collection tube (similar to the normal Eppendorf). Add 30-50 µl RNase-free water directly to the RNeasy spin column membrane. Close the lid and centrifuge for 1 minute at ≥10'000 rpm (p.e. 10'500 rpm). SAVE THE FLOW-THROUGH.

- Repeat elution with another 50 µl RNase-free water applied directly to the RNeasy spin column membrane. Close the lid and centrifuge for 1 minute at ≥10'000 rpm (p.e. 10'500 rpm). SAVE THE FLOW-THROUGH.

- Discard the RNeasy spin column (pink) column and save the flow-through (Extracted RNA solution) in the -80ºC.

8.4 Annex 4: RT^2 array protocol

(Provided in informatic support)

8.5 Annex 5: Bioanalyzer protocol

(Provided in informatic support)

8.6 Annex 6: RT^2 arrays reports-

a. UP-029

b. SEBTA-03

(Provided in informatic support)